WIND-TUNNEL RESEARCH ON THE MECHANICS OF PLUMES IN THE ATMOSPHERIC SURFACE LAYER

by

J. E. Cermak[1], P. K. Shrivastava[2]

and M. Poreh[3]

**FLUID MECHANICS AND
WIND ENGINEERING PROGRAM**

COLLEGE OF ENGINEERING

COLORADO STATE UNIVERSITY
FORT COLLINS, COLORADO

WIND-TUNNEL RESEARCH ON THE MECHANICS OF
PLUMES IN THE ATMOSPHERIC SURFACE LAYER

by

J. E. Cermak[1], P. K. Shrivastava[2]

and M. Poreh[3]

prepared for

December 1983   CER83-84JEC-PKS-MP12
                                                 Project No. 5-3 2512

[1]Professor-in-Charge, Fluid Mechanics and Wind Engineering Program, and
 Director, Fluid Dynamics and Diffusion Laboratory, Colorado State
 University.
[2]Doctoral Candidate, Department of Civil Engineering, Colorado State
 University.
[3]Visiting Professor, Colorado State University.

REPORT DOCUMENTATION PAGE		READ INSTRUCTIONS BEFORE COMPLETING FORM
1. REPORT NUMBER CER83-84JEC-PKS-MP12	2. GOVT ACCESSION NO.	3. RECIPIENT'S CATALOG NUMBER
4. TITLE (and Subtitle) Wind Tunnel Research on the Mechanics of Plumes in the Atmospheric Surface Layer		5. TYPE OF REPORT & PERIOD COVERED Annual Progress Report
		6. PERFORMING ORG. REPORT NUMBER
7. AUTHOR(s) J. E. Cermak, P. K. Shrivastava, M. Poreh		8. CONTRACT OR GRANT NUMBER(s) DAAK11-82-K-0004
9. PERFORMING ORGANIZATION NAME AND ADDRESS Fluid Dynamics and Diffusion Laboratory Department of Civil Engineering Colorado State University Fort Collins, Colorado 80523		10. PROGRAM ELEMENT, PROJECT, TASK AREA & WORK UNIT NUMBERS 1L161102A71A-D
11. CONTROLLING OFFICE NAME AND ADDRESS Contracts and Grants Administrator Office of Sponsored Research Colorado State University Fort Collins, Colorado 80523		12. REPORT DATE December 1983
		13. NUMBER OF PAGES
14. MONITORING AGENCY NAME & ADDRESS(If different from Controlling Office) CDR/DIR Chemical Systems Laboratory Attn: DRDAR-CLB-PS (Dr. E. Stuebing) Aberdeen Proving Ground, Maryland 21010		15. SECURITY CLASS. (of this report) UNCLASSIFIED
		15a. DECLASSIFICATION/DOWNGRADING SCHEDULE NA

16. DISTRIBUTION STATEMENT (of this Report)

Approved for public release; distribution unlimited.

17. DISTRIBUTION STATEMENT (of the abstract entered in Block 20, if different from Report)

18. SUPPLEMENTARY NOTES

This study was sponsored by the Army Smoke Research Program, Chemical Systems Laboratory, Aberdeen Proving Ground, Maryland.

19. KEY WORDS (Continue on reverse side if necessary and identify by block number)

Plume Mechanics	Dispersion of Gases	Meteorological Wind Tunnel
Turbulent Diffusion	Dispersion of Particles	Turbulence Distributions
Boundary Layers	Physical Modeling	Concentration Distribu- tions
Atmospheric Stability	Atmospheric Surface Layer	Temperature Distributions

20. ABSTRACT (Continue on reverse side if necessary and identify by block number)

The diffusion of a neutrally buoyant gas emitted from point sources into neutral, stable and unstable boundary layers that simulated atmospheric conditions were studied in a meteorological wind tunnel for flow over two surface roughnesses. Measurements were made of the mean flow velocities and temperatures, turbulence intensities, velocity correlations and gas concentrations in the diffusing plume. Empirical models were developed for predicting diffusion under all three stabilities studied.

DD FORM 1 JAN 73 1473 EDITION OF 1 NOV 65 IS OBSOLETE

TABLE OF CONTENTS

LIST OF FIGURES

LIST OF TABLES

LIST OF SELECTED SYMBOLS

Symbol	Definition	Dimension
C	Normalized observed concentration	L^{-2}
C_{max}	Maximum normalized plume concentration	L^{-2}
C_p	Specific heat at constant pressure	$L^2 T^{-2} t^{-1}$
d_y	Horizontal drift of maximum concentration	L
g	Acceleration due to gravity	LT^{-2}
h	Height of temperature gradient inversion	L
H	Source height above the surface	L
H_o	Wall heat flux	$H L^{-2} T^{-1}$
k	von Karman constant	-
L	Monin-Obukhov length scale	L
n	Exponent of velocity profile	
N.C.	Normalized concentration	L^{-2}
Q	Source strength	LT^{-1}
Ri	Richardson number $= \dfrac{g}{T} \dfrac{\left(\dfrac{\partial \theta}{\partial z}\right)}{\left(\dfrac{\partial u}{\partial z}\right)^2}$	-
s	Vertical plume spread exponent	-
T	Temperature	t
T^*	Friction temperature	t
u, v, w	Mean velocity in the x, y, z directions	LT^{-1}
u', v', w'	Turbulent fluctuating velocity in the x, y, z direction	LT^{-1}
u_∞	Free-stream velocity	LT^{-1}
u^*	Shear velocity	LT^{-1}
U_{ref}	Reference velocity	LT^{-1}

Symbol	Definition	Dimension
V	Volume flowrate	L^3T^{-1}
w*	Convective velocity	LT^{-1}
x, y, z	A right-hand coordinate system with origin at the base of the simulated point source	L
X	Dimensionless distance	-
z_o	Aerodynamic surface roughness length	L
z^s	Source height	L
δ	Momentum boundary layer thickness	L
δ_z	Vertical plume spread	L
ρ_o	Mass density	ML^{-3}
θ	Temperature (in absolute units)	t
λ_y	Horizontal plume spread constant	L
λ_z	Vertical plume spread constant	L
σ_y	Standard deviation of the horizontal plume spread	L
σ_z	Standard deviation of the vertical plume spread	L
τ_o	Shear stress at boundary (z=0)	$ML^{-1}T^{-2}$
χ	Measured concentration	ppm
χ_o	Source strength	ppm

L - length
T - time
M - mass
t - temperature
H - heat

I. INTRODUCTION

1.1 Purpose

The three-year research program is intended to establish the foundations for a long-range comprehensive investigation of aero-collodial dispersion and evolution in the atmospheric-surface-layer (ASL) environment through use of simulated ASL flows. It was formulated to achieve the following objectives:

1. Establishment of a set of reference data on mean flow and turbulence characteristics for the full-range of possible ASL simulations in the Meteorological Wind Tunnel (MWT) of the Fluid Dynamics and Diffusion Laboratory (FDDL).

2. Development of dispersion data for the reference flows that will serve as reference plumes to evaluate effects of aero-colloids on dispersion mechanics.

3. Design and initiate studies to determine the effects of aero-colloidal particle size and concentration on concentration distributions and surface deposition.

4. Design and develop a capability for research on aerocolloidal kinetics in the MWT.

5. Establish the foundation for a long-range research program on plume mechanics.

The proposed research objectives are further described in specific tasks planned for each of the three years.

1.2 First-Year Tasks

Initial efforts of the research program were directed to the development of reference data for a wide range ASL simulations in the MWT. Mean flow, turbulence characteristics and dispersion data were investigated and carefully documented. Additionally, the design of

1

second-year experiments with aerocolloidal particles was initiated. These three first-year objectives are expanded upon in the task descriptions which follow:

Task 1-A: Establish characteristics of meteorological variables for simulated ASL's in the MWT that include full range of the wind tunnel capability to simulate stable and unstable thermal stratification beginning at ground level and elevated inversions. Careful documentation of the mean flow and turbulence characteristics is required to provide basic reference flow fields for the plume dispersion studies.

A. Flow Variables
   1. Lower boundary -- plane
   2. Boundary roughness -- 2 cases (smooth, 1 rough)
   3. Thermal stratification -- 4 cases (neutral, 1 stable, 1 unstable, 1 elevated inversion)

B. Measurements (for each combination of flow variables)
   1. Mean velocity and temperature -- 5 vertical profiles; along centerline at x = 15,16,17,19, 22 m from test-section entrance
   2. Turbulence intensities -- 5 vertical profiles; same location as for mean velocity and temperature
   3. Velocity-velocity correlations ($\overline{u'w'}$, $\overline{u'v'}$, $\overline{v'w'}$) -- 1 vertical profile, x = 16 m on centerline
   4. Velocity power spectra (u', v', w') -- 5 points; x = 16 m
   5. Turbulence scales (longitudinal, lateral, vertical) -- 5 points; x = 16 m

Task 1-B: Develop a set of reference plume characteristics for the reference flow fields. The reference plumes are intended to provide basic characterization of turbulent diffusion by atmospheric turbulence without modifications caused by the diffusing material. Reference plumes developed by a single source emission at several distinct elevations in the simulated ASL, including ground level, are proposed for reference documentation.

2

A. Flow Variables: same as Task 1-A

B. Material Source Variables
   1. Time: steady
   2. Spatial: point; 3 elevations at x = 16 m
   3. Material: non-reacting gas, with hydrocarbon tracer,
                 neutral buoyancy relative to atmospheric
                 density at release elevation
   4. Momentum: near zero

C. Measurements
   1. Mean concentration of source material: distributions to
      describe cross section of plume at 4 locations downwind of
      source

Task 1-C: Design experiments to investigate plume mechanics for

          stable aerocolloidal particles in the simulated ASL.

A plume study to be performed in Year 2 will be designed to include
the following general specifications --

A. Flow Variables: same as Task 1-A

B. Material Source Variables:
   1. Time: steady
   2. Spatial: point
   3. Material (tentative): monodisperse polystyrene latex
                             spheres (0.5 - 5.0 μm)
C. Measurements
   1. Mean concentration distributions in plume
   2. Surface deposition

1.3 Report Organization

The MWT was operated in several different configurations to achieve

the thermal stratifications and boundary roughnesses specified in the

preceding Tasks 1-A and 1-B. These configurations, as well as descrip-

tions of the test instrumentation and measurement apparatus, are re-

corded in the next section.

Experiments were conducted to obtain reference data for three

differing atmospheric stabilities. The results of these experiments are

discussed in Sections 3.0, 4.0 and 5.0 for neutral, stable and unstable

flow, respectively. Each section adheres to a similar format. The

3

velocity profiles obtained above a smooth floor are first described, followed by the velocity fields recorded over the rough floor. The final part of each section contains a discussion of the measured concentration fields for both roughness conditions. Tabulated data and graphic comparisons used in the presentations are contained in tables and figures located at the end of each section.

Section 6.0 contains Conclusions and Commentary from the previously discussed experiments.

The appendices to this report contain development of special topics entitled "Wind-Tunnel Simuluation of Particle-Plumes in the Atmospheric Surface Layer" and "Length-Scales Describing the Vertical Diffusion from Ground-Level Sources".

2.0 EXPERIMENTAL PROCEDURES

2.1 Wind-Tunnel Configuration

All experiments were conducted in the MWT at CSU. Design and operation of the wind tunnel are described in detail by Cermak (1981). Elevation and plan views of the MWT are shown in Figure 2-1.

Figure 2-2 is a three-dimensional representation of the entrance to the MWT test section. All four surfaces immediately preceding the test section were lined with gravel. The sawtooth shaped trip which framed the entrance was also used as a reference for locating the point source within the test section.

Four evenly spaced 91 cm tall spires were placed across the tunnel, next to the sawtooth trip, to simulate the desired ABL within the test section. Pertinent theories of ABL simulation are discussed in detail by Cermak (1971, 1982). Figure 2-3 contains a close-up pictorial representation of the MWT entrance configuration, while Figure 2-4 contains a dwonwind view of the entire MWT test section, without roughness.

A portion of the twelve auxiliary cooling plates, which covered one third of the floor upwind of the test section, is visible in the photo reproduced in Figure 2-5. These plates, which remained in place during tests in all three stratifications, have a slightly rougher surface than the permanently installed aluminum plates, which make up the next 12.28 m of tunnel floor.

A change in the aerodynamic surface roughness, z_o, from a lower value for the 'smooth' case to a higher value for the 'rough' case was achieved by the installation of 1.6 cm twisted-link chain elements placed 21.6 cm apart along the entire test section of the MWT. The

origin of the coordinate system used to reference the velocity and concentration measurements was established at the location of the ground-level point source (16.12 m downwind of the sawtooth trip). Figure 2-6 shows the arrangement of the roughness chains.

A schematic drawing summarizing the configuration of the MWT is presented in Figure 2-7. This drawing also shows the location of the measurement stations which are described in the next sub-section.

2.2 Test Measurements and Instrumentation

The neutral boundary layer was simulated in the MWT with existing ambient conditions whereas stratified boundary layers were simulated by controlling the environment in the wind-tunnel. Table 2-1 presents the mean velocity and temperature conditions maintained in the MWT during experiments with each of the three stabilities. Free-stream velocity and temperature were continuously monitored with a pitot tube and thermistor positioned 1.09 m above the floor, and 0.85 m upwind of the source (see Figures 2-6 and 2-7).

To create the stable boundary layer, an ethylene-glycol solution was circulated through the auxiliary cooling plates and the permanent aluminum plates to chill the floor, while the air circulating in the closed-loop tunnel was heated.

The unstable boundary layer was simulated by electrically heating the aluminum plates and simultaneously, cooling the air circulating in the MWT.

Using the location of the ground-level source as a coordinate reference, velocity, turbulence and temperature data for each stability and surface roughness condition were measured at downwind distances of 0, 2.80 and 6.05 m along the centerline. These measurements were

6

obtained with a constant temperature cross-film anemometer, TSI model 1241-10, and a resistance wire temperature sensor mounted in close proximity to each other. Prior to taking data, the sensors were calibrated in a temperature and velocity controlled enclosure. Empirical equations were developed to relate anemometer voltage, velocity and temperature. Using these equations, an on-line computer permitted nearly instantaneous output of the velocity and temperature data measured in the MWT.

Two orientations of the cross-film furnished velocity and turbulence data along all three primary axes. Mean and cross-correlation values were computed from 600-1000 instantaneous readings per second, recorded over a period of 60-120 seconds with sampling rate and duration dependent upon the relative stability of test conditions.

Neutrally buoyant hydrocarbon tracers were released from 0.635 cm diameter brass tubes (referred to elsewhere, and here, as the point sources), located at heights of $z^s \cong 0$, 10.00 and 20.0 cm above the floor. The effective height of the ground-level source was one-half the tube diameter, or approximately 3 mm. Figure 2-8 illustrates the arrangement of the point sources.

The tracers (9.98% ethane, 4% CO_2, 86.0% N_2 or 5.6% propane, 94.38% N_2) were released through the sources with an exit velocity $\cong$ 88 cm/sec while being maintained at the average temperature existing at source height.

Tracer concentrations were measured at distances of 0.85, 1.95, 2.80, 3.90 and 6.05 m downwind from the source for all three stabilities. Rapid diffusion in the unstable flow dictated additional measurements at 0.45 and 1.35 m.

Samples of the tracer were drawn by a near-isokinetic sampling system through 1.59 mm I.D. tubes into a gas chromatograph analyzer. The sampling tubes, mounted on a rake, as shown in Figure 2-9, provided a grid for measuring diffusion within the tracer plume. Up to 40 five-minute tracer samples were simultaneously collected by the sampler, shown in Figure 2-10a, for analysis int he Hewlett-Packard gas chromatograph (GC), shown in Figure 2-10b.

The tracer gas data obtained from the GC analyses wer normalized using the equation

$$ N.C. = \frac{\chi u_\infty}{\chi_o V} \qquad (2-1) $$

where   N.C. = normalized concentration (m^{-2})

χ = measured concentration (ppm)

u_∞ = free-stream velocity (m/s)

χ_o = source strength (ppm)

V = volume flowrate (m^3/s).

All diffusion data included in this report are in this normalized for.

2.3 Flow Visualization

Titanium dioxide (TiO_2) 'smoke' was released from the point sources for each stratification to observe plume behavior and to ascertain the normal operation of lthe MWT. Plume diffusions for the three stratifications and three source heights were documented on 16 mm movie film and 35 mm photos. Representative plumes from a ground-level source for stable, neutral and unstable atmospheric conditions are presented in Figures 2-11 and 2-12.

Table 2-1. Temperature and Velocity Conditions in the MWT for Plume Mechanics Experiments

Atmospheric Condition	Roughness	T_F (°C)	$\overline{T}_\infty$ (°C)	$\overline{u}_\infty$ (m/s)
Neutral	smooth	-	23.2 (22.5 to 24.0)	3.00 (2.88 to 3.06)
	rough	-	23.5 (22.5 to 25.0)	2.99 (2.91 to 3.05)
Stable	smooth	~±1	77.0 (75.7 to 79.3)	2.45 (2.43 to 2.47)
	rough	~±1	78.7 (73.0 to 80.3)	2.44 (2.39 to 2.51)
Unstable	smooth	157	7.7 (7.4 to 8.4)	2.43 (2.40 to 2.46)
	rough	146	7.5	2.44

T_F Floor Temperature

$\overline{T}_\infty$ Mean Free-Stream Temperature

$\overline{u}_\infty$ Mean Free-Stream Velocity

(Range of Values)
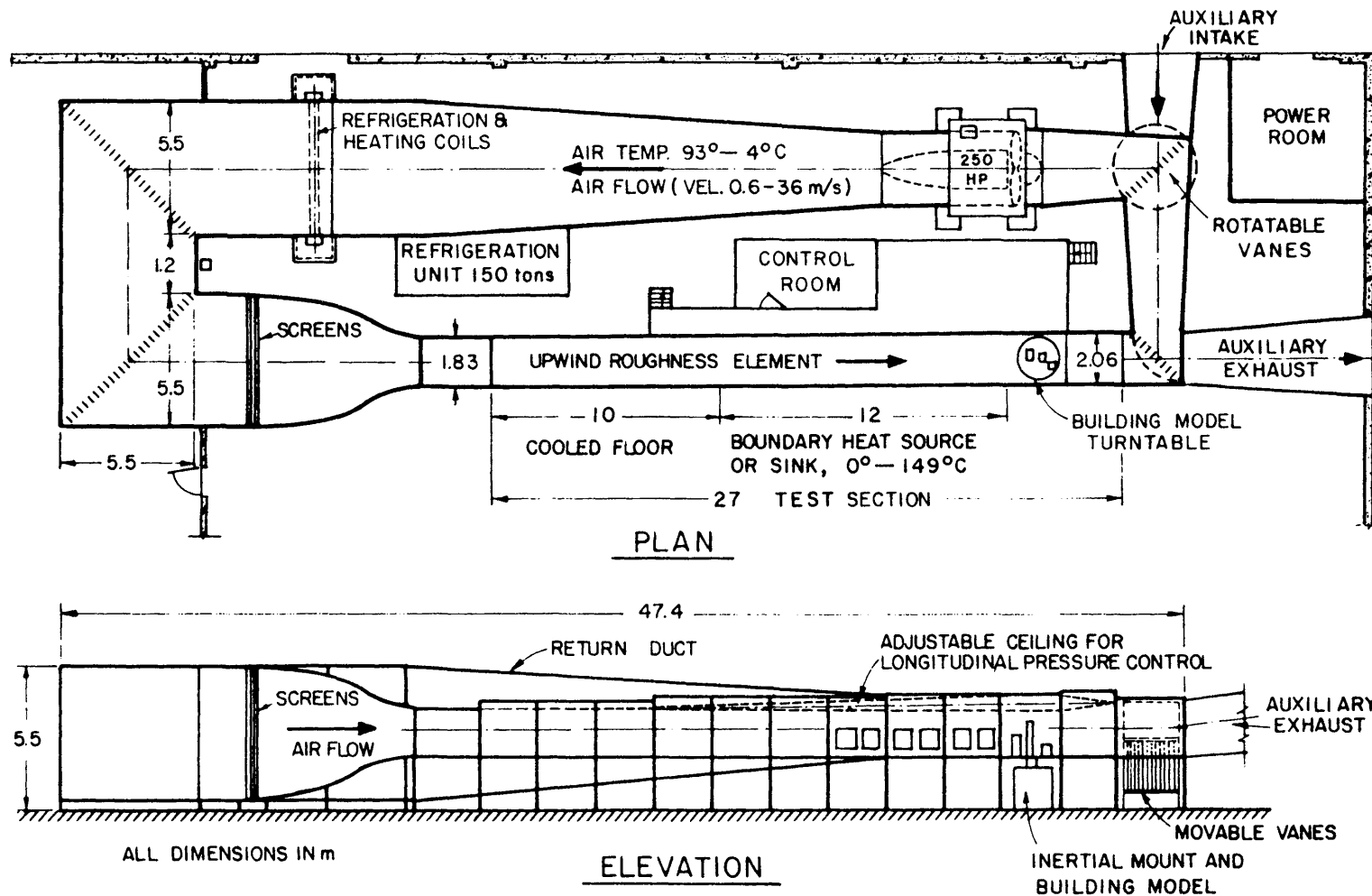
Figure 2-1. Meteorological Wind Tunnel, Fluid Dynamics and Diffusion Laboratory, Colorado State University.

Wind Direction

Ç Test Section

z

6' (1.83m)

0.25"(0.64cm) to 0.75"(1.91cm) Dia. Gravel Lining

x

y

3" (7.62cm)

1½" (3.81cm)
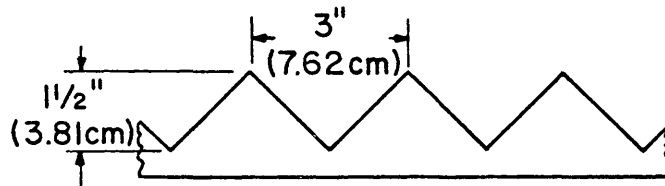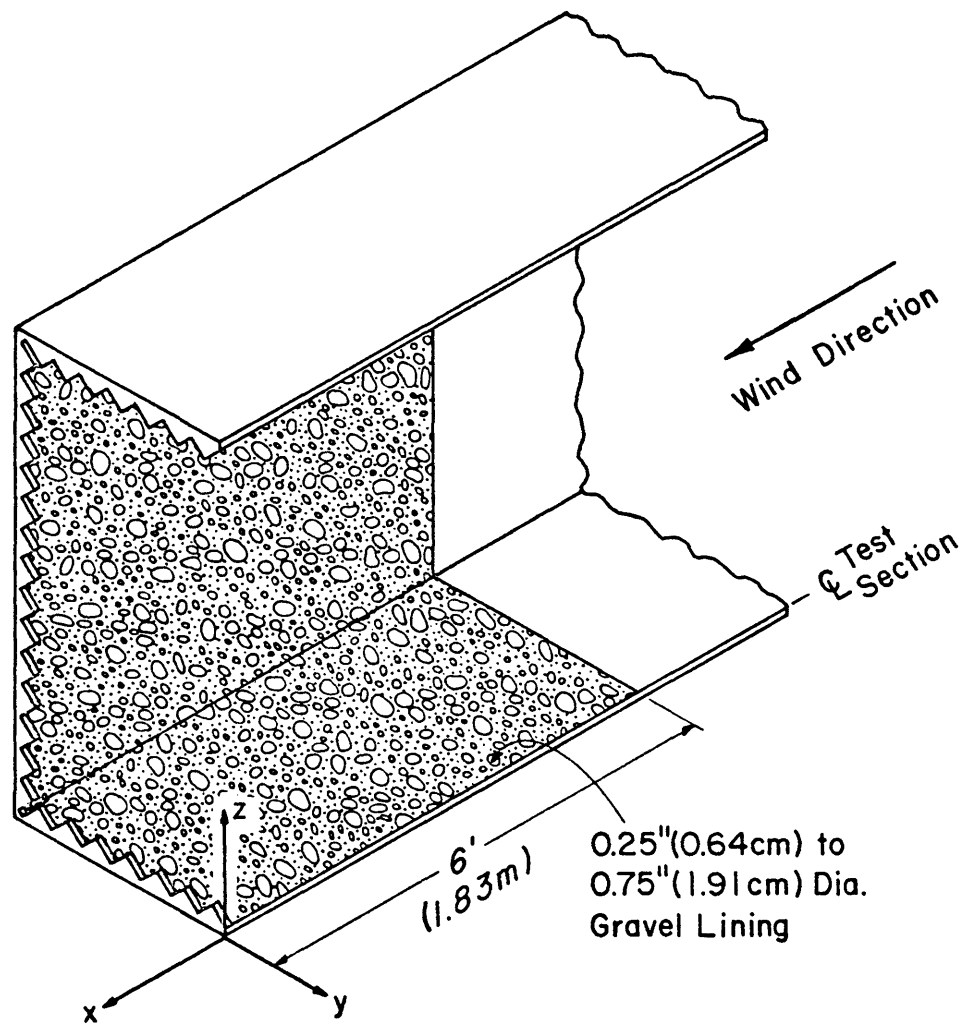
Sawtooth Detail

Figure 2-2. Three-dimensional drawing of sawtooth-roughness boundary layer trip at entrance to MWT test-section.

Figure 2-3. Close-up photograph of MWT entrance configuration.

Figure 2-4. Appearance of MWT test-section viewed from entrance.
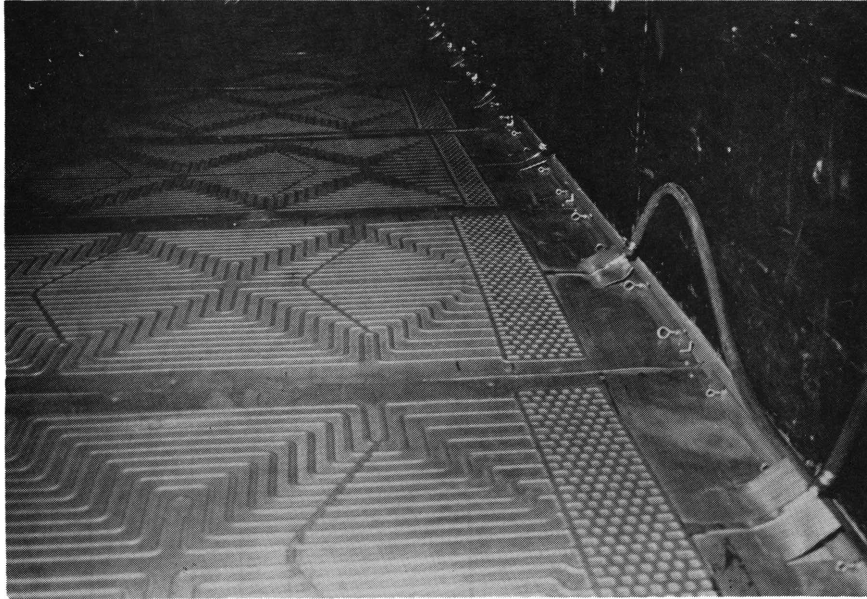
Figure 2-5. Auxiliary cooling plates which covered upwind one-third of MWT test-section.
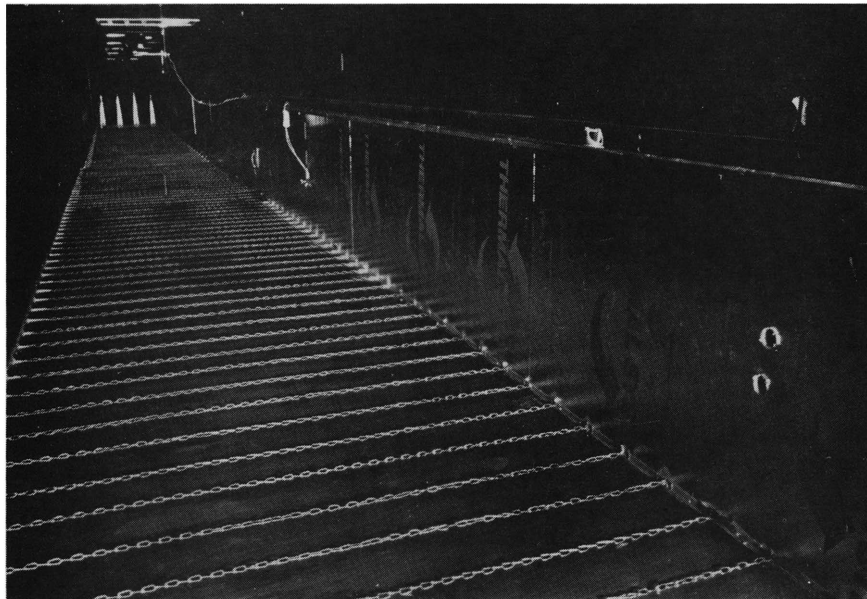
Figure 2-6. Upwind view of MWT test-section with roughness in place.
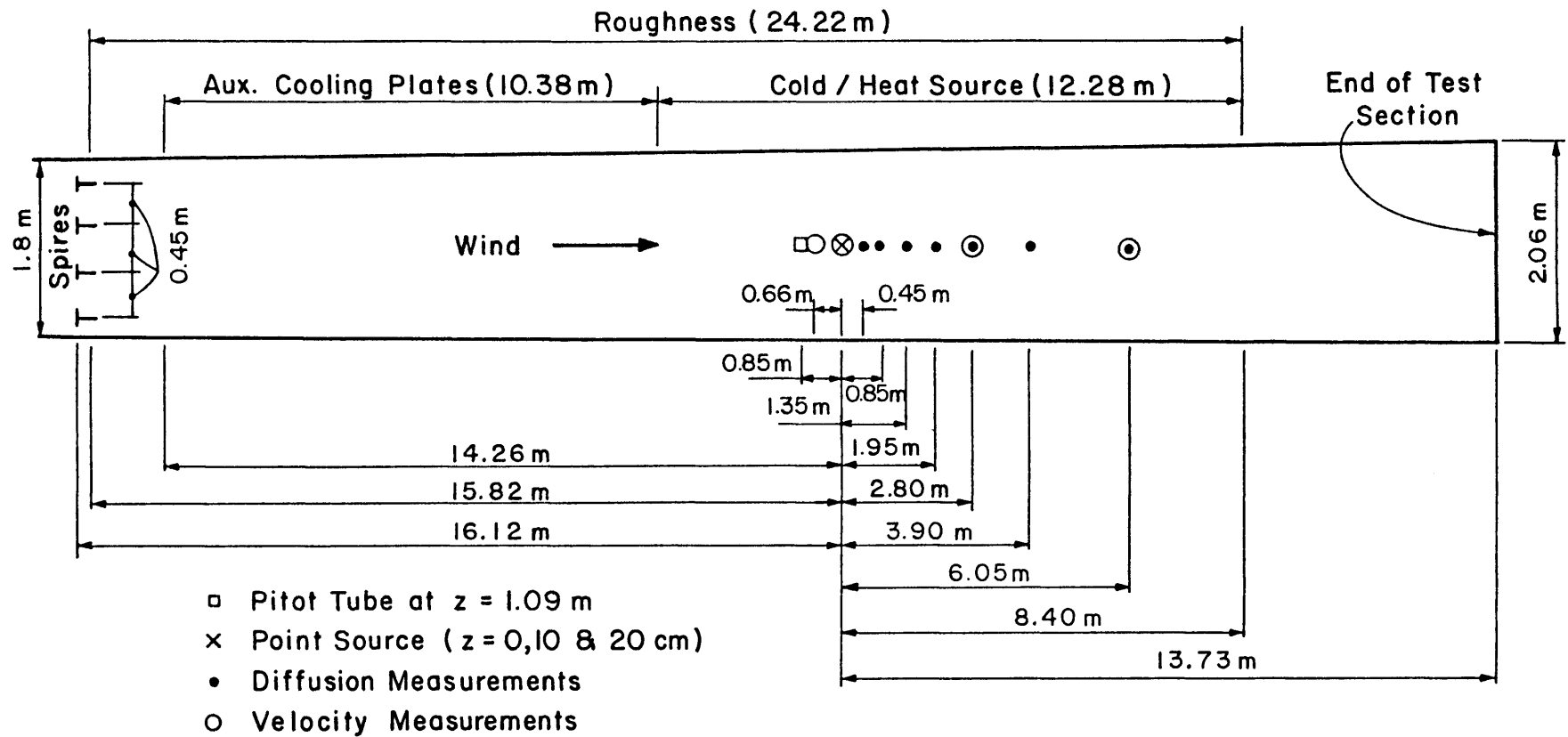
Figure 2-7. Schematic of MWT configuration and measurement locations.
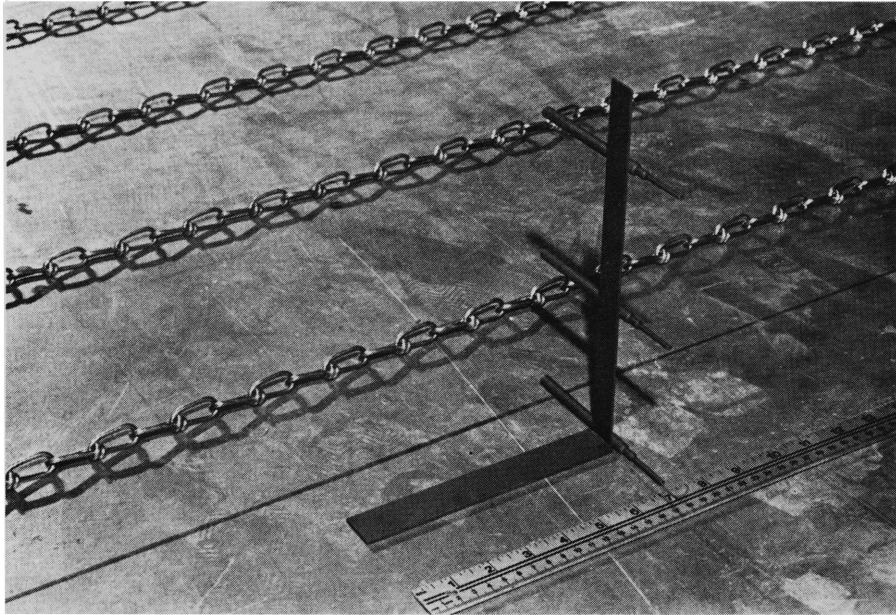
Figure 2-8. Point sources located 16.12 m downwind at ground-level, 10 cm, and 20 cm heights.
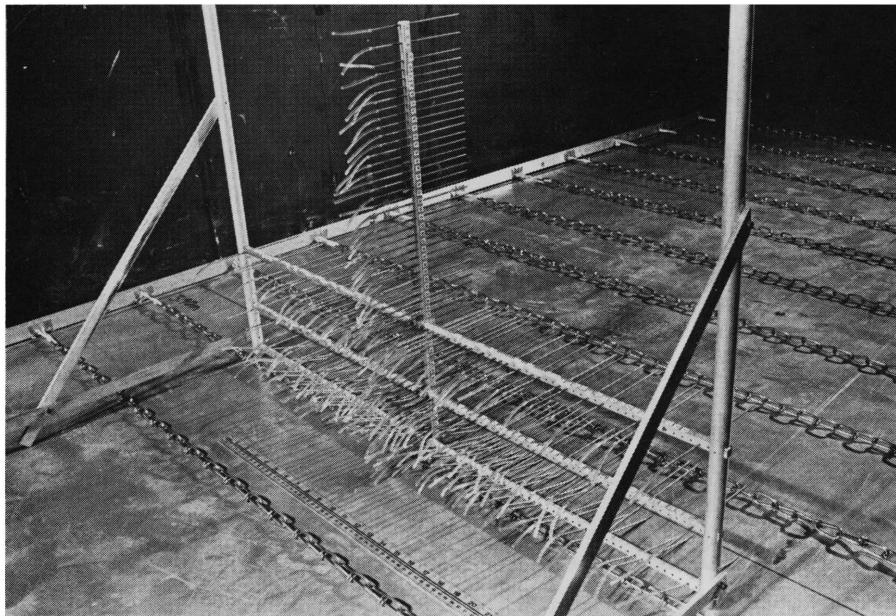
Figure 2-9. Sampling rake used to measure diffusion patterns.
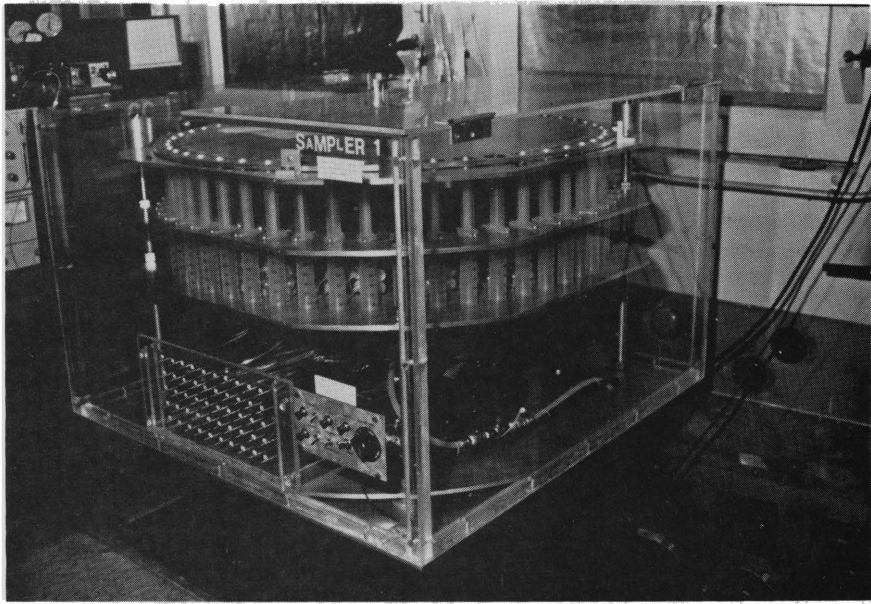
(a)
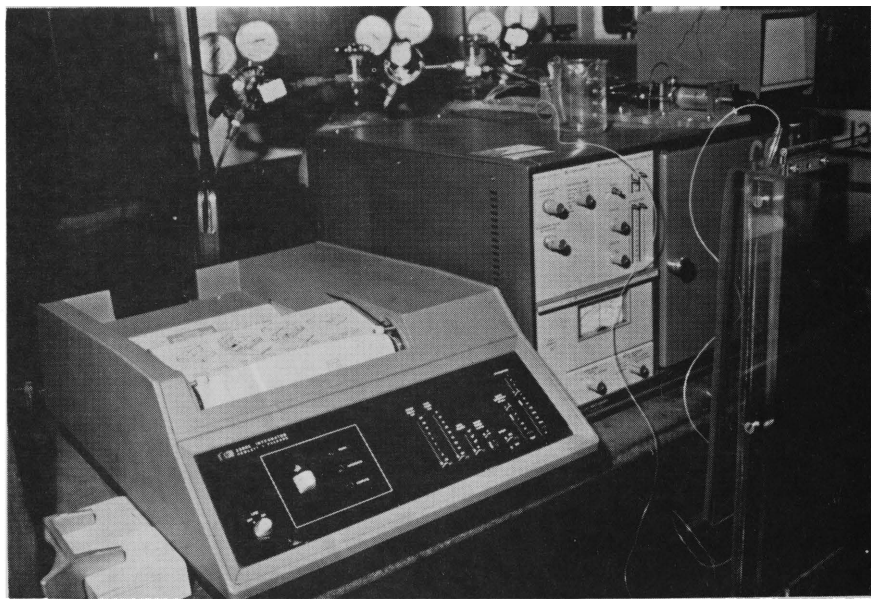
(b)

Figure 2-10.   Photographs of (a) the Tracer Sampling System and (b)
the HP Integrator and Gas Chromatograph

STABLE   NEUTRAL   UNSTABLE

Figure 2-11.   Flow visualization from a ground-level source over a smooth surface
              for three simulated atmospheric conditions.
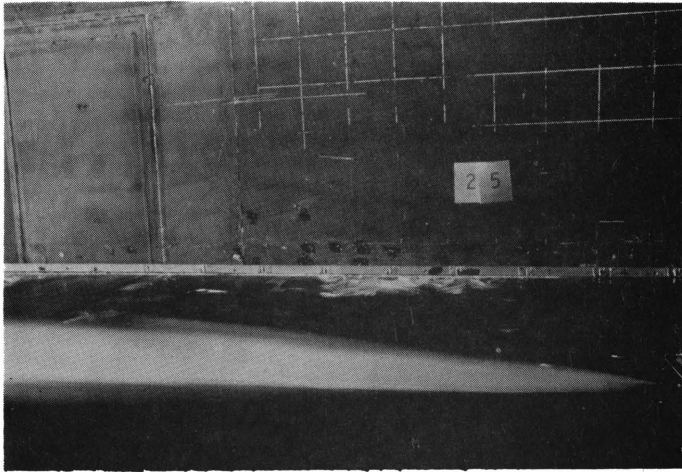
STABLE

NEUTRAL
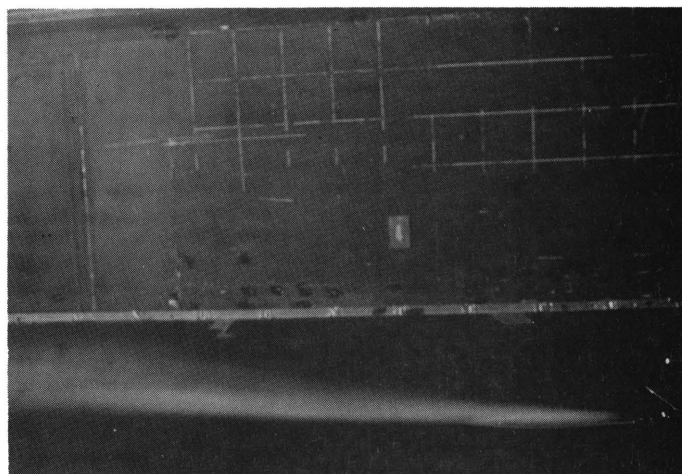
UNSTABLE

Figure 2-12. Flow visualization from a ground-level source over
a smooth surface for three simulated atmospheric
conditions.

3.0 NEUTRAL FLOW

3.1 Velocity Field Over the Smooth Floor

Mean velocity distributions u(z) were measured at distances of
x = 0.0, 2.80 and 6.05 m with respect to the source. These velocity
profiles are presented in Figure 3-1 and indicate good horizontal homo-
geneity. However, since the flow transitions from a slightly rough to
smooth surface, in accordance with Antonia and Luxton's (1972) findings,
the shear stress in the central region of the boundary layer increases
while the surface shear stress is reduced. With increasing distance
from the transition of the surface roughness, the surface shear stress
gradually increases. These effects can be seen in Figure 3-2 which
presents the shear stress measurements at distances of x = 0.0, 2.80 and
6.05 m from the source.

The average value of the shear velocity for this flow in the region
of interest is estimated from Figure 3-2 to be $u^* = 0.09$ m/sec. The
measured longitudinal turbulence intensity (u_{rms}/U) and vertical turbu-
lence intensity (w_{rms}/U) distributions are presented in Figures 3-3 and
3-4 for measurements made at distances of x = 0.0, 2.80 and 6.05 m from
the source.

From the velocity and turbulence data for neutral flow over the
smooth floor it may be concluded that the boundary layer developed in
the wind tunnel was not a perfect model of an ideal neutral boundary
layer. However, its major characteristics are typical of many real
neutral atmospheric boundary layers.

3.2 Velocity Field Over the Rough Floor

The mean velocity distributions u(z) measured at distances
of x = 0.0, 2.80 and 6.05 m with respect to the source are presented in

Figure 3-5. These velocity profiles also indicate good horizontal homogeneity. The transition in surface roughness in this case is comparatively smaller than that for the case of flow over the smooth surface. Hence distributions of the shear stress at distances of x = 0.0, 2.80 and 6.05 m from the source, presented in Figure 3-6 exhibit the familiar monotonically decreasing behavior throughout the central region of the boundary layer.

The average shear velocity for this flow in the region of interest is estimated from Figure 3-6 to be $u^* = 0.135$ m/sec. The longitudinal turbulence intensity and vertical turbulence intensity distributions are presented in Figures 3-7 and 3-8 for measurements made at distances of x = 0.0, 2.80 and 6.05 m from the source.

Table 3-1 compares some properties of the simulated wind flow in the wind tunnel with Robins' (1978) data, and with typical values of these properties found in the atmospheric boundary layer. In the table, z_o denotes the roughness length, u^* the friction velocity, U_{ref} the reference velocity, u, v and w the turbulence components in the longitudinal, lateral and vertical directions, and n the exponent of the velocity profile:

$$\frac{u^*}{U_{ref}} = (\frac{z}{z_{ref}})^n \quad . \tag{3-1}$$

The table shows that the present data closely matches Robins' with regard to simulation of atmospheric flows in the wind tunnel.

3.3 Measured Concentration Field

For the two surface-roughness conditions in the region of interest concentration profiles were measured for a continuous point source located firstly at ground level and then at a height of 10 cm above

the surface. The measurements were made at downstream distances of x = 0.85, 1.95, 2.80, 3.90 and 6.05 m from the source. The data corresponding to the ground-level source were fitted to the empirical semi-equation

$$\frac{C}{C_{max}(x)} = \exp[(-\ell n2)(\frac{y-dy}{\lambda y})^2]\exp[(-\ell n2)(\frac{z}{\lambda z})^s] \; , \qquad (3-2)$$

where the knowns are C: normalized observed concentration, m^{-2}

y,z: measuring location, cm

and the unknowns are

$C_{max}(x)$: maximum normalized plume concentration, m^{-2}

dy: horizontal drift of maximum concentration, cm

λy: horizontal plume spread constant, cm

λz: vertical plume spread constant, cm

s: vertical plume spread exponent.

Estimates of the five unknowns in the above equation for the five downstream measurement stations are presented in Table 3-2.

Data collected in the horizontal and vertical planes corresponding to the source located at a height of 10 cm above the surface were fitted to the semi-empirical equations

$$\frac{C}{C_{max}(x)} = \exp[(-\ell n2)(\frac{y-dy}{\lambda y})^2] \qquad (3-3)$$

and

$$\frac{C}{C_{max}(x)} = \exp[(-\ell n2)(\frac{z-H}{\lambda z})^2]+\exp[(-\ell n2)(\frac{z+H}{\lambda z})^2] \; , \qquad (3-4)$$

where H is the known source height above the surface. Estimates of the four unknowns $C_{max}(x)$, dy, λy and λz in the above equations for the five downstream measurement stations are presented in Table 3-3.

21

Equations for diffusion in the horizontal plane from the ground level as well as the elevated sources were based on a Gaussian diffusion model. Figures 3-9 and 3-10 show typical horizontal concentration profiles, measured as well as predicted by these equations using the computed values of the unknowns, downstream from the ground-level and elevated sources respectively. These figure clearly demonstrate that the Gaussian model is suitable for horizontal diffusion.

Diffusion in the vertical plane is fairly well described by the Gaussian model for the case of the elevated source, as can be seen in Figure 3-11, but this model fails to accurately describe the diffusion in the vertical plane from a ground-level source. Hence for the ground-level source, diffusion in the vertical plane is described by a non-Gaussian, variable-exponent model. Figure 3-12 illustrates the suitability of an exponential model in the present investigation. Non-Gaussian distributions of tracer material were also observed in the diffusion experiments of the Prairie Grass Project (Barad and Haugen, 1959) and the Green Glow program (Barad and Fuquay, 1962).

Diffusion data in the vertical plane from the elevated source, for flow over both surface roughnesses considered, shows that near the source the maximum concentration occurs at the height of the source, then it rapidly approaches the ground with increasing distance from the source.

Figures 3-13, 3-14, 3-15 and 3-16 show the distributions of $\lambda_y(x)$, $\sigma_y(x)$, $\lambda_z(x)$, and $\sigma_z(x)$ for the two source heights and two surface roughnesses considered. The $\sigma_y(x)$ and $\sigma_z(x)$ are standard deviations of the horizontal and vertical plume spreads, respectively. The variation of the normalized peak concentrations, with distance downstream from the

22

source, are presented in Figures 3-17 and 3-18, and the variation of the normalized ground-level concentration, with distance downstream from the source, for the elevated source, is presented in Figure 3-19.

Figures 3-20 and 3-21 compare the present diffusion data for ground-level sources with Robins' data for urban and rural flows. These figures show good agreement between the two data sets. Figure 3-22 compares the vertical plume spread of the present data with Robins' and Pasquill's estimates. Once again, the three data sets show a good match.

Table 3-1.   Comparison of Simulated and Atmospheric Flows

Category	δ (m)	z_o (m at full scale)	n	u^*/U_{ref}	u_{rms}/u^*	v_{rms}/u^*	w_{rms}/u^*
Present data							
Smooth	0.95	0.01	0.15	0.037	2.1	1.1	1.0
Rough	0.90	0.16	0.25	0.055	2.5	0.8	0.8
Robins' data							
Rural	0.6	0.03	0.14	0.045	2.4	-	1.2
Urban	2.0	1.3	0.22	0.063	2.6	2.0	1.4
Atmosphere#							
Rural	600	0.01-0.07	1/7	0.037-0.045	2.5	1.9	1.3
Suburban	600	1.0-1.5	1/5	0.045-0.055	2.5	1.9	1.3
Urban	600	1.0-4.0	1/4	0.040-0.060	2.5	1.9	1.3

#Source: Counihan (1975)

Table 3-2. Unknowns for Ground-level Source in Neutral Flow

Variable	Distance Downstream from Source (m)					Roughness
	x = 0.85	x = 1.95	x = 2.80	x = 3.90	x = 6.05	
$C_{max}(x)$	124.02	36.42	19.22	11.85	5.93	Rough
(m^2)	328.88	73.04	37.34	20.22	9.92	Smooth
dy	1.70	2.58	2.43	3.93	4.52	Rough
(cm)	0.56	0.36	0.91	-1.06	2.83	Smooth
λ_y	14.08	21.93	26.60	29.83	36.59	Rough
(cm)	7.56	13.36	17.51	24.09	27.61	Smooth
λ_z	7.12	13.92	17.61	23.22	32.31	Rough
(cm)	3.32	7.52	10.96	13.60	21.66	Smooth
s	1.60	1.60	1.52	1.60	1.68	Rough
(-)	1.20	1.31	1.41	1.39	1.47	Smooth

Table 3-3. Unknowns for 10 cm Source in Neutral Flow

| Variable | Distance Downstream from Source (m) | | | | | Roughness |
	x = 0.85	x = 1.95	x = 2.80	x = 3.90	x = 6.05	
Horizontal Profile						
$C_{max}(x)$	58.01	22.21	15.08	9.70	5.19	Rough
(m^2)	76.96	19.81	13.17	10.34	6.35	Smooth
dy	0.43	1.15	2.09	2.15	4.45	Rough
(cm)	-0.35	-1.30	-0.79	-2.77	1.37	Smooth
λ_y	10.16	20.15	26.28	30.53	36.73	Rough
(cm)	8.68	15.92	18.77	25.33	28.51	Smooth
Vertical Profile						
$C_{max}(x)$	58.46	14.19	7.98	5.02	2.65	Rough
(m^2)	85.32	11.51	8.11	5.56	3.17	Smooth
λ_z	6.94	16.15	20.29	26.00	33.61	Rough
(cm)	5.54	20.10	21.07	21.64	28.89	Smooth

NEUTRAL   SMOOTH FLOOR
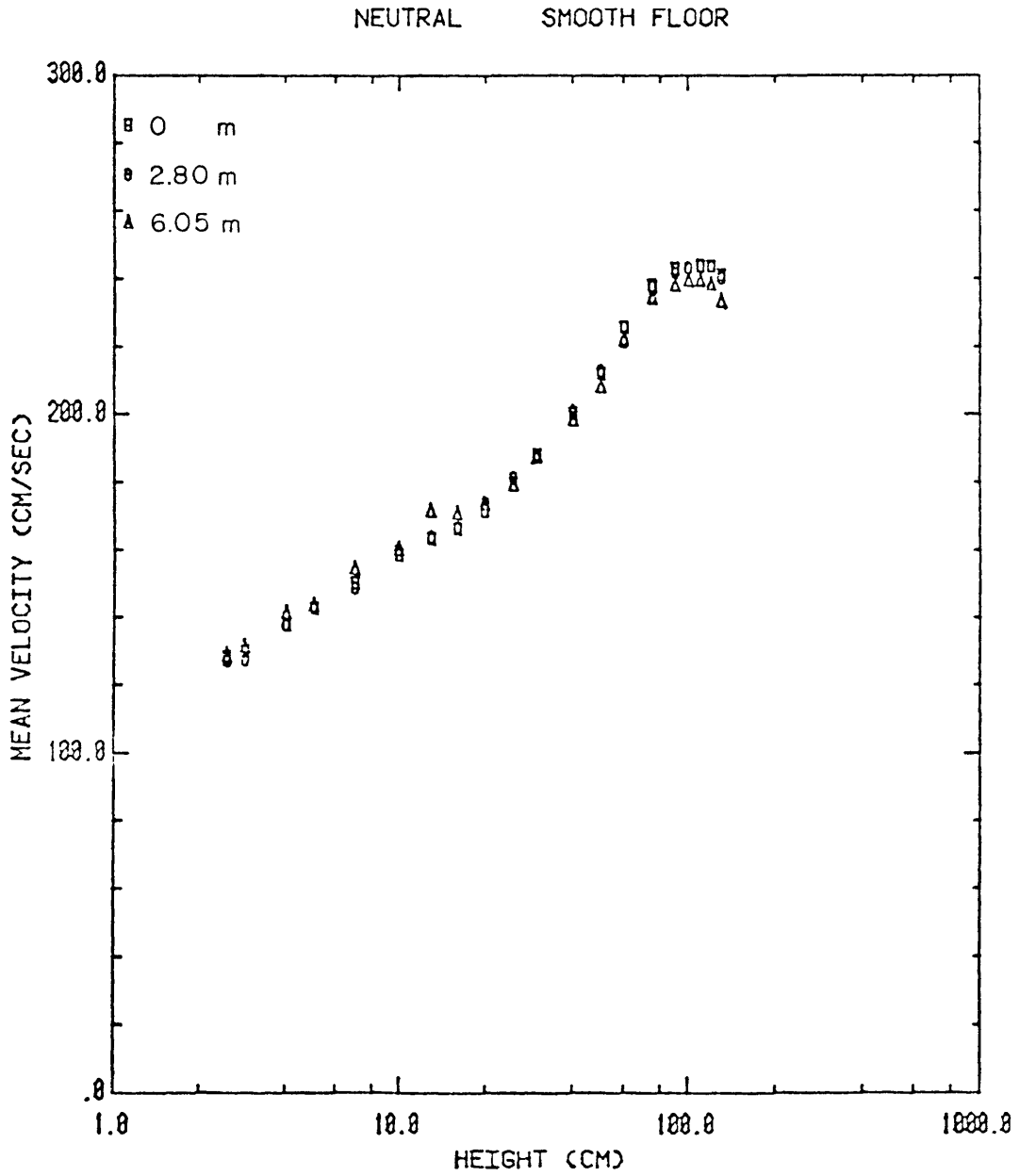
Figure 3-1. Mean velocity profiles, smooth floor.

27
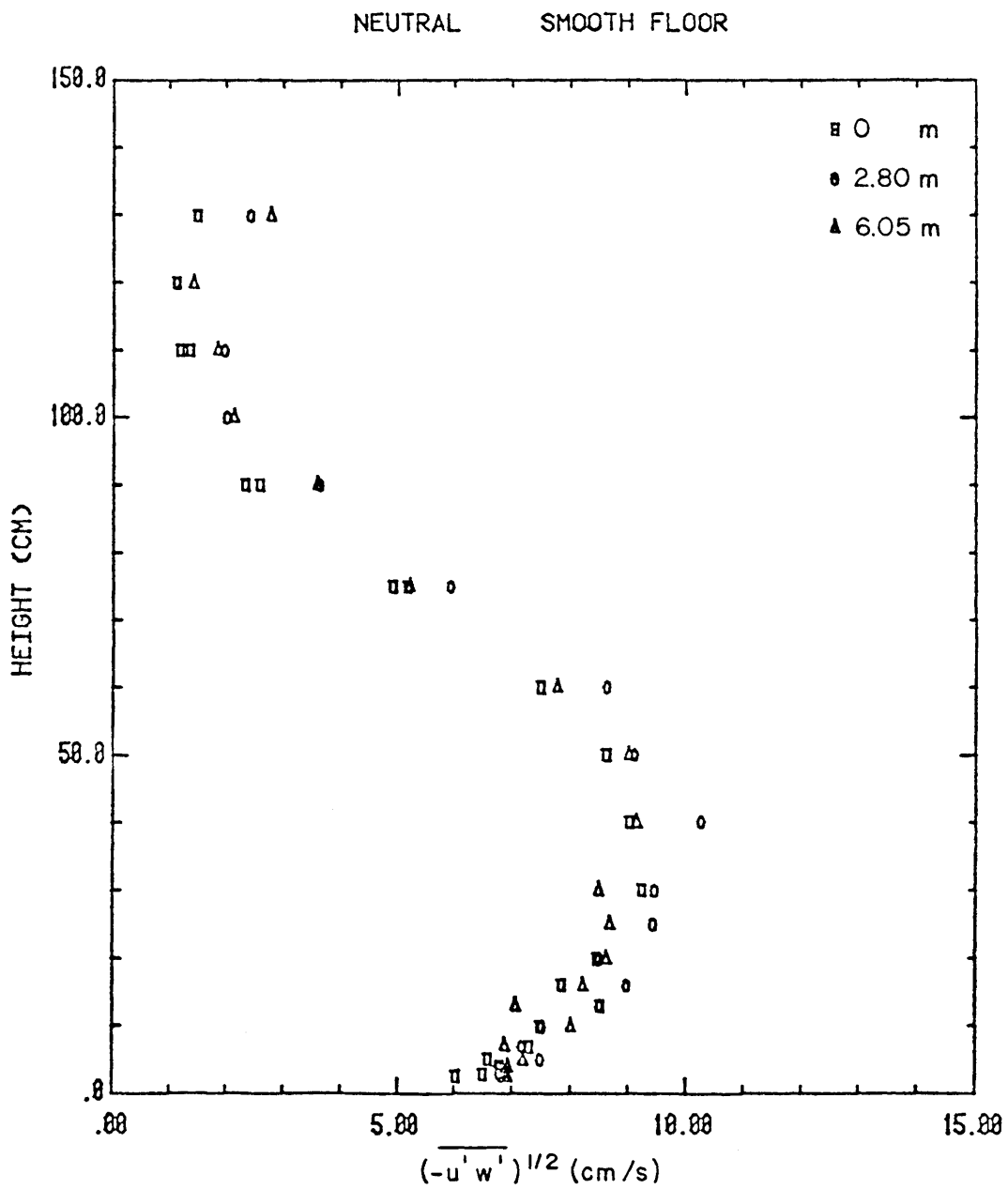
Figure 3-2. Vertical distribution of shear stress $(\overline{-u'w'})^{\frac{1}{2}}$, smooth floor.

NEUTRAL   SMOOTH
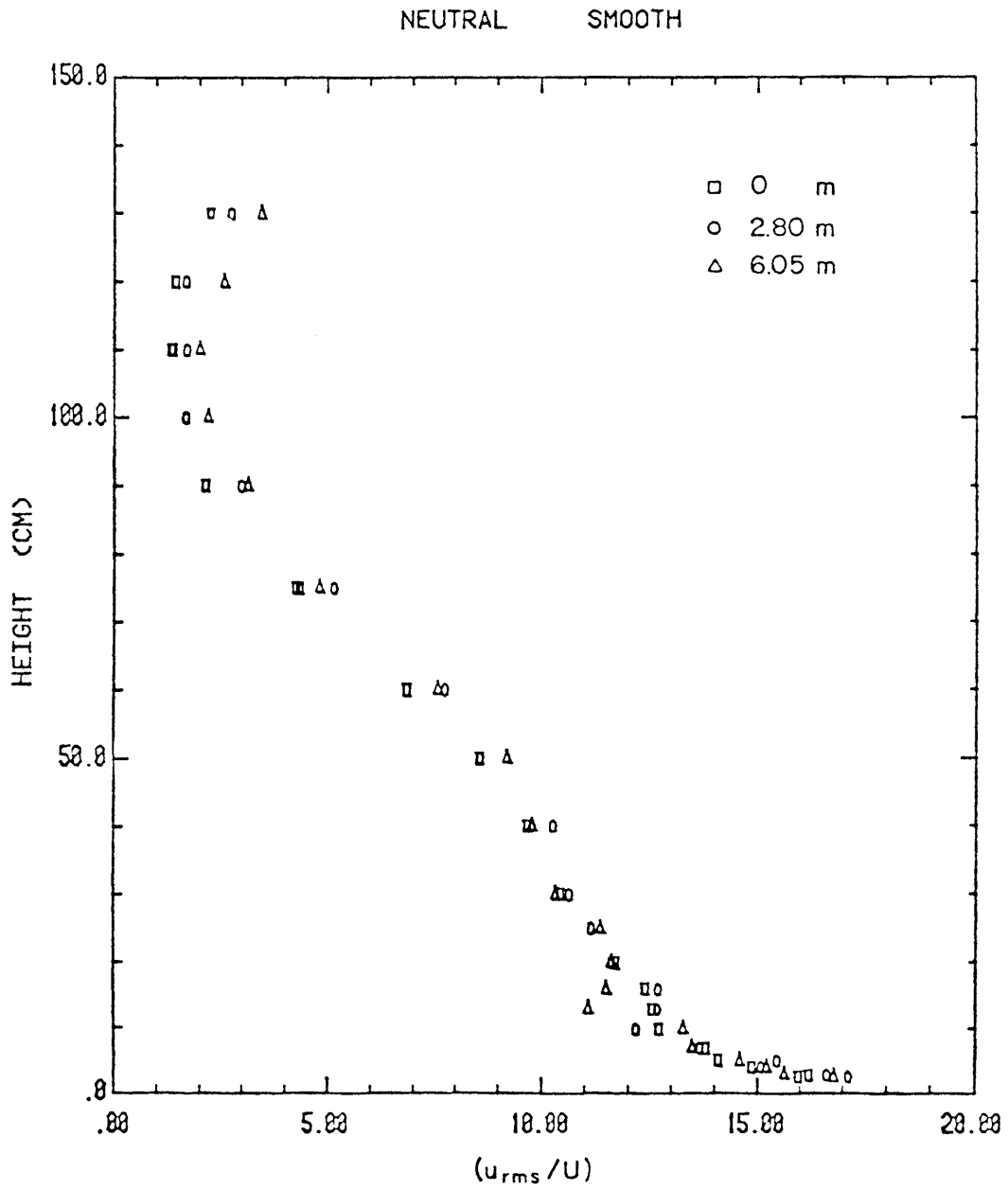
Figure 3-3. Longitudinal turbulence intensity (u_{rms}/U), smooth floor.

NEUTRAL   SMOOTH FLOOR
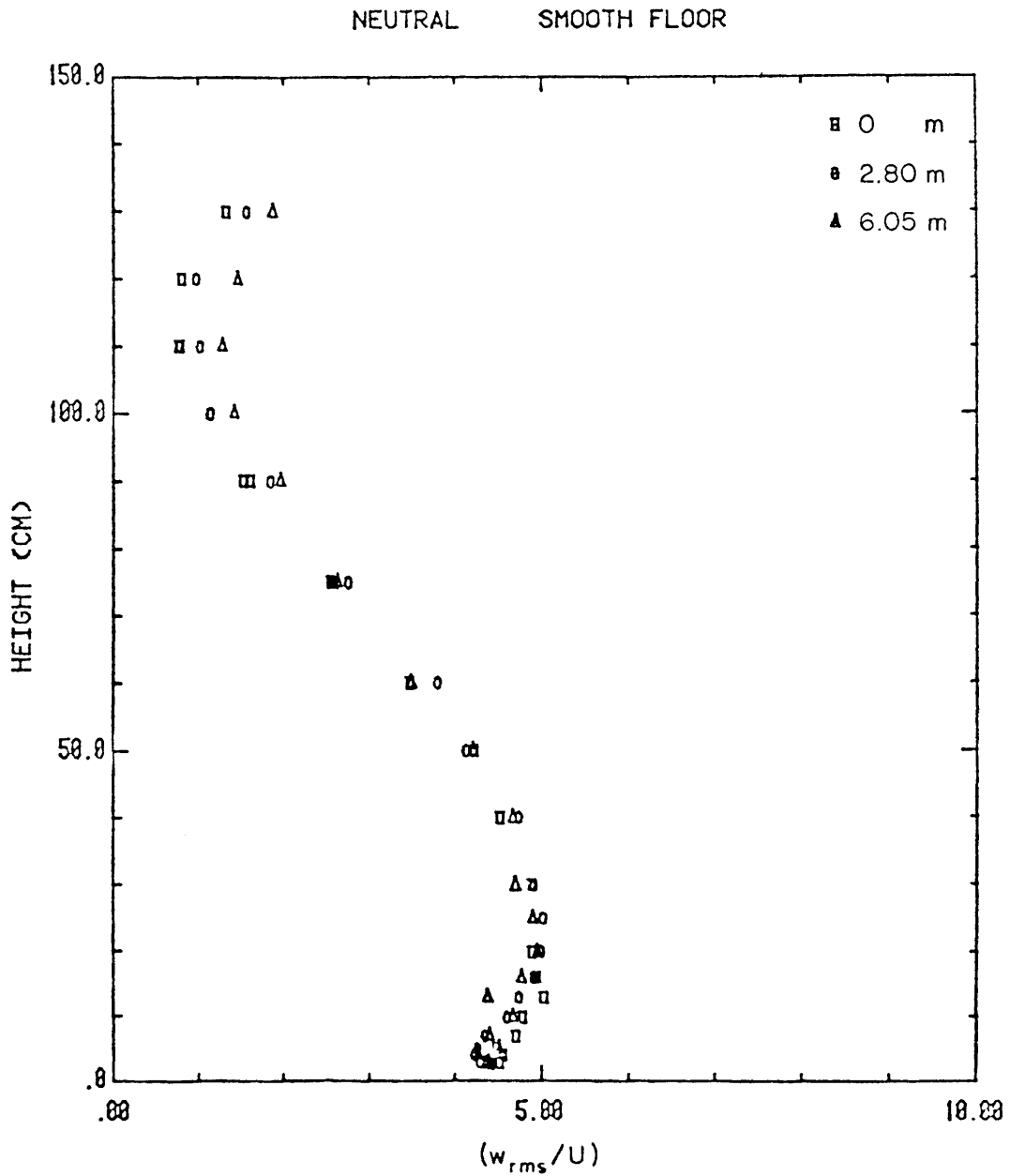
Figure 3-4.   Vertical turbulence intensity (w_{rms}/U), smooth floor.

NEUTRAL   ROUGH FLOOR
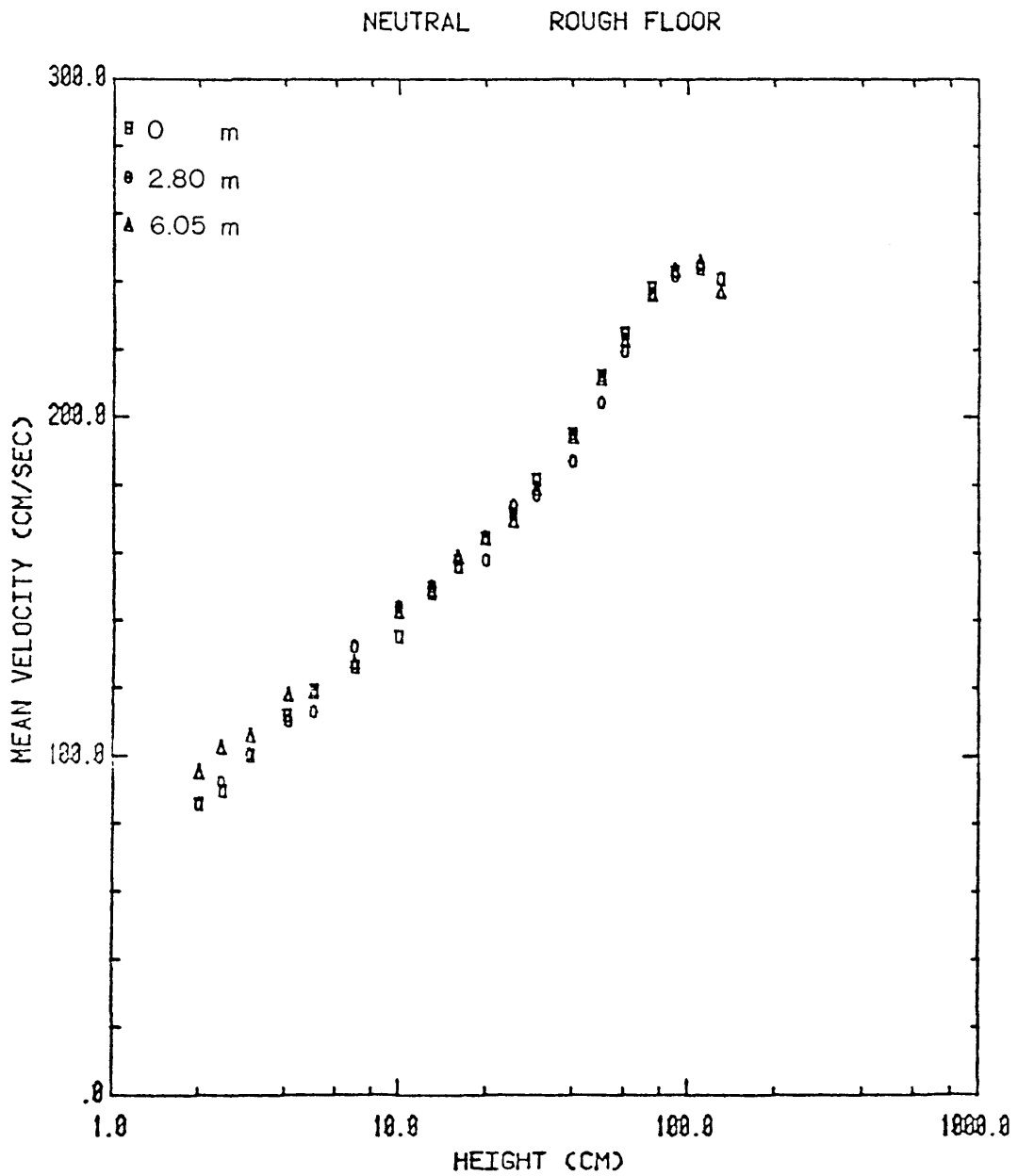
Figure 3-5. Mean velocity profiles, rough floor.

31

NEUTRAL   ROUGH FLOOR
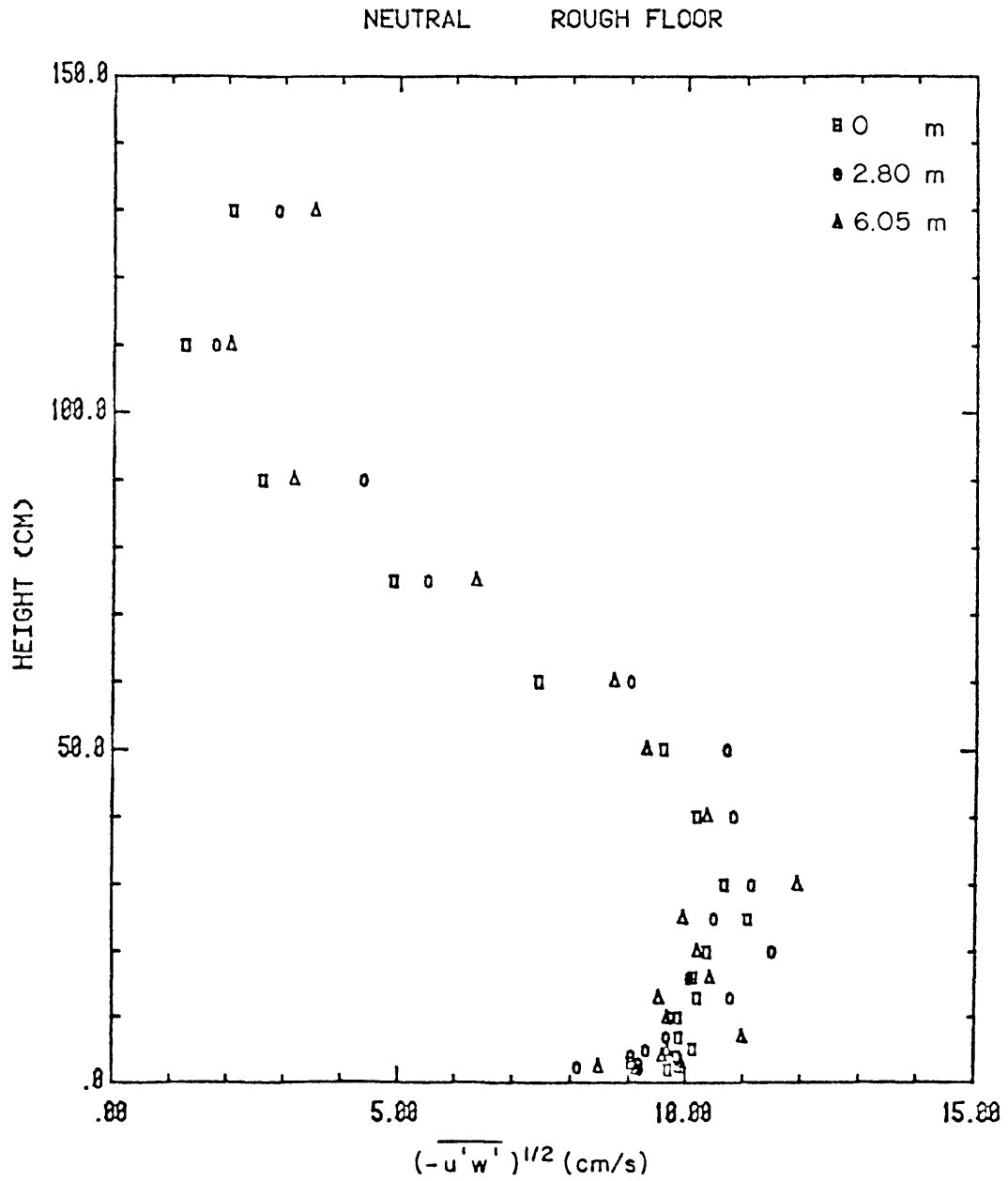
Figure 3-6. Vertical distribution of shear stress $(\overline{-u'w'})^{\frac{1}{2}}$, rough floor.
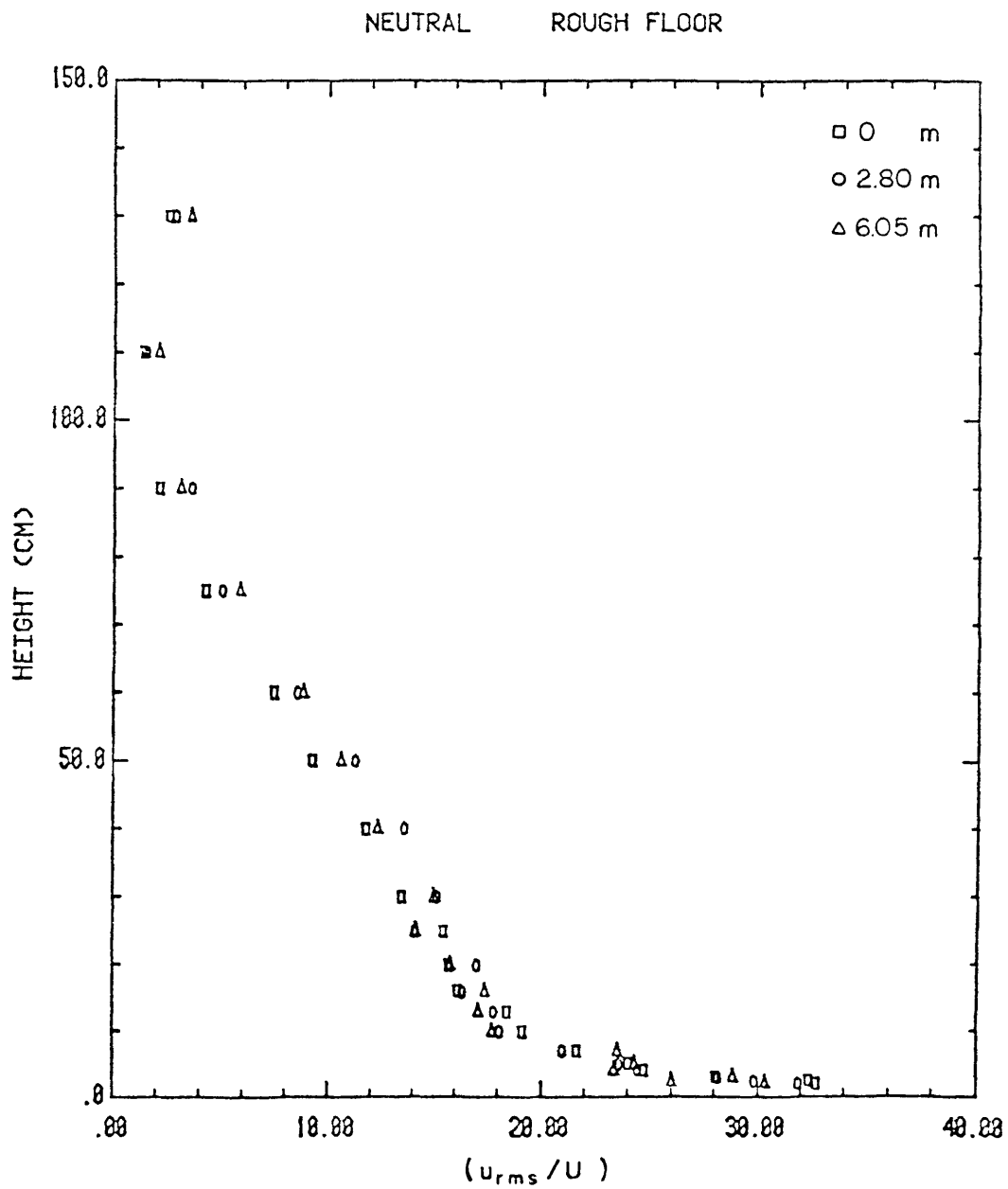
Figure 3-7. Longitudinal turbulence intensity (u_{rms}/U), rough floor.
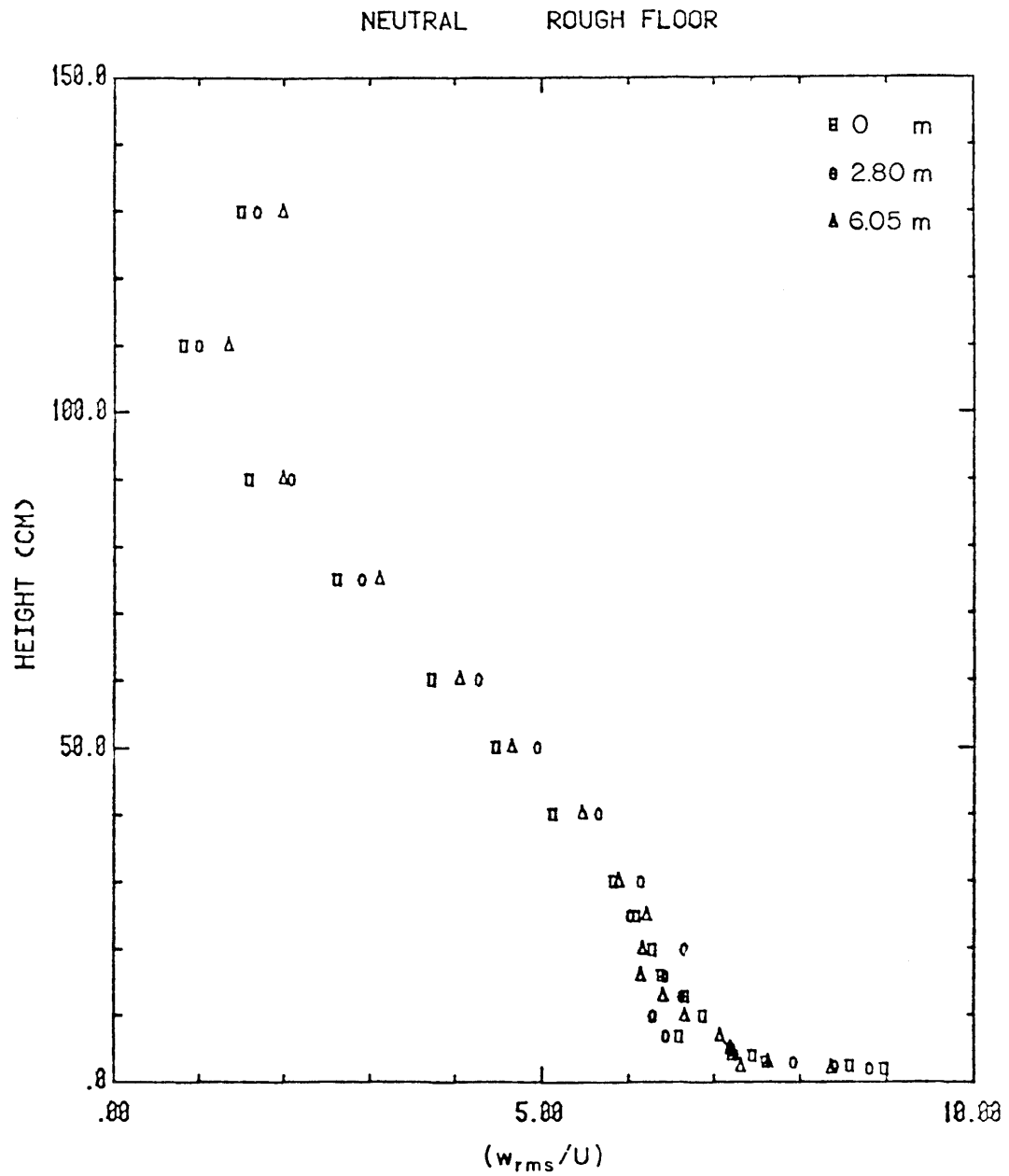
Figure 3-8. Vertical turbulence intensity (w_{rms}/U), rough floor.

34
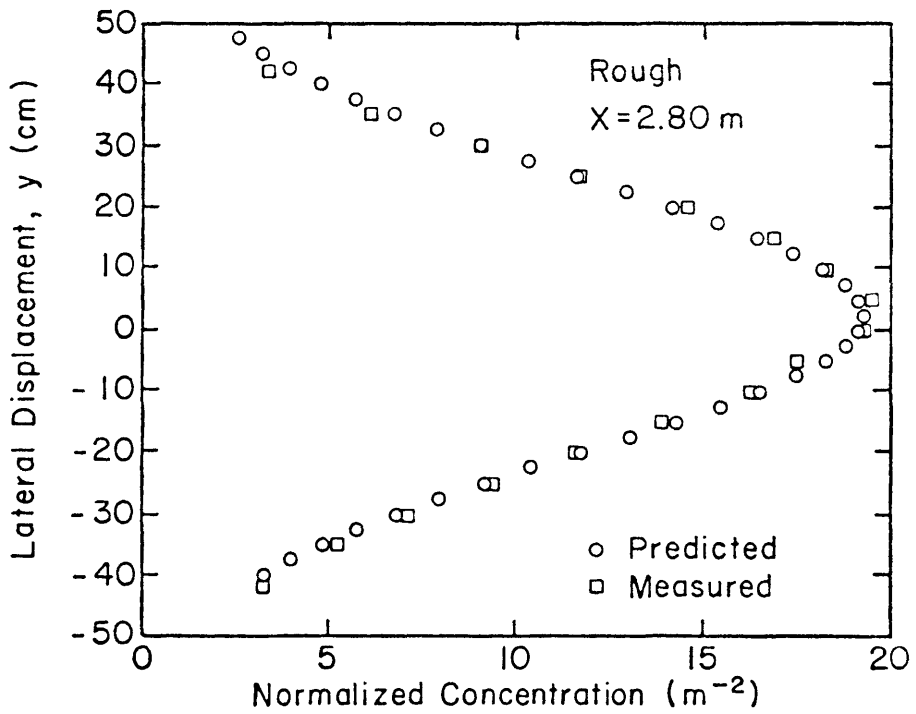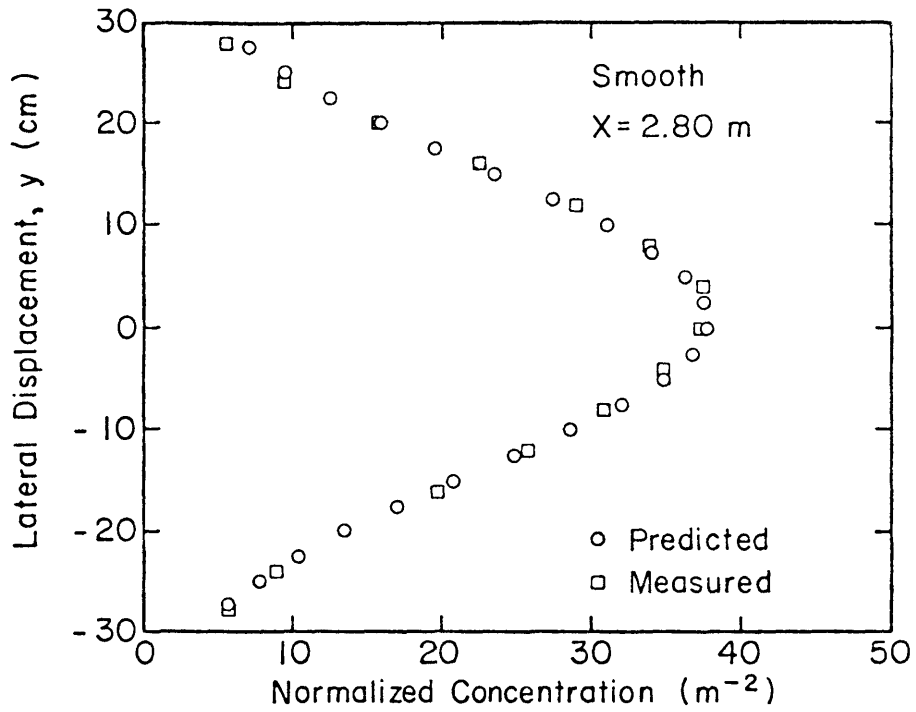
Figure 3-9. Horizontal concentration profiles for a ground-level source in neutral flow.
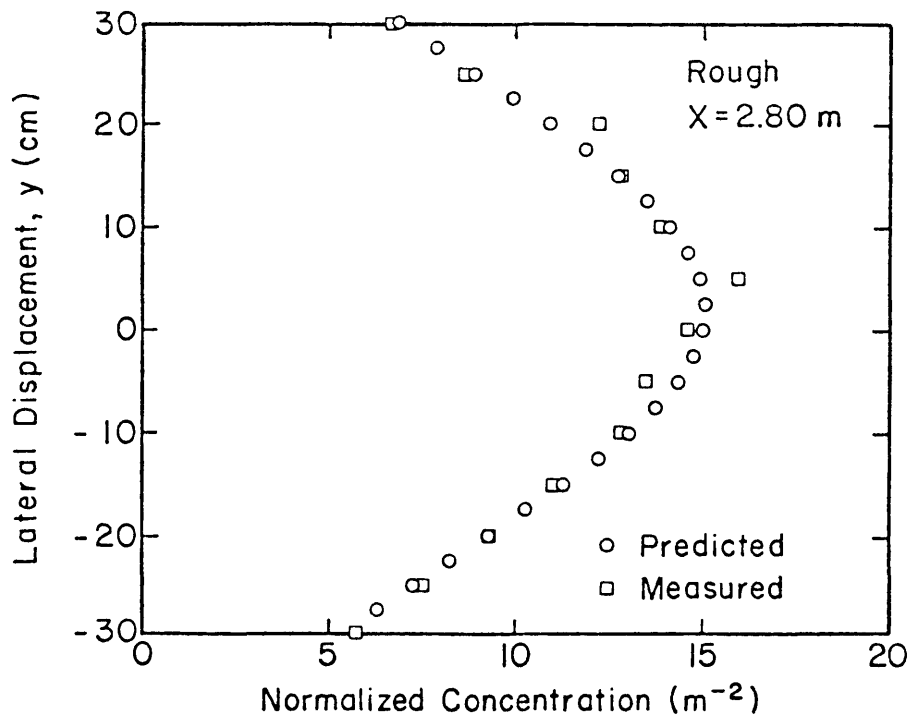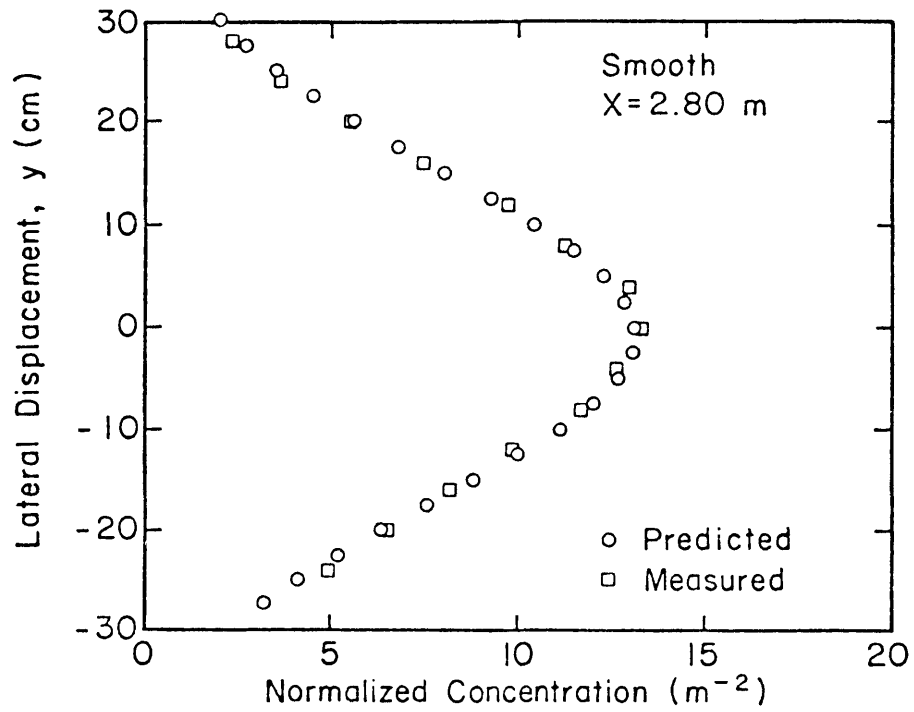
Figure 3-10.   Horizontal concentration profiles for a 10 cm source
in neutral flow.
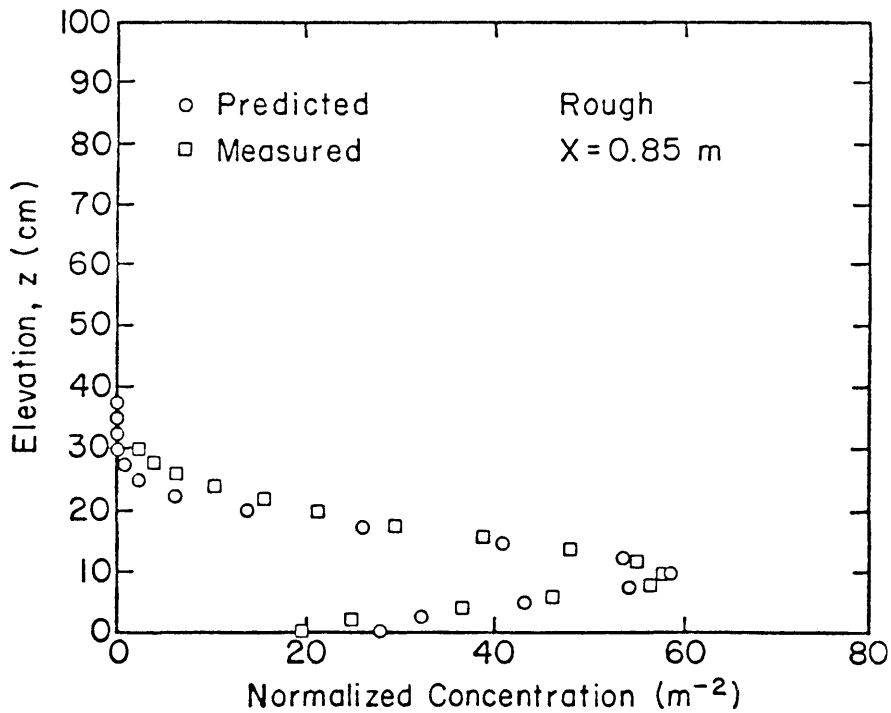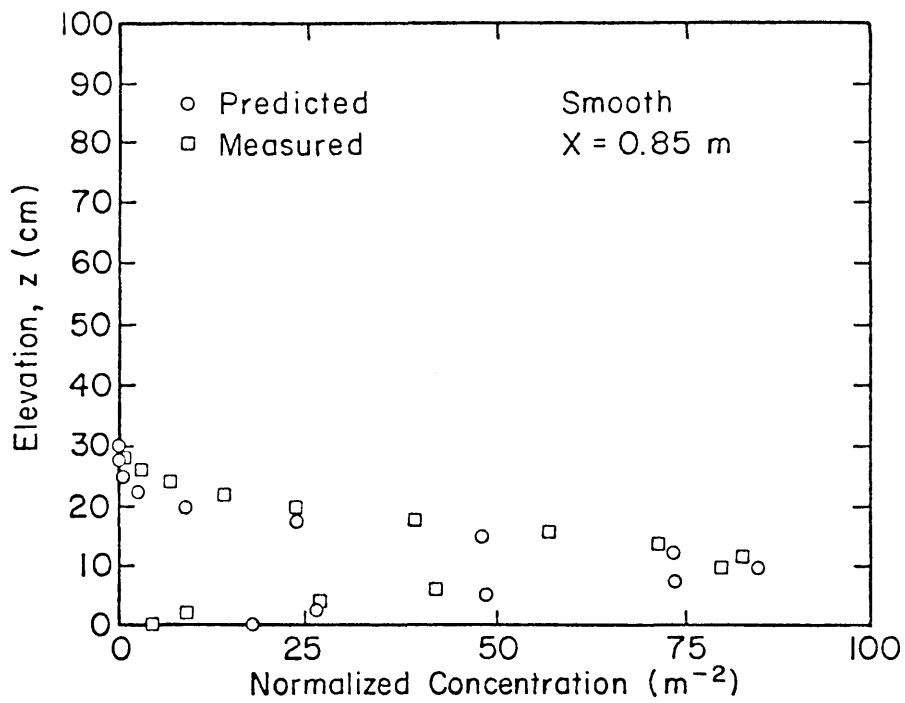
Figure 3-11.   Vertical concentration profiles for a 10 cm source in neutral flow.
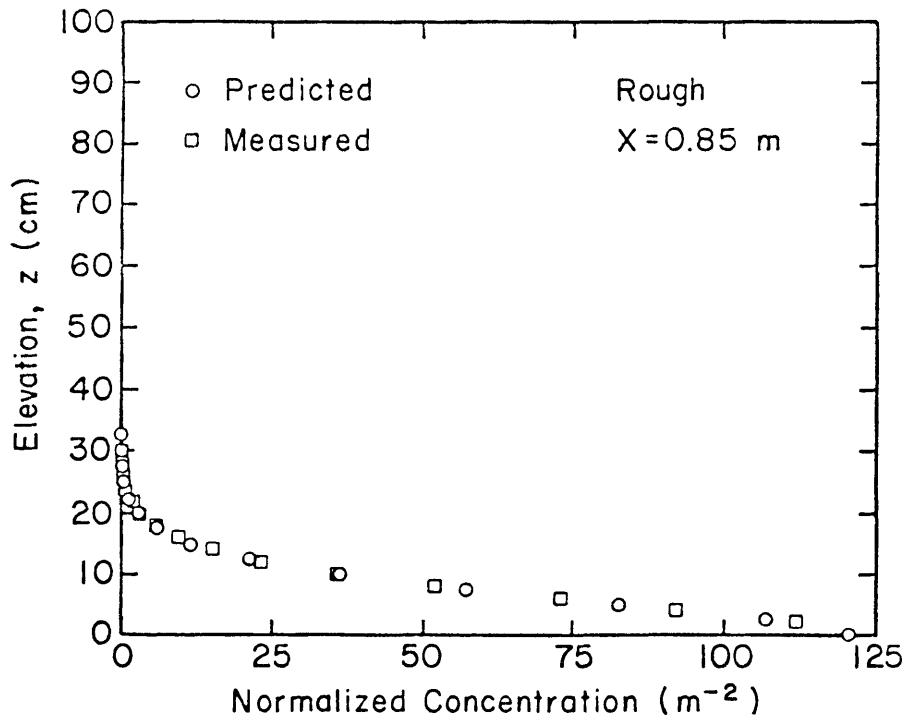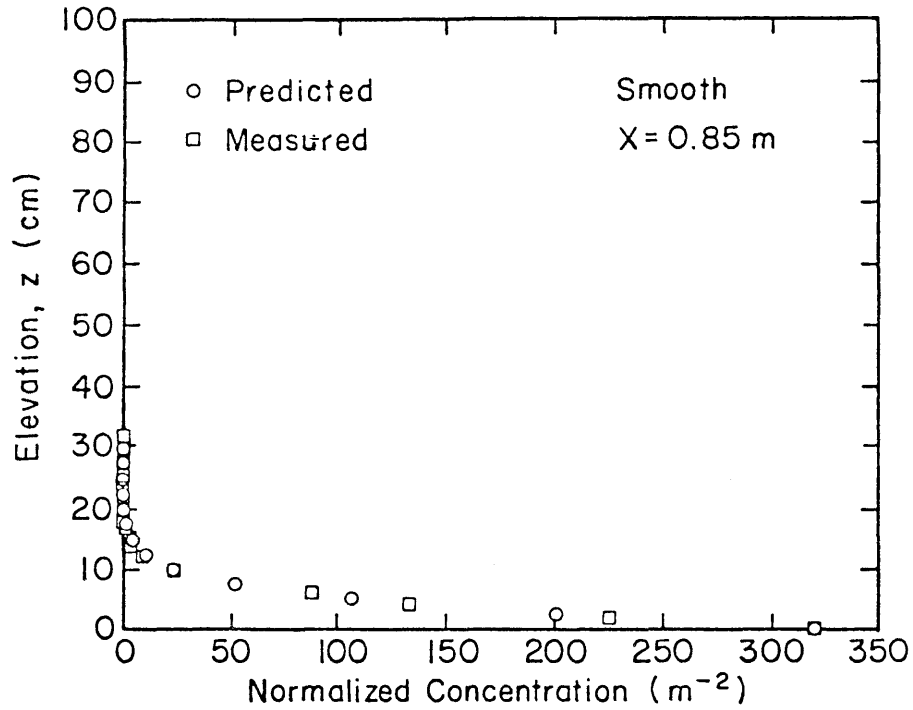
Figure 3-12.   Vertical concentration profiles for a ground-level source in neutral flow.
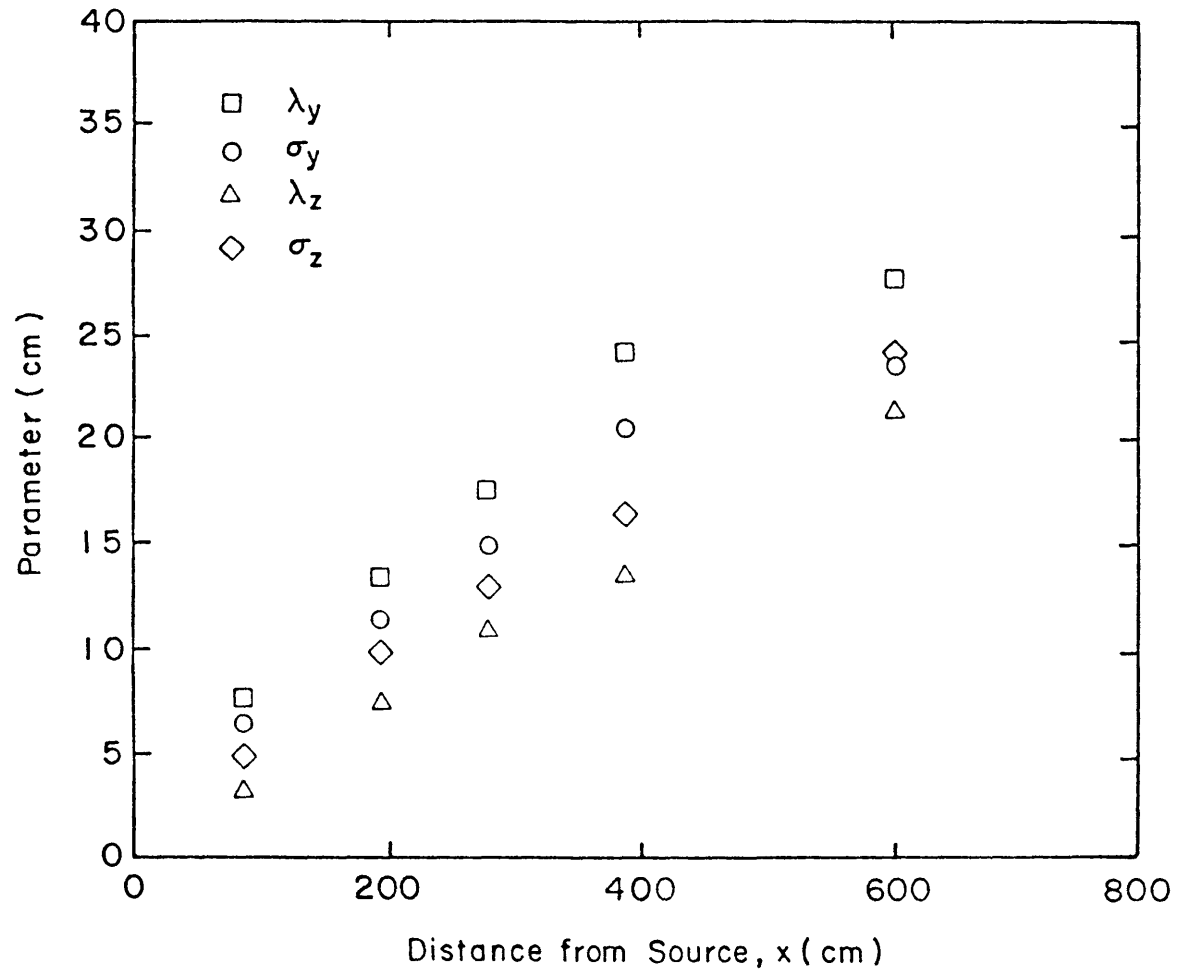
Figure 3-13. Plume spread parameters for ground-level source, smooth floor.
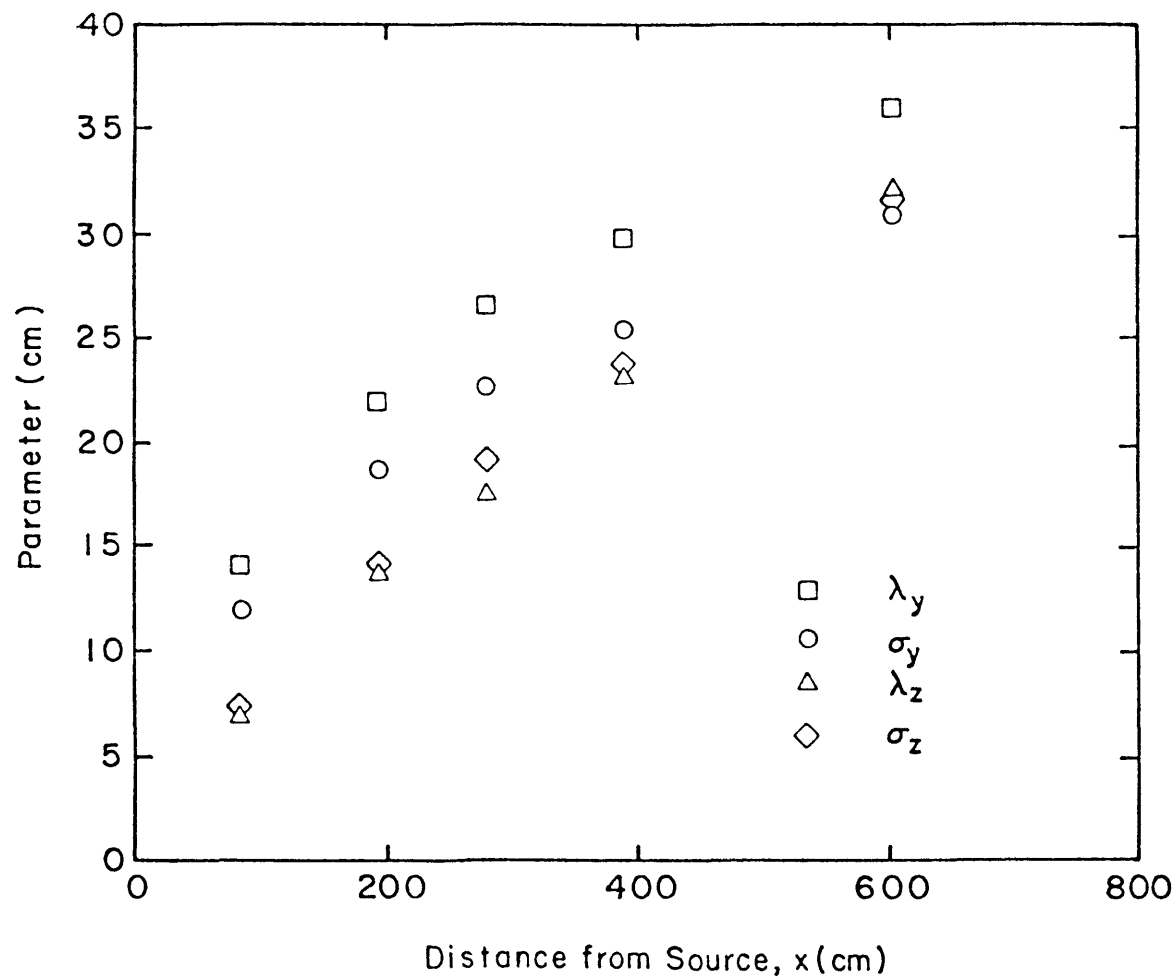
Figure 3-14. Plume spread parameters for ground-level source, rough floor.
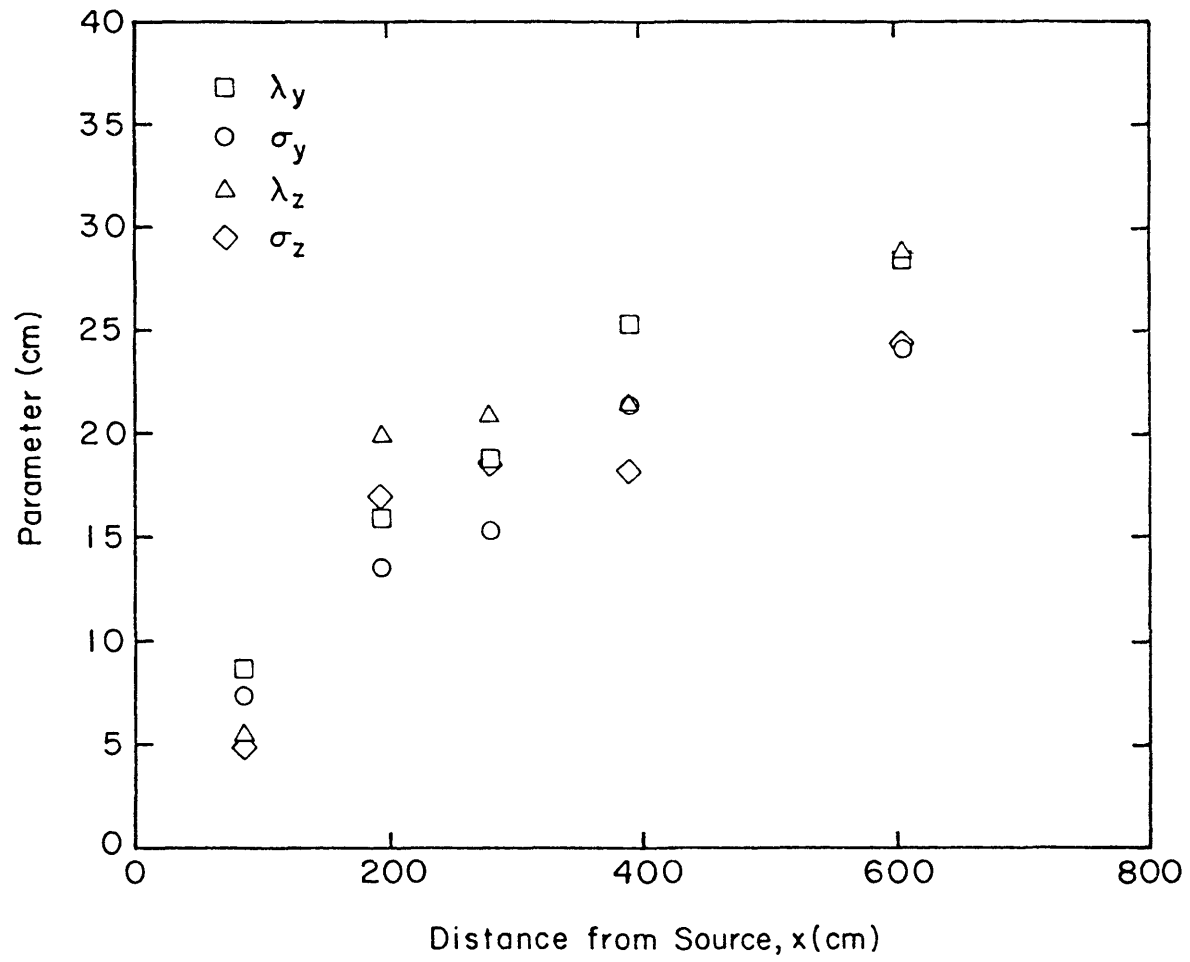
Figure 3-15. Plume spread parameters for 10 cm source, smooth floor.
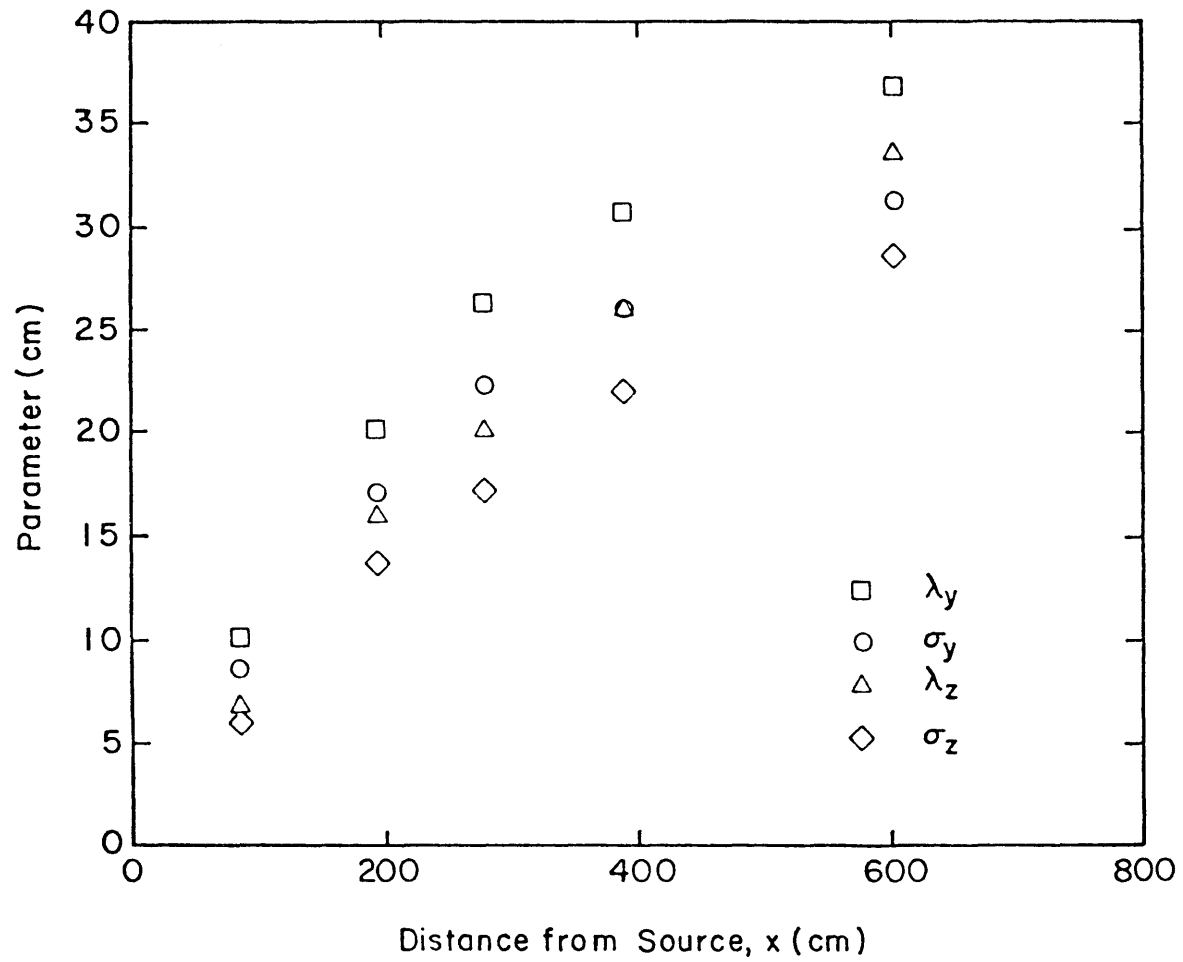
Figure 3-16. Plume spread parameters for 10 cm source, rough floor.
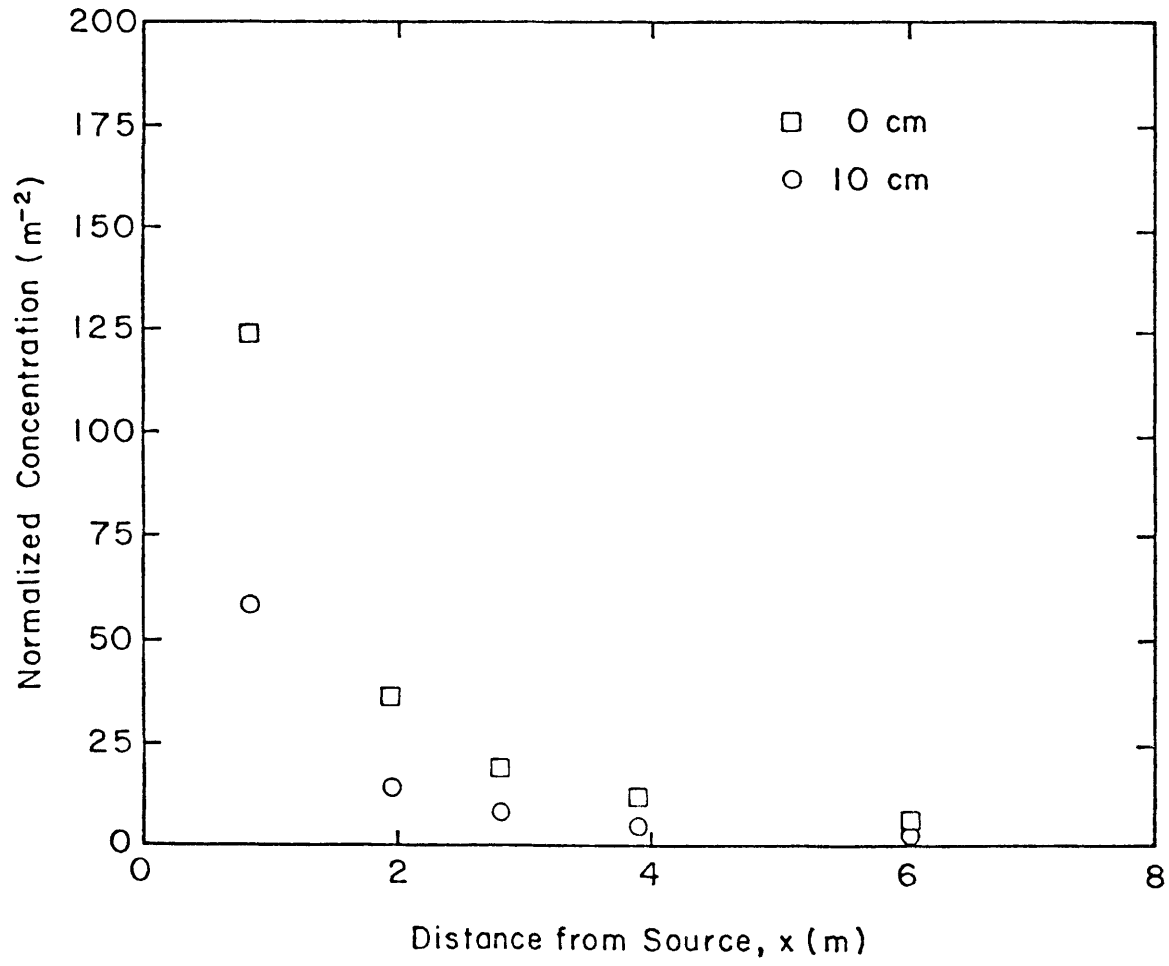
Figure 3-17. Normalized peak concentrations for two source heights, rough floor.
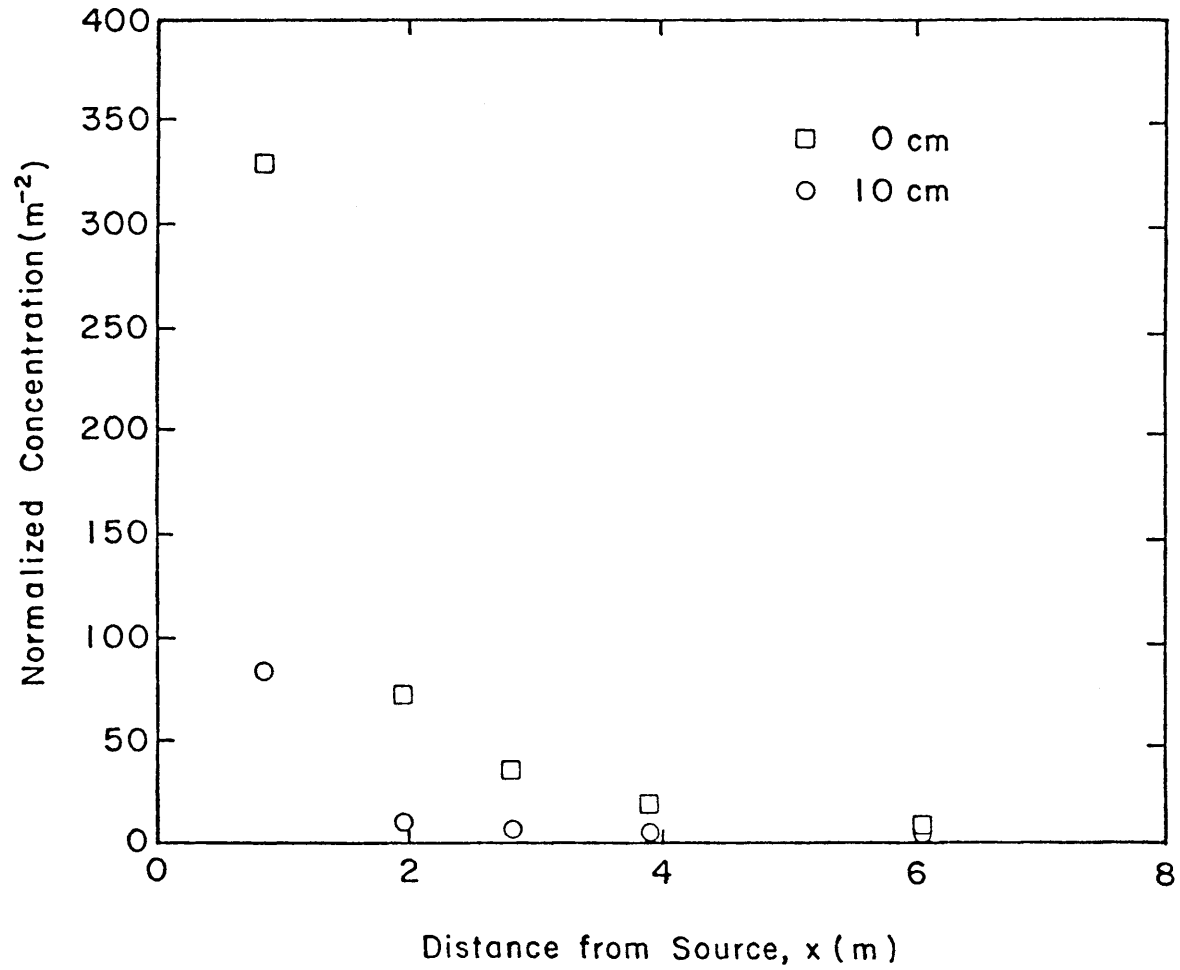
Figure 3-18. Normalized peak concentrations for two source heights, smooth floor.
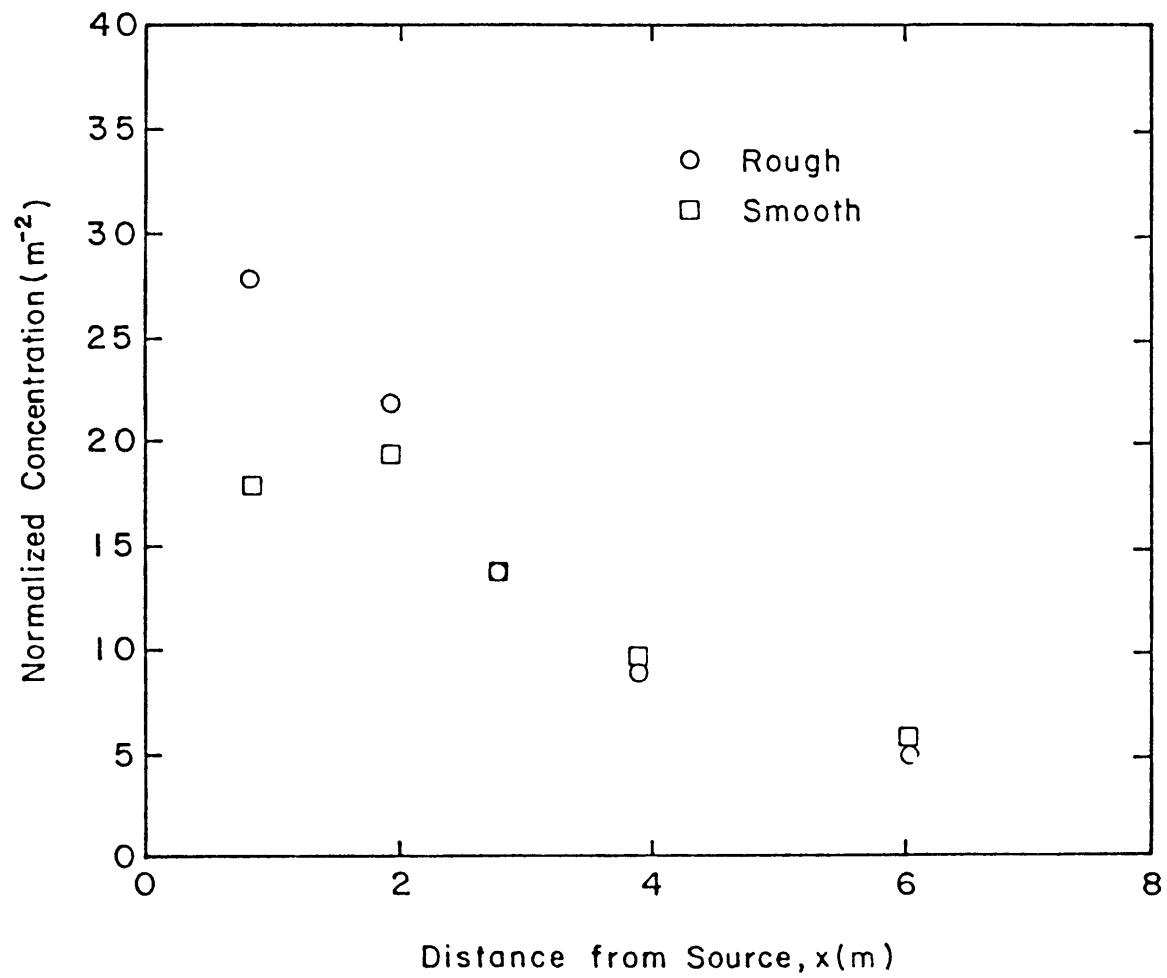
Figure 3-19. Normalized ground-level concentrations for two roughnesses, 10 cm source.
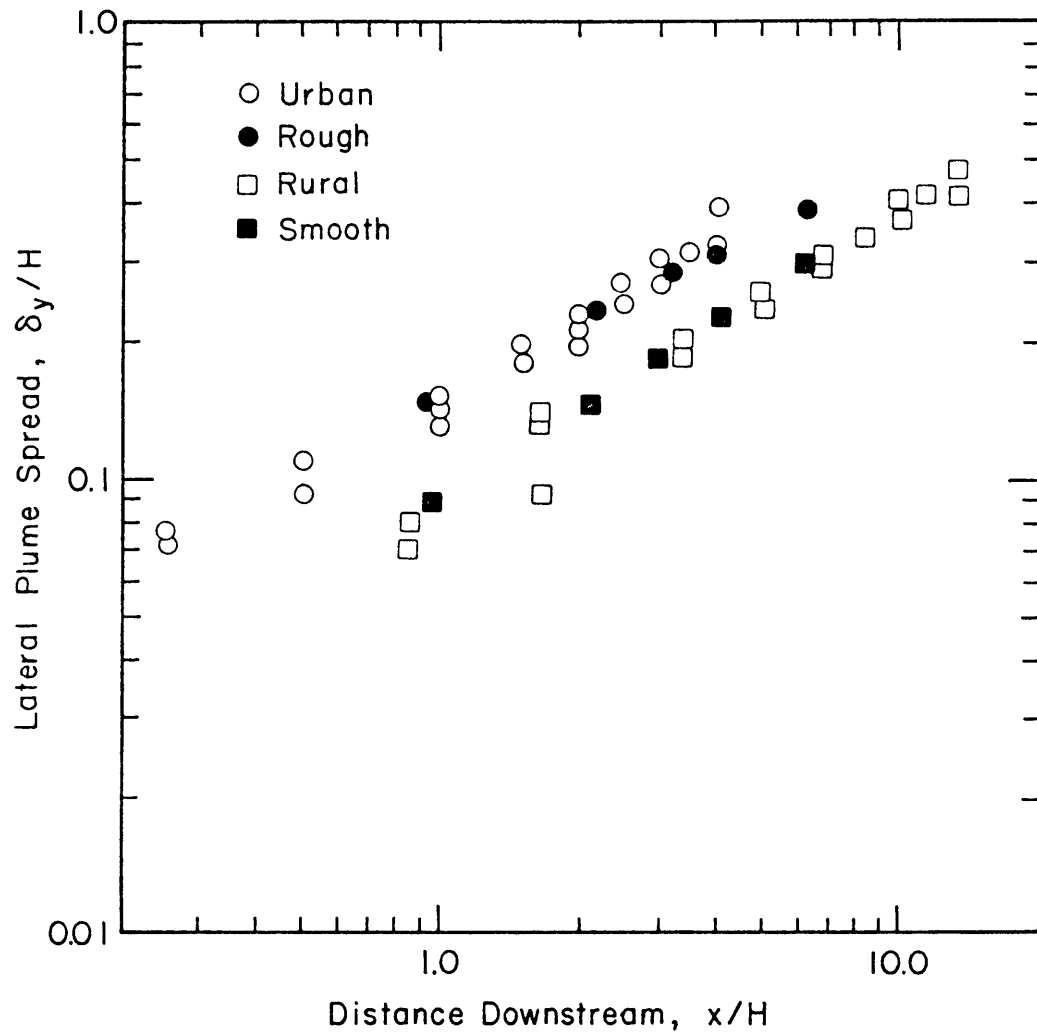
Figure 3-20. Comparison of measured lateral plume spread with Robins (1978) urban and rural flow experimental data.
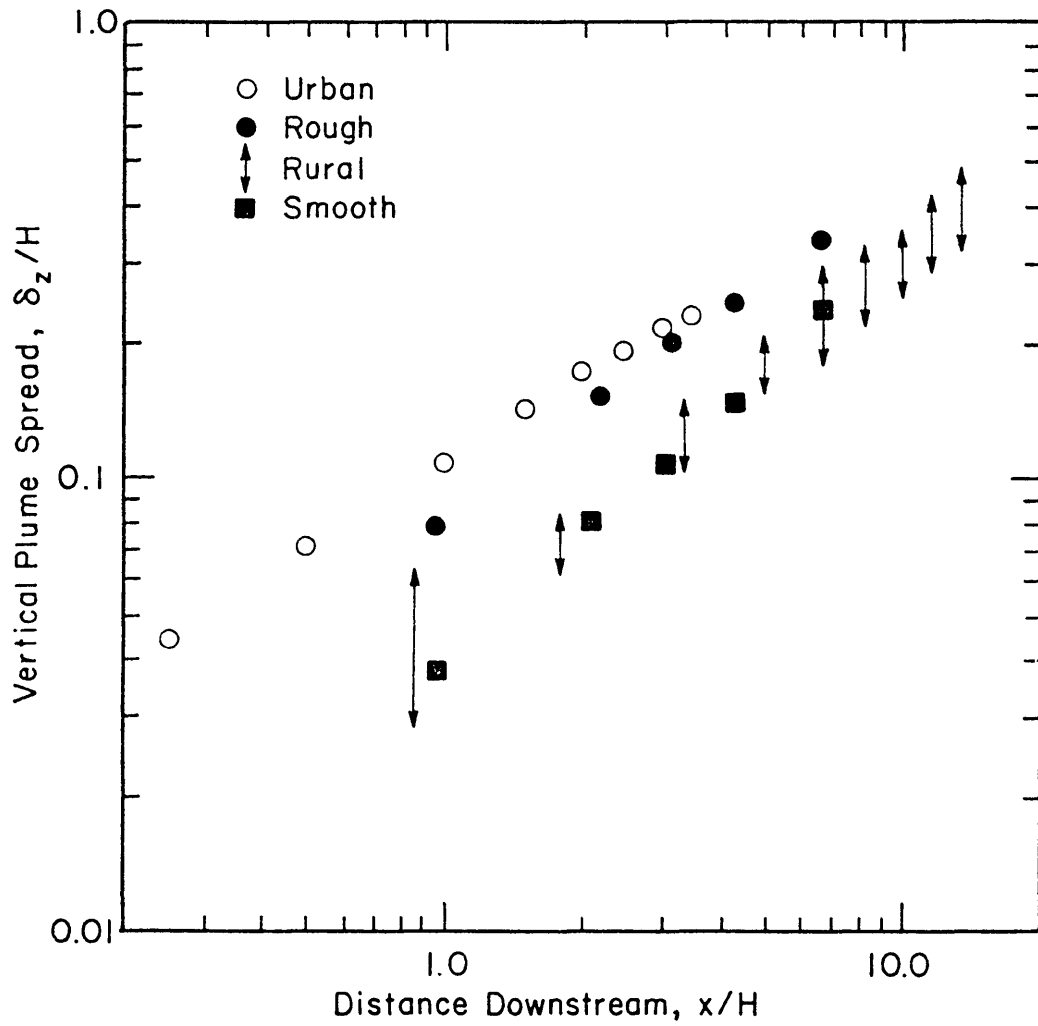
Figure 3-21. Comparison of measured vertical plume spread with Robins (1978) urban and rural flow experimental data.
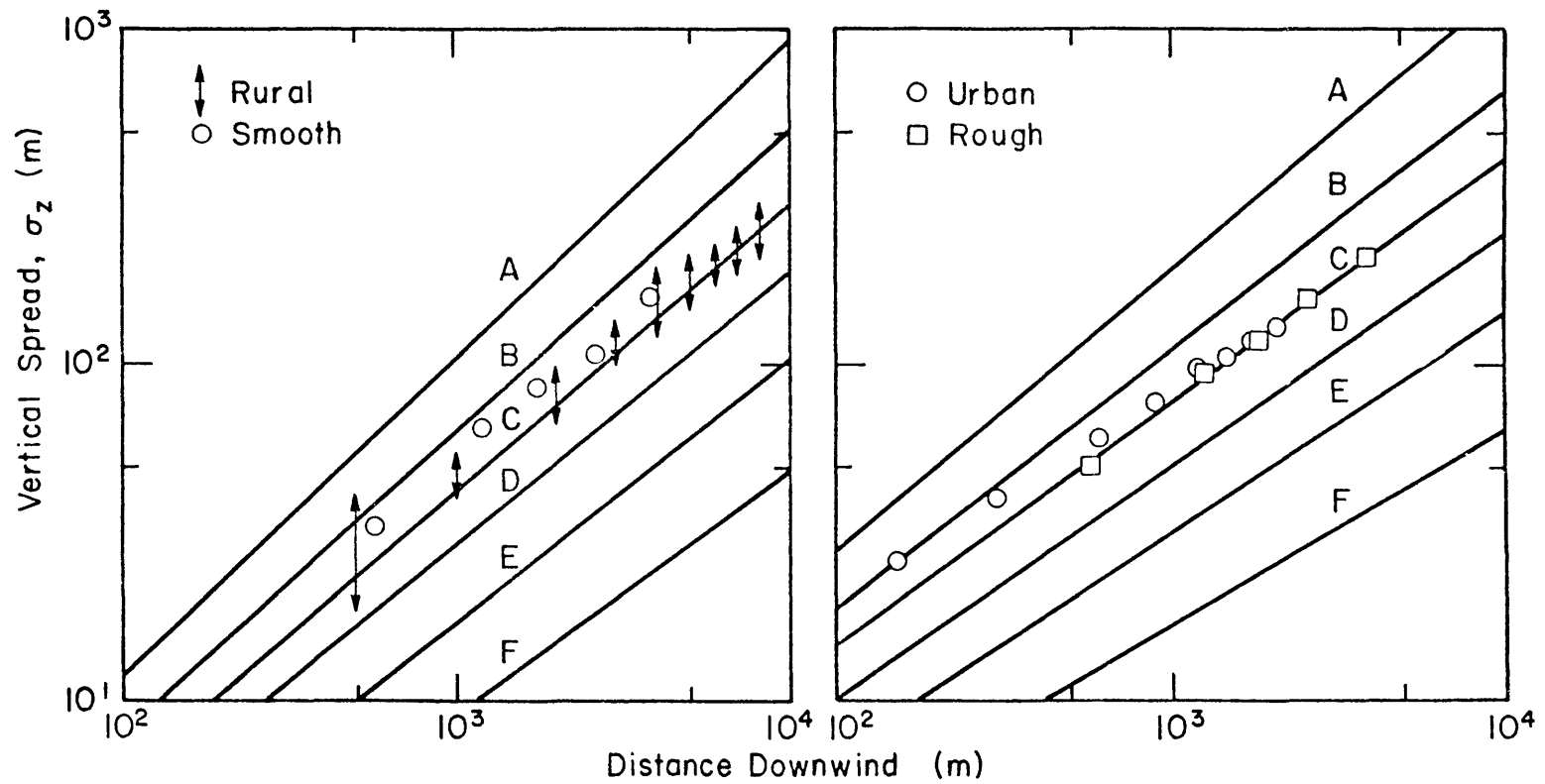
Figure 3-22. Comparison of Robins (1978) urban and rural flow experimental data and present measurements with Pasquill's vertical plume spread estimates.

4.0 STABLE FLOW

4.1 Velocity Field over the Smooth Floor

Temperature profiles $T(z)$ were measured at distances of $x = 0.0$, 2.80 and 6.05 m from the source. These profiles are presented in Figure 4-1 and show good horizontal homogeneity.

Mean velocity distributions, $u(z)$, measured at distances of $x = 0.0$, 2.80 and 6.05 m from the source are presented in Figure 4-2. These profiles also show good horizontal homogeneity, however, they also indicate that the flow was not ideal. Such a behavior of the flow field, which is typical of real atmospheric flows, can be attributed to the step change in surface roughness from rough to smooth, as discussed in an earlier section on neutral flows. Under these conditions, the selection of idealized parameters such as the shear velocity, u^*, the surface roughness, z_o, and the Monin-Obukhov length scale, L, is affected.

Shear measurements made at distances of $x = 0.0$, 2.80 and 6.05 m from the source are presented in Figure 4-3. These profiles, too, clearly show the effect of flow transition from rough to smooth surface. Since stable flows are very strongly affected by the transition in surface roughness, the average value of the shear velocity, u^*, for this flow in the region of interest is estimated by fitting data near the surface to the log-linear equation,

$$u(z) = \frac{u^*}{K} \left[\ell n (\frac{z}{z_o}) \right] , \qquad (4\text{-}1)$$

where $u(z)$ is the mean velocity at elevation z, k is von Karman's constant, and z_o is the aerodynamic surface roughness. The value of the shear velocity thus obtained is $u^* = 0.11$ m/s.

From the similarity theory of Monin and Obukhov, which is based on the assumption that the flow is plane homogeneous and that vertical fluxes are constant, the following velocity, temperature and length scales are obtained:

The shear velocity u^*:

$$u^* = (\tau_o/\rho_o)^{\frac{1}{2}} \tag{4-2}$$

The friction temperature T^*:

$$T^* = -H_o/(\rho_o C_p K u^*) \tag{4-3}$$

The stability length L:

$$L = -u^{*3}/(K \frac{g}{T_a} \frac{H_o}{\rho_o C_p}) \quad , \tag{4-4}$$

where ρ_o is the density, τ_o is the wall shear stress, H_o is the wall heat flux, and g/T_a is the stability parameter.

For stable flow over a smooth surface, the friction temperature is estimated from Figure 4-1 to be $T^* = 11C^\circ$. Combining equations 4-3 and 4-4, the stability length is expressed as

$$L = u^{*2}/(K^2 \frac{g}{T_a} T^*) \quad . \tag{4-5}$$

Using the above equation, L is approximately 16 cm for this flow. Figure 4-4 shows the variation of the point Richardson number with z/L in this case.

Distributions of the longitudinal turbulence intensity (u_{rms}/U) and the vertical turbulence intensity (w_{rms}/U), measured at distances of x = 0.0, 2.80 and 6.05 m from the source, are presented in Figures 4-5 and 4-6.

4.2 Velocity Field over the Rough Floor

Temperature profiles T(z) measured at distances of x = 0.0, 2.80 and 6.05 m from the source are presented in Figure 4-7.

Mean velocity distributions, u(z), measured at distances of x = 0.0, 2.80 and 6.05 m from the source are presented in Figure 4-8. These profiles show good horizontal homogeneity and resemble profiles for ideal flows. As discussed in the section on neutral flow over a rough surface, in this flow, too, the change in surface roughness near the region of interest is considerably smaller in comparison to the case of flow over the smooth surface. Hence the shear stress profiles presented in Figure 4-9 for measurements made at distances of x = 0.0, 2.80 and 6.05 m from the source more closely resemble profiles obtained in ideal flows. The average shear velocity for this flow in the region of interest is estimated to be $u^* = 0.13$ m/s from curve fitting data to equation 4-1.

The friction temperature for this flow is estimated from Figure 4-7 to be $T^* = 14C^\circ$. The stability length is calculated from equation 4-5 to be $L \cong 25$ cm. Figure 4-10 shows the variation of the point Richardson number with z/L for this flow.

The longitudinal and vertical turbulence intensity distributions are presented in Figures 4-11 and 4-12, respectively, for measurements made at distances of x = 0.0, 2.80 and 6.05 m from the source.

4.3 Measured Concentration Field

In stable flow, diffusion data were measured for two surface roughness conditions, for a continuous point source located at elevations of ~0.0, 10.0 and 20.0 cm above the floor of the wind tunnel. Concentration measurements were made at distances of x = 0.85, 1.95, 2.80, 3.90 and 6.05 m downstream of the source location. Data corresponding to the ground-level source were fitted to the semiempirical equation 3-2 which yielded the five unknowns $C_{max}(x)$, d_y, λ_y, λ_z and s,

51

listed in Table 4-1, for the various measurement distances from the source.

Concentration data corresponding to the two elevated sources were fitted to semiempirical equations 3-3 and 3-4. Estimates of the four unknowns $C_{max}(x)$, d_y, λ_y and λ_z obtained from these regressions, for the five downstream measurement stations, are presented in Tables 4-2 and 4-3.

As observed in the neutral case, Figures 4-13, 4-14 and 4-15 demonstrate the adequacy of the Gaussian model to accurately describe lateral diffusion in the stable case, regardless of the surface rough-ness or source height. Figures 4-16 and 4-17 further show the suit-ability of the same model in describing diffusion (in the vertical plane) from elevated sources. Vertical diffusion from the ground level source in stable flow, as for the neutral flow, is modelled by a non-Gaussian, variable exponent model. Figure 4-18 illustrates the suitability of this model.

Table 4-1.   Unknowns for Ground-level Source in Stable Flow

| Variable | Distance Downstream from Source (m) | | | | | Roughness |
	x = 0.85	x = 1.95	x = 2.80	x = 3.90	x = 6.05	
$C_{max}(x)$	1307.22	418.89	227.48	122.56	81.36	Rough
(m^2)	3321.90	1343.29	762.24	468.16	188.49	Smooth
dy	-0.34	0.64	1.44	1.74	1.18	Rough
(cm)	1.16	1.00	2.83	-3.27	-2.01	Smooth
λ_y	8.57	12.63	15.93	20.77	26.95	Rough
(cm)	4.56	7.90	10.07	11.84	14.77	Smooth
λ_z	2.91	4.51	5.96	7.68	8.82	Rough
(cm)	1.11	-	2.29	-	3.95	Smooth
s	1.80	1.83	1.96	2.09	2.11	Rough
(-)	1.32	-	1.69	-	2.07	Smooth

Table 4-2.   Unknowns for 10 cm Source in Stable Flow

Variable	Distance Downstream from Source (m)					Roughness
	x = 0.85	x = 1.95	x = 2.80	x = 3.90	x = 6.05	

Horizontal Profile

Variable	x = 0.85	x = 1.95	x = 2.80	x = 3.90	x = 6.05	Roughness
$C_{max}(x)$	146.77	83.24	66.51	55.31	39.99	Rough
(m^2)	343.23	120.35	79.37	55.50	38.53	Smooth
dy	-0.07	-0.93	0.22	-0.03	1.17	Rough
(cm)	-0.13	-0.78	0.76	-0.39	0.37	Smooth
λ_y	7.39	10.69	12.29	15.21	20.95	Rough
(cm)	4.15	7.85	10.30	13.08	17.41	Smooth

Vertical Profile

Variable	x = 0.85	x = 1.95	x = 2.80	x = 3.90	x = 6.05	Roughness
$C_{max}(x)$	146.45	80.10	62.31	50.17	34.53	Rough
(m^2)	342.34	120.18	78.35	53.93	37.64	Smooth
λ_z	4.91	6.98	8.31	9.07	10.14	Rough
(cm)	-	5.13	5.72	7.22	7.17	Smooth

Table 4-3. Unknowns for 20 cm Source in Stable Flow

| Variable | Distance Downstream from Source (m) | | | | | Roughness |
	x = 0.85	x = 1.95	x = 2.80	x = 3.90	x = 6.05	
	Horizontal Profile					
$C_{max}(x)$	91.93	52.61	37.53	27.27	19.91	Rough
(m^2)	218.83	64.37	37.94	26.08	17.12	Smooth
dy	-0.11	0.16	0.94	0.21	0.69	Rough
(cm)	0.72	1.51	-0.03	-0.47	0.06	Smooth
λ_y	7.51	10.30	12.40	14.06	17.53	Rough
(cm)	4.43	8.56	11.03	13.80	17.09	Smooth
	Vertical Profile					
$C_{max}(x)$	90.71	52.48	36.61	26.76	19.63	Rough
(m^2)	216.90	62.96	39.20	26.44	17.30	Smooth
λ_z	5.59	7.13	8.40	9.42	11.09	Rough
(cm)	3.58	6.20	8.29	9.61	10.66	Smooth
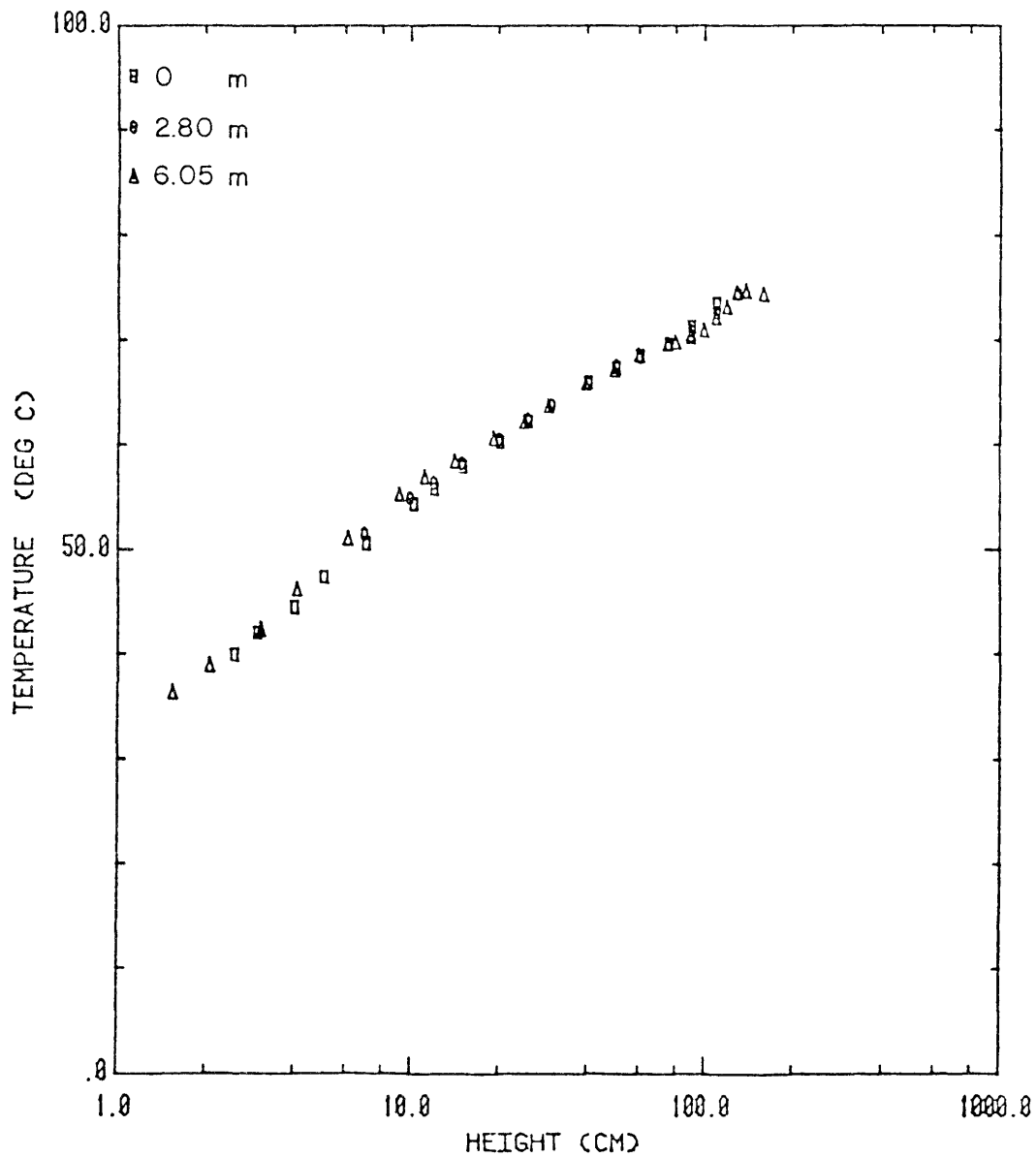
Figure 4-1. Temperature profiles, smooth floor.

Figure 4-2. Mean velocity profiles, smooth floor.

57
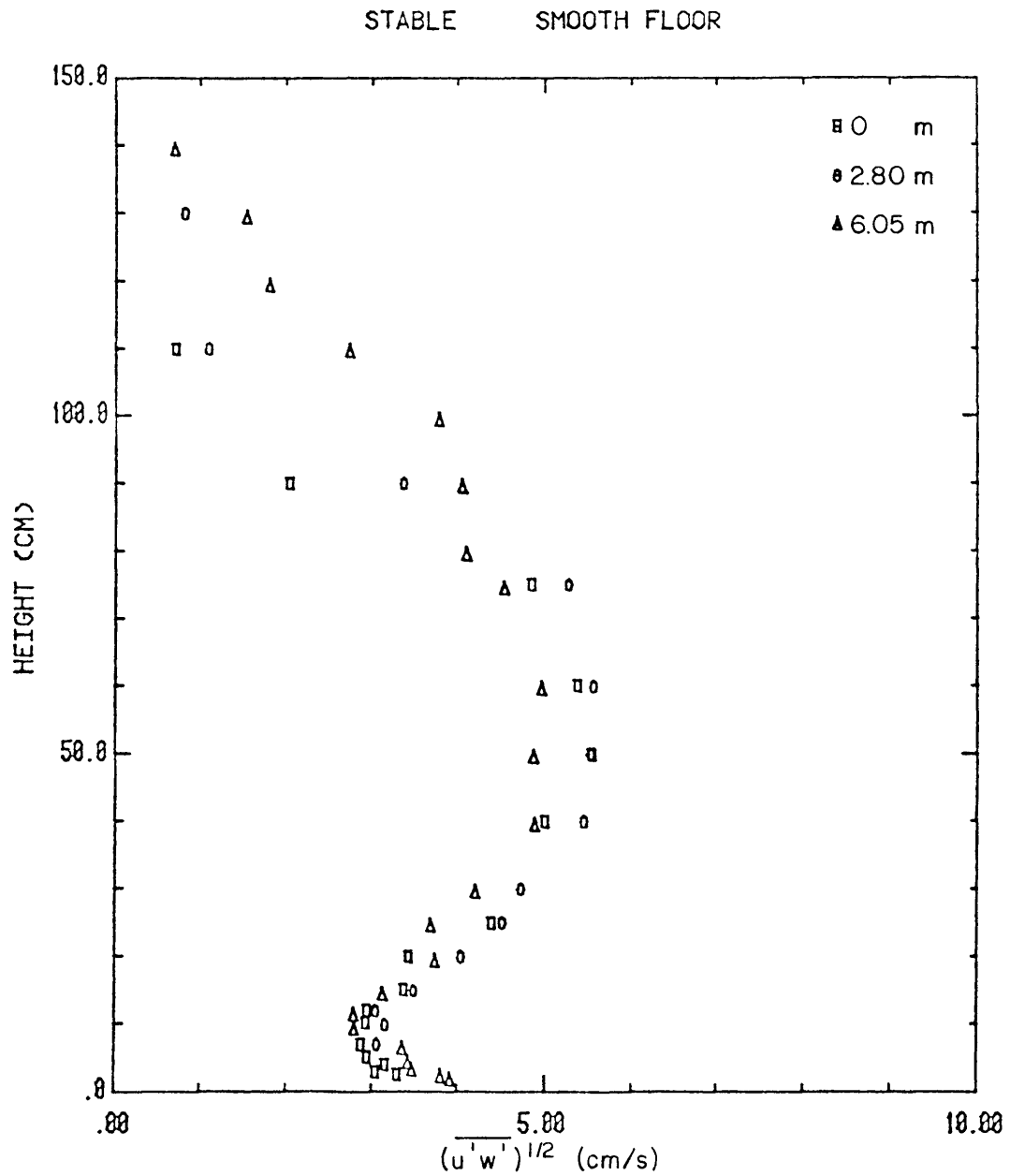
Figure 4-3. Vertical distribution of shear stress $(\overline{u'w'})^{\frac{1}{2}}$, smooth floor.
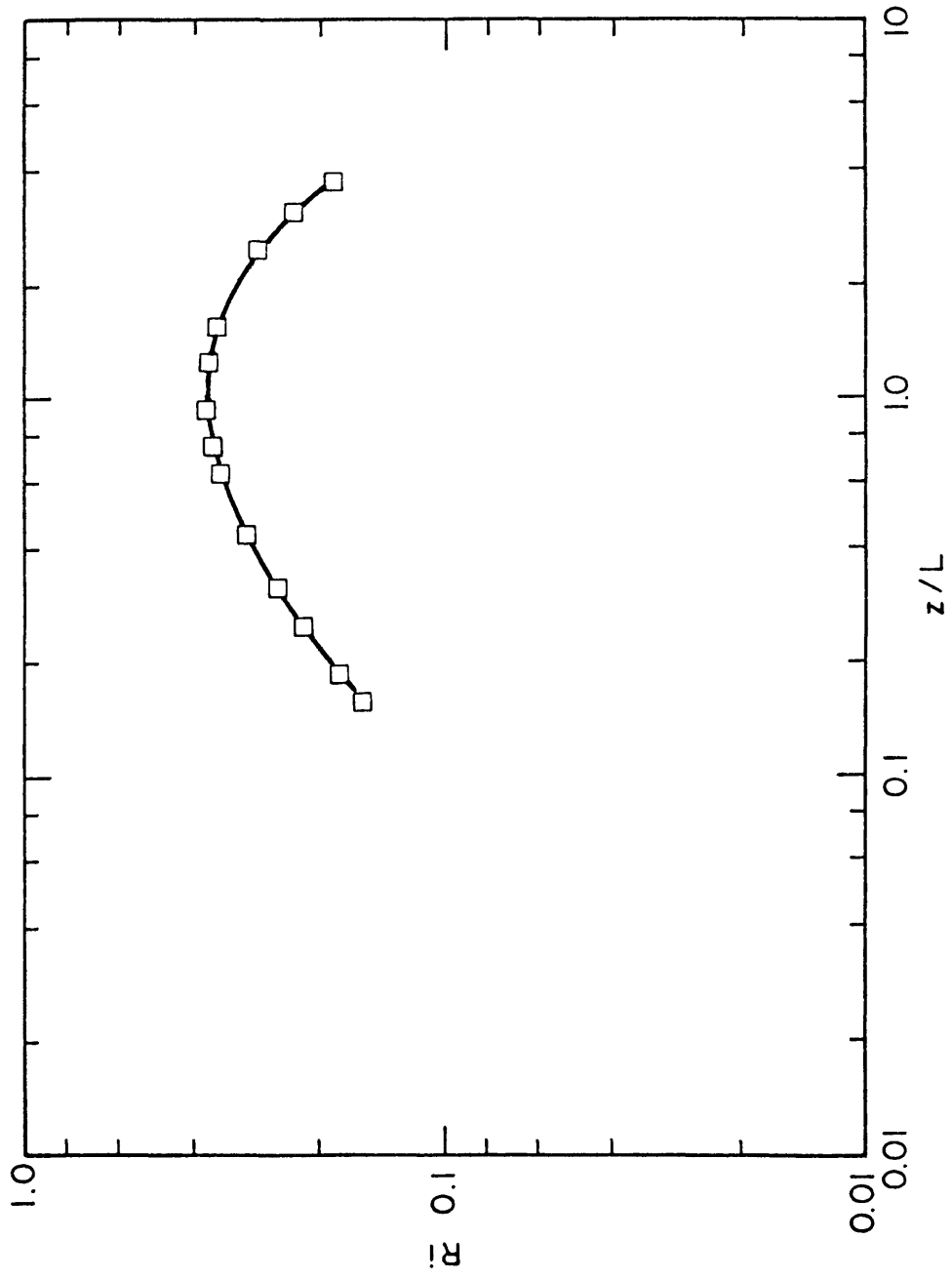
Figure 4-4. R_i as a function of z/L, for a smooth floor.

STABLE   SMOOTH FLOOR
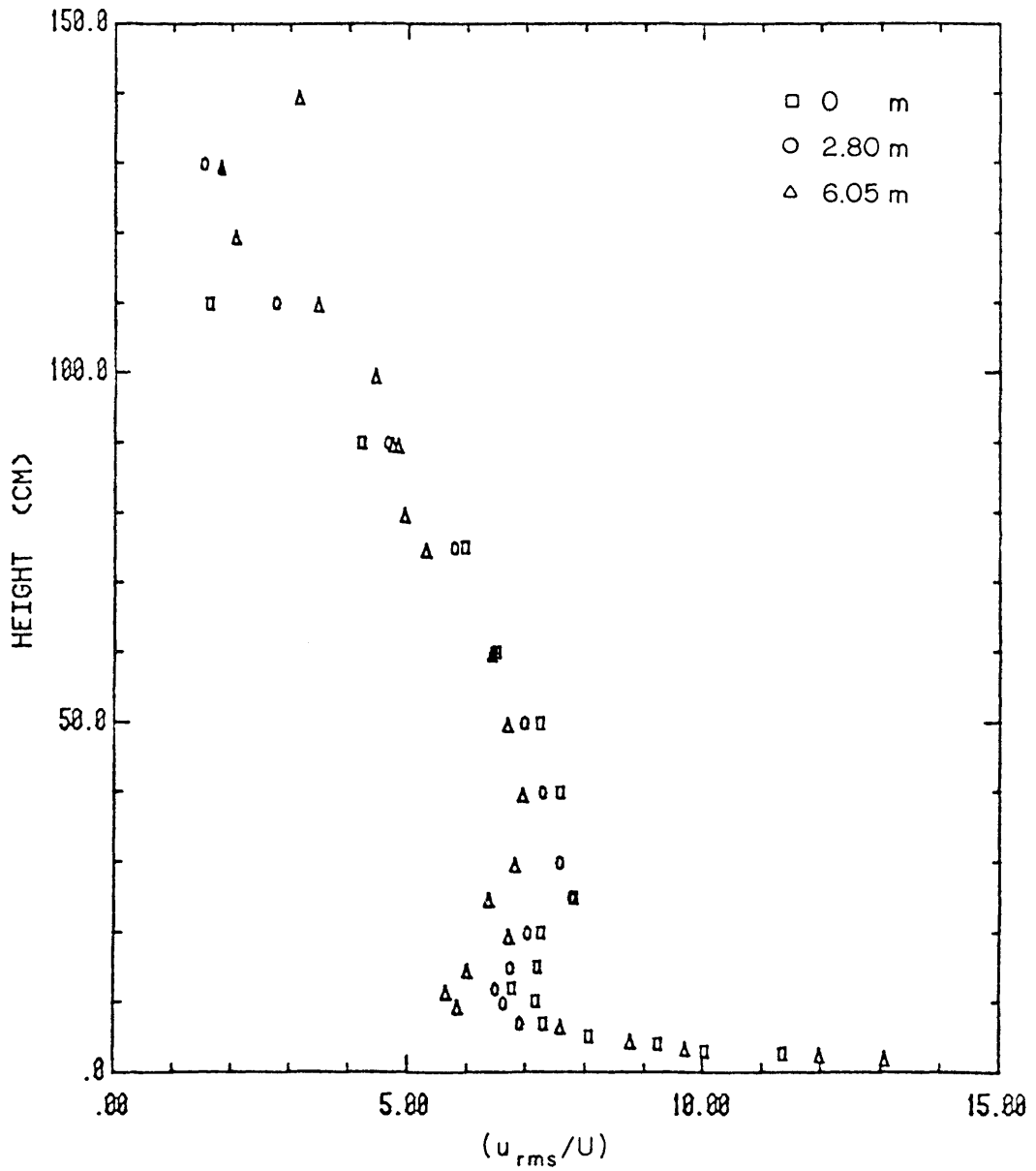
Figure 4-5.   Longitudinal turbulence intensity (u_{rms}/U), smooth floor.
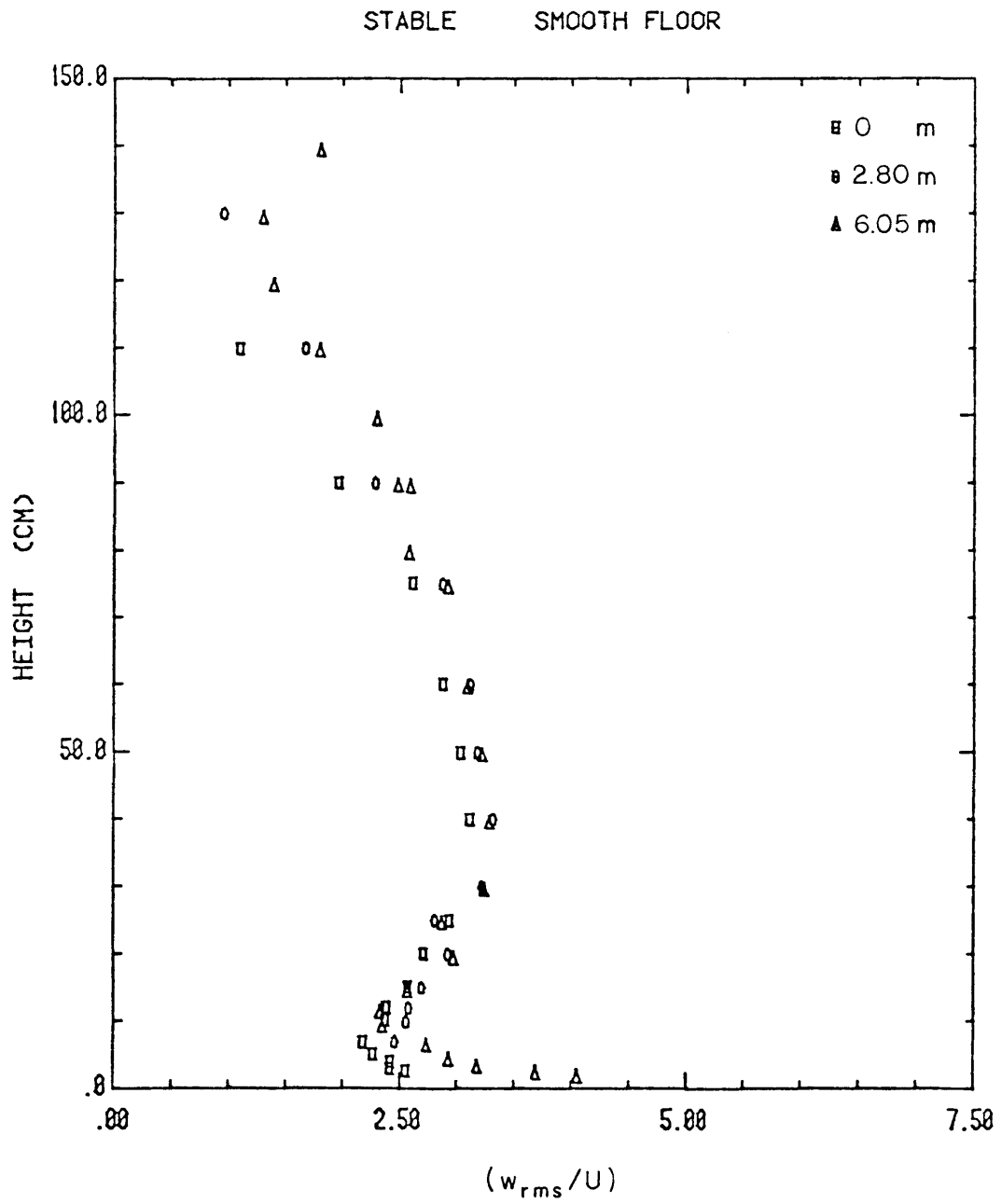
Figure 4-6. Vertical turbulence intensity (w_{rms}/U), smooth floor.
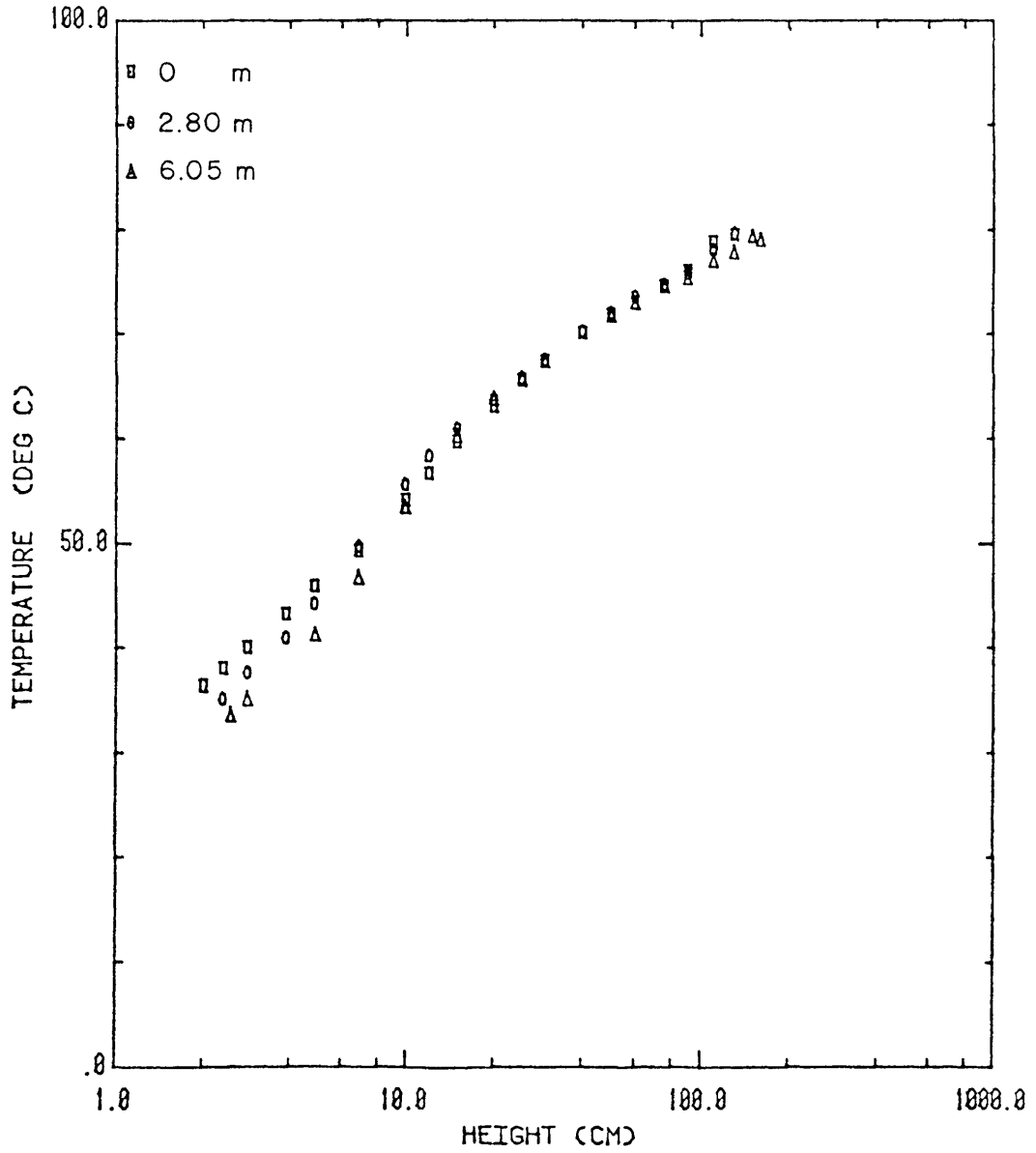
Figure 4-7.   Temperature profiles, rough floor.

STABLE   ROUGH FLOOR
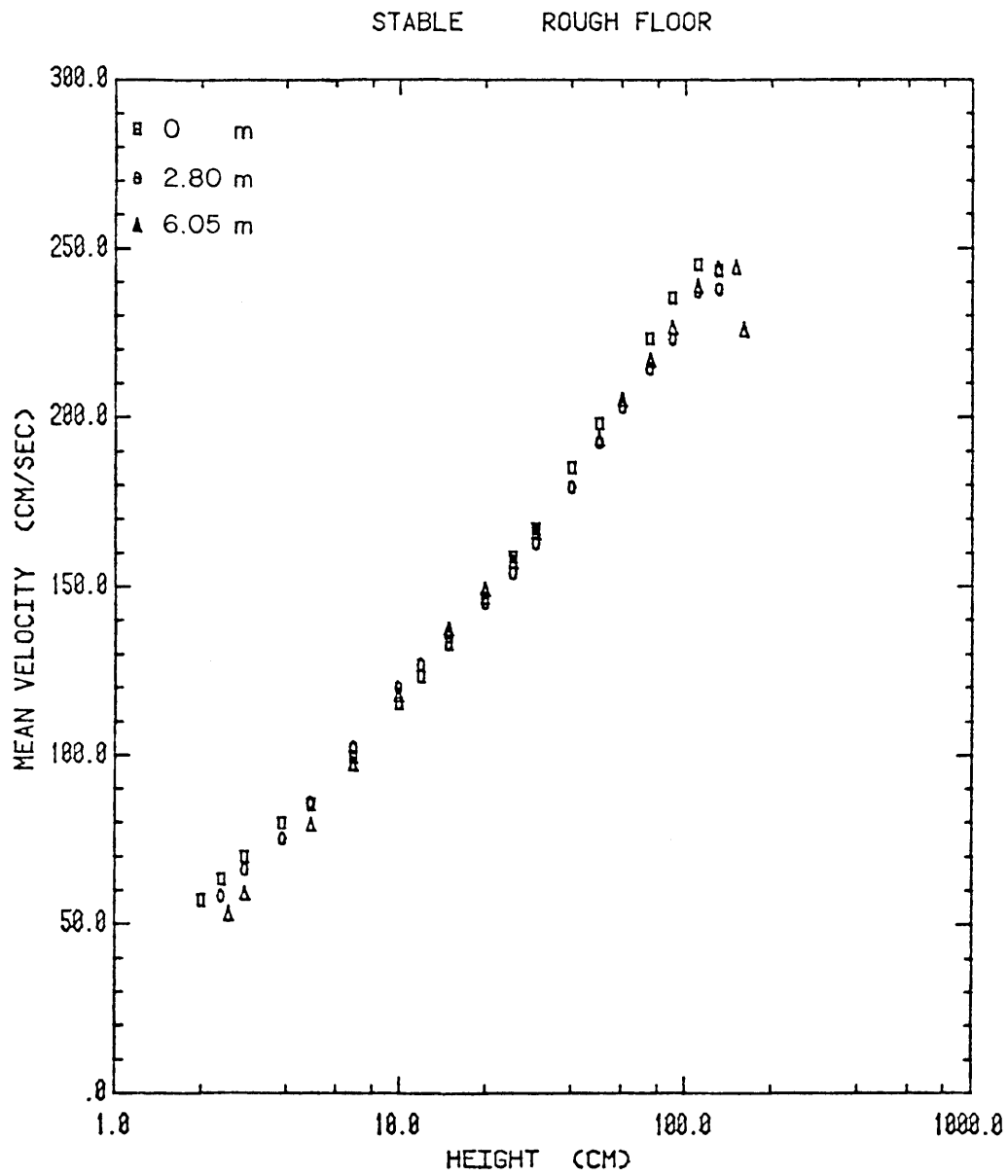
Figure 4-8. Mean velocity profiles, rough floor.

STABLE   ROUGH FLOOR
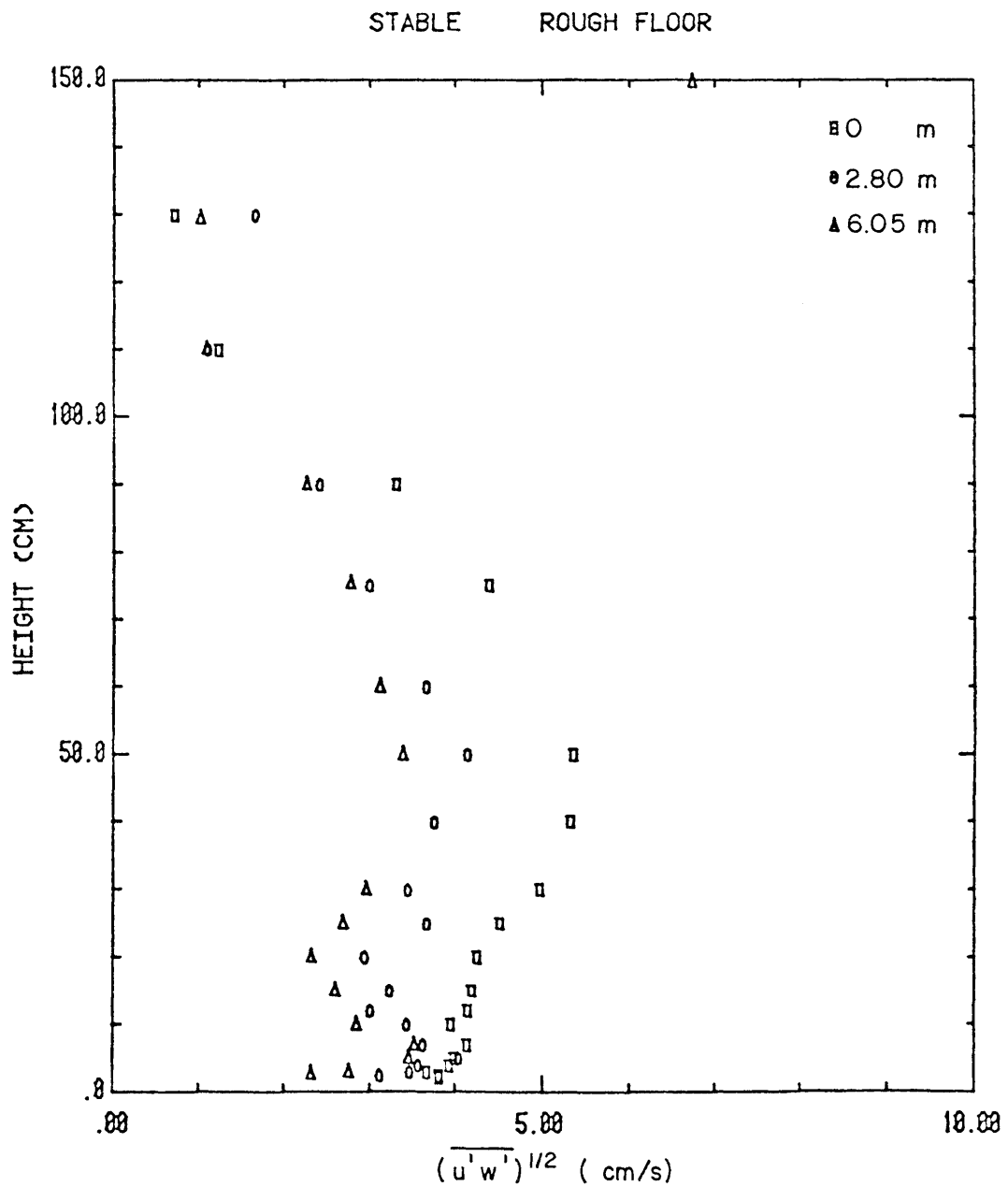
Figure 4-9. Vertical distribution of shear stress $(\overline{u'w'})^{\frac{1}{2}}$, rough floor.

64
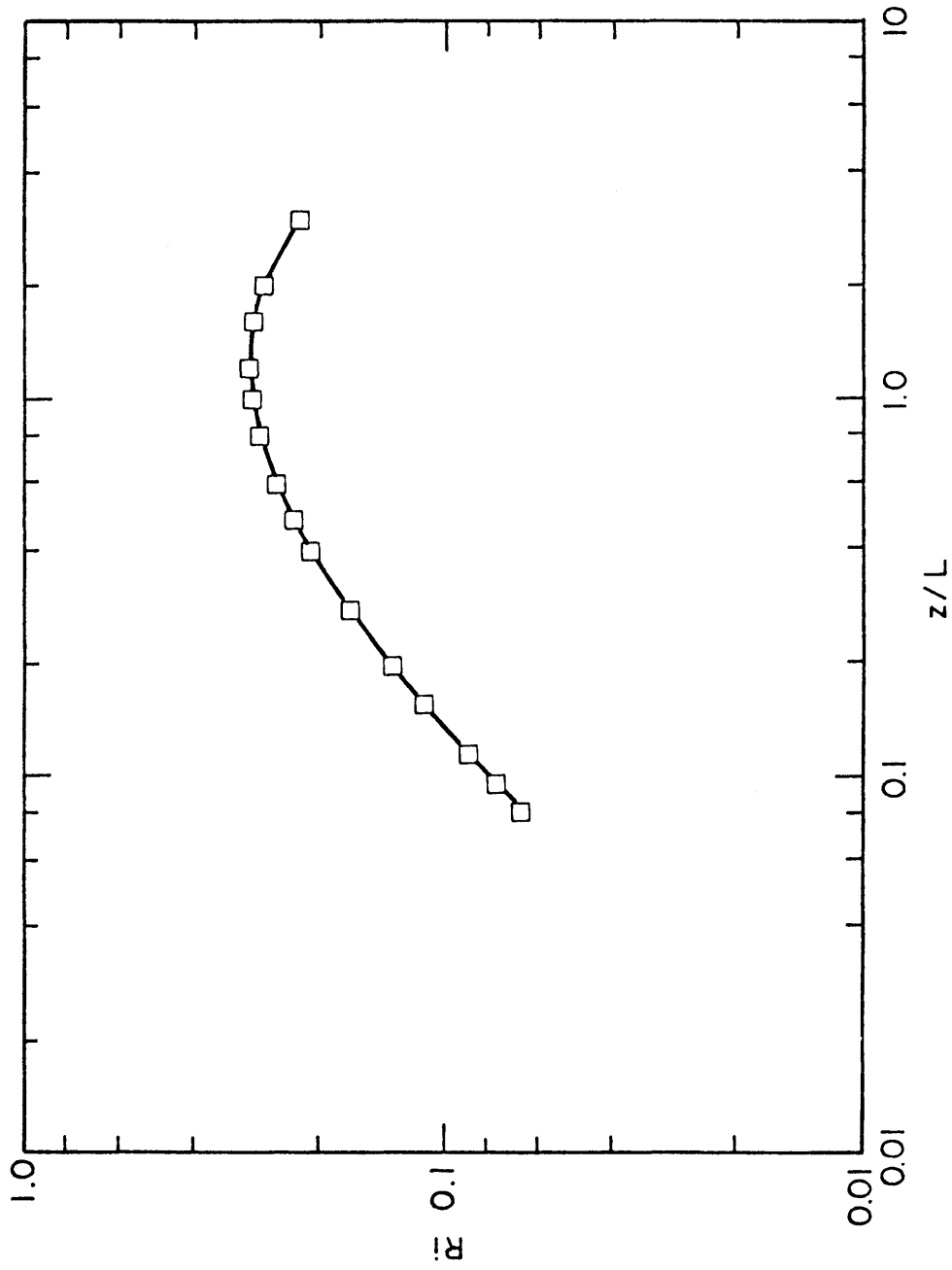
Figure 4-10. R_i as a function of z/L, for a rough floor.
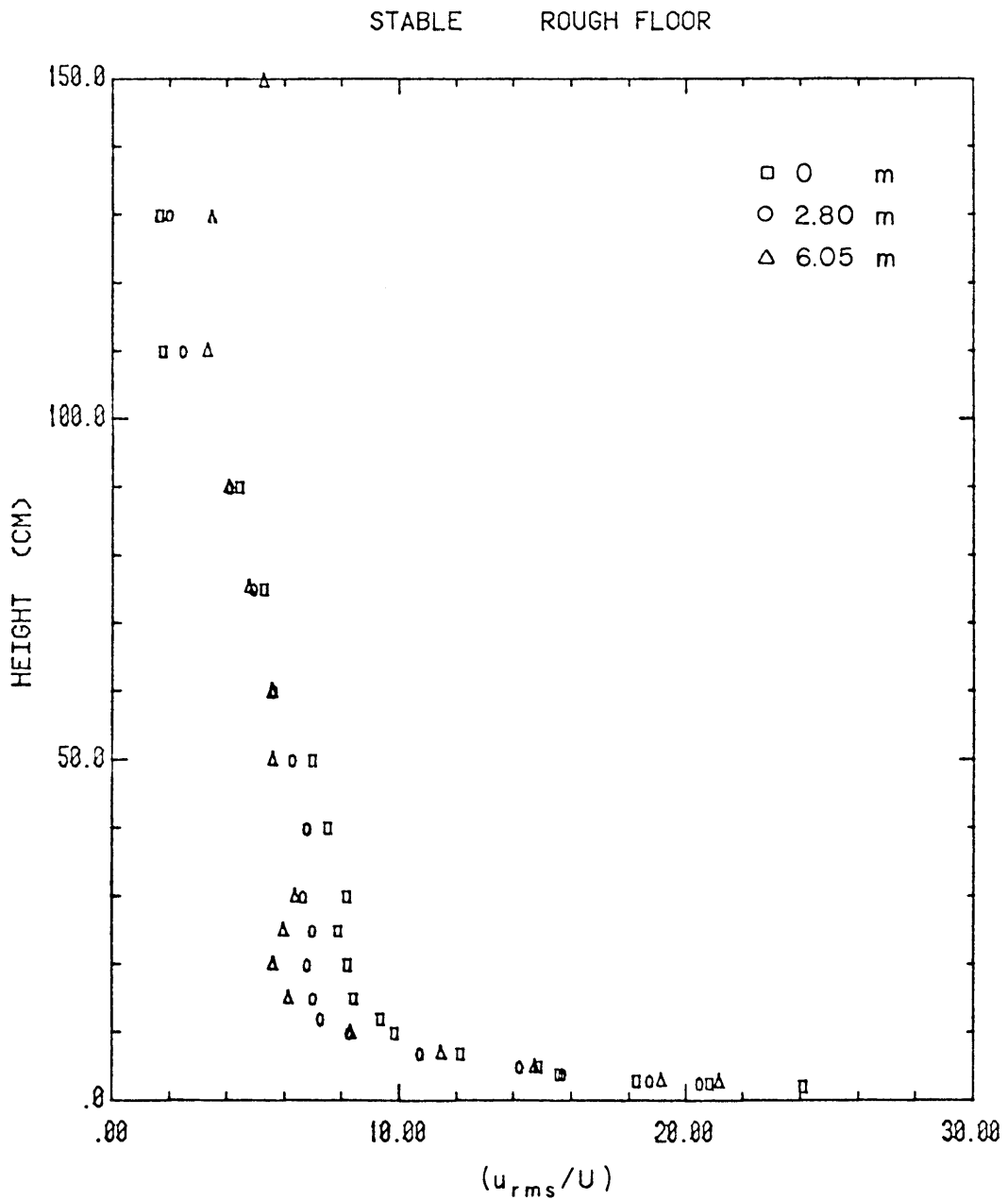
Figure 4-11. Longitudinal turbulence intensity (u_{rms}/U), rough floor.
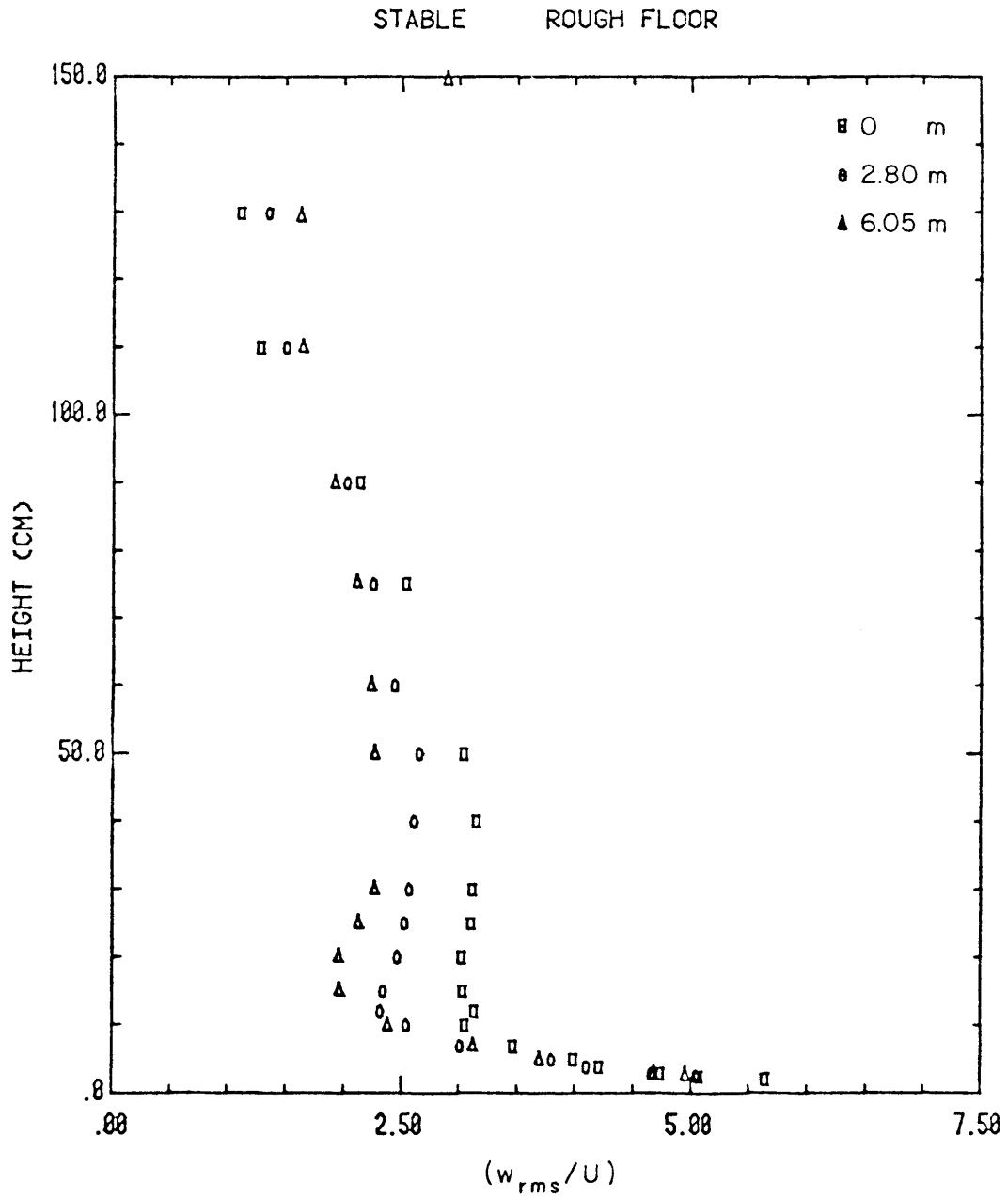
Figure 4-12. Vertical turbulence intensity (w_{rms}/U), rough floor.
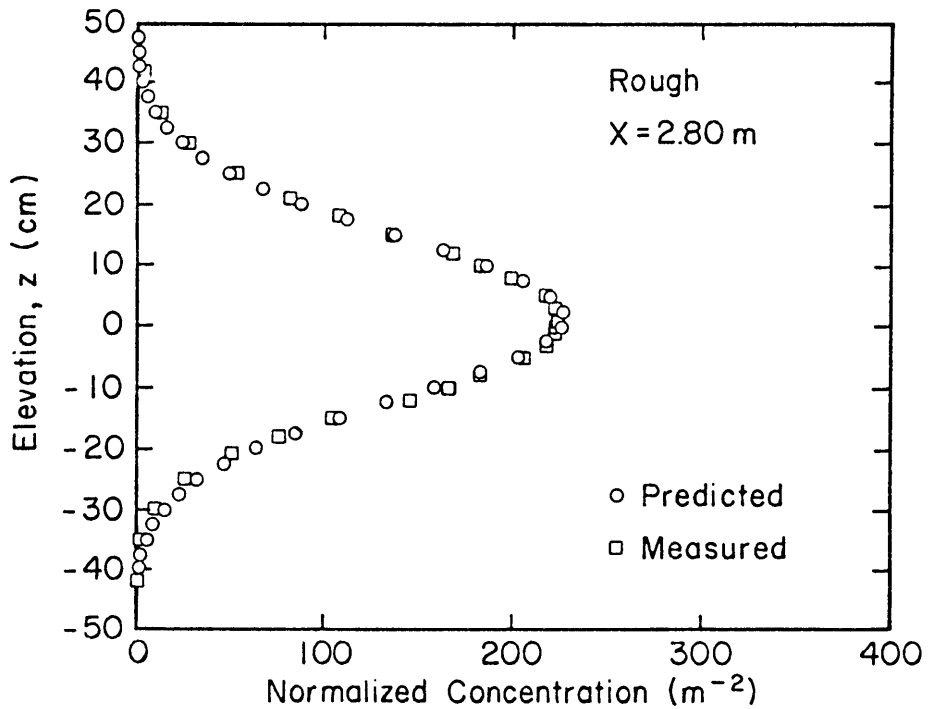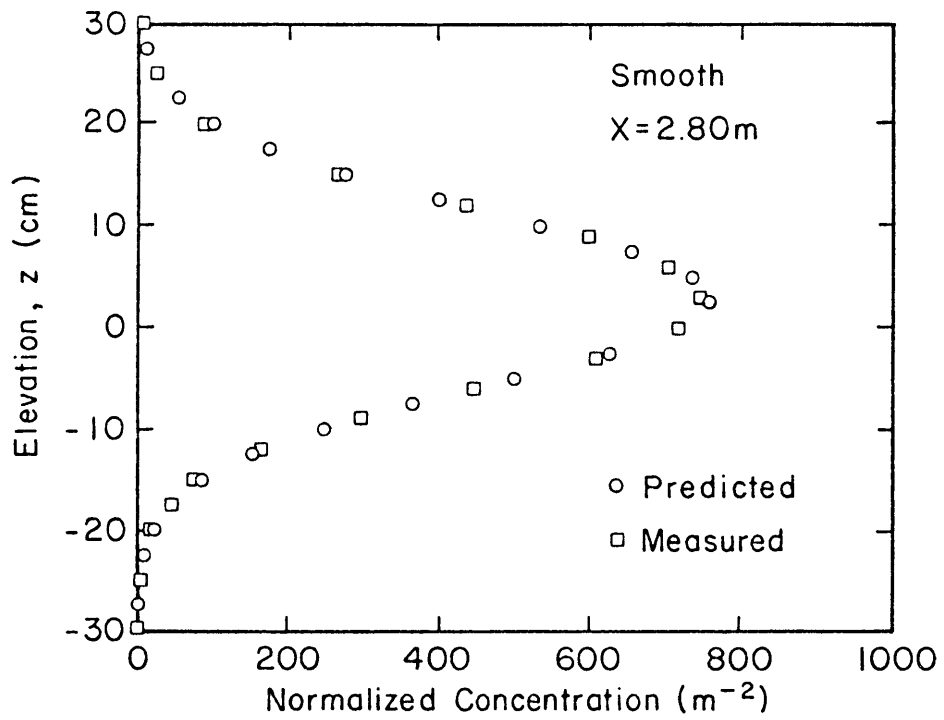
Figure 4-13. Horizontal concentration profiles for a ground-level source in stable flow.
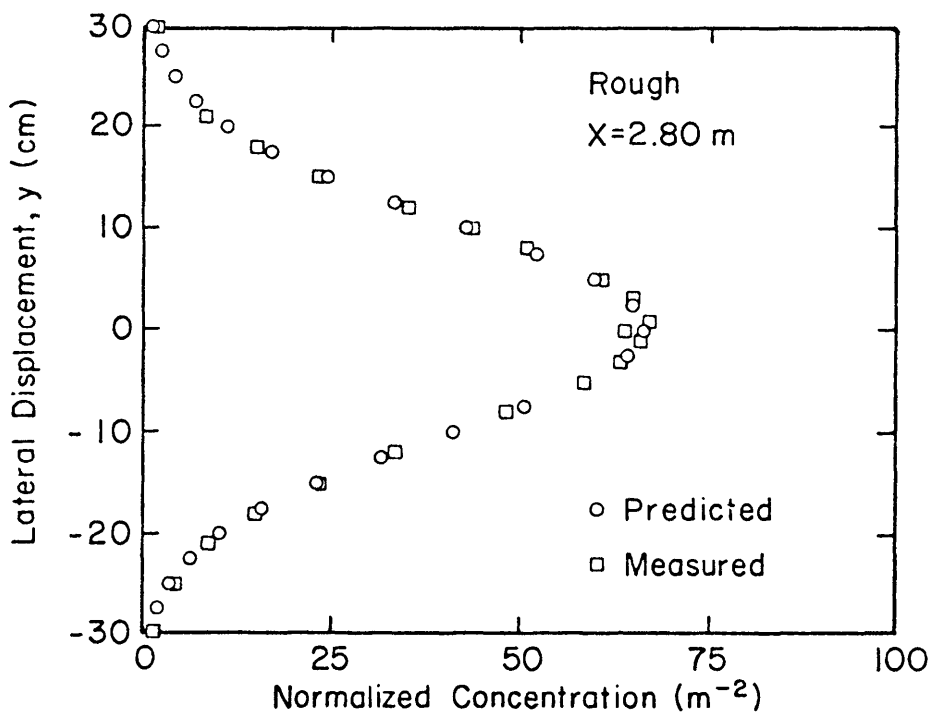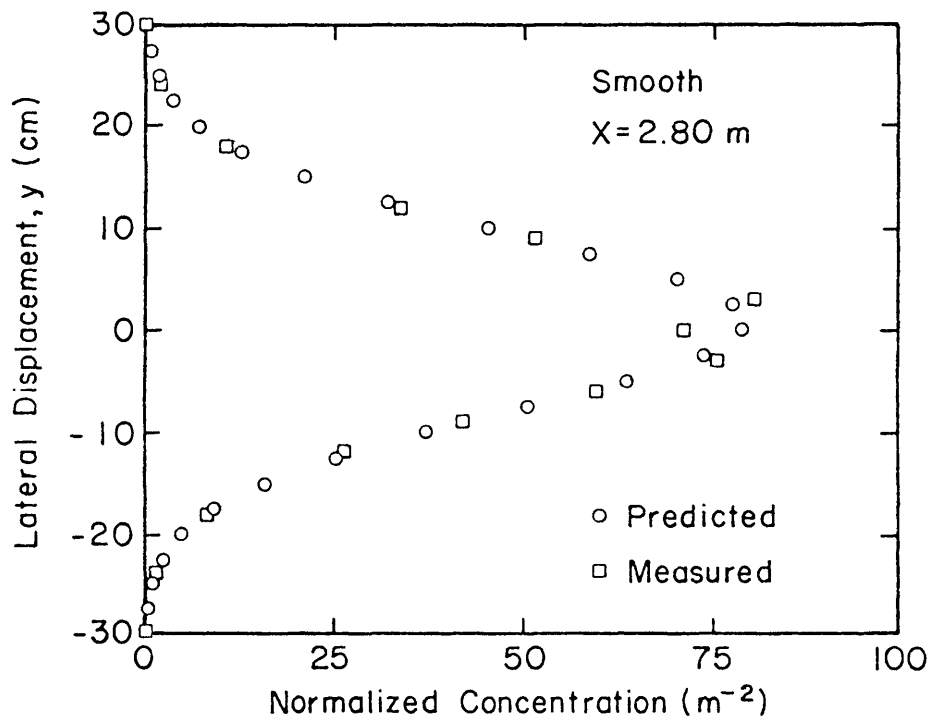
Figure 4-14. Horizontal concentration profiles for a 10 cm source in stable flow.
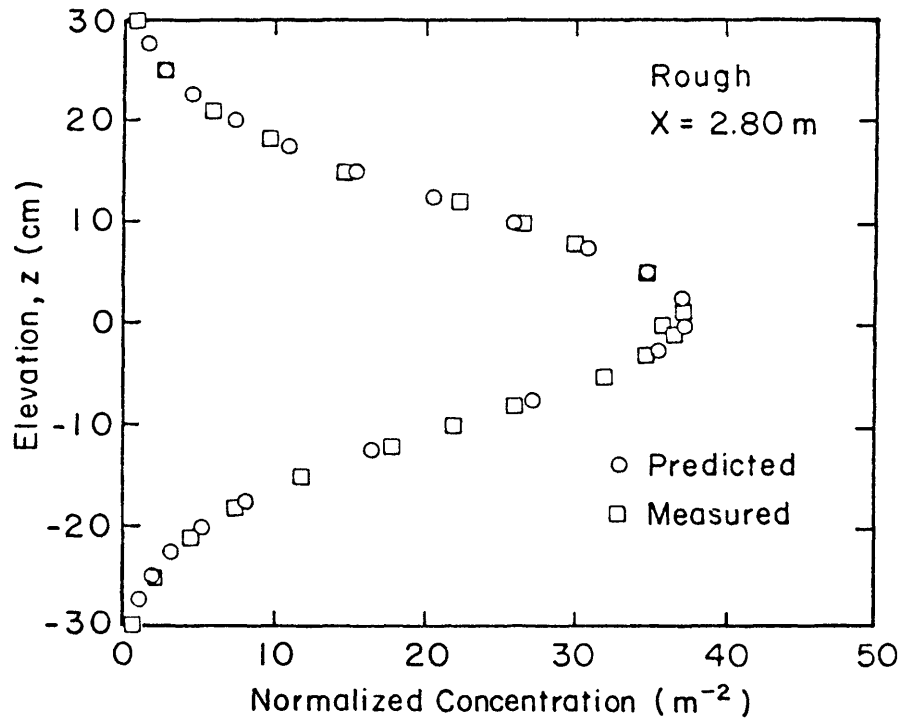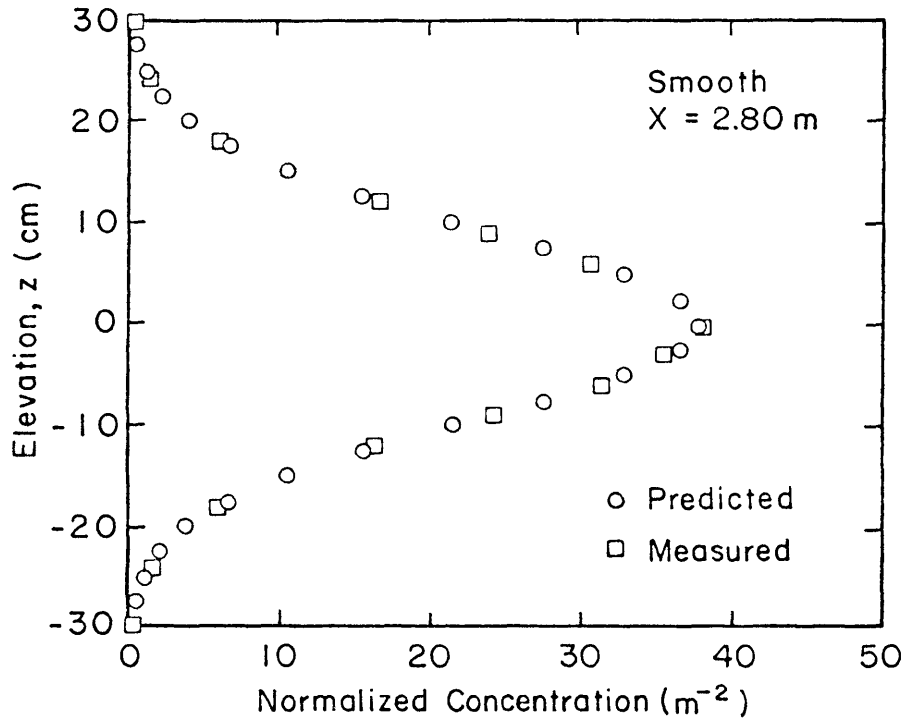
Figure 4-15. Horizontal concentration profiles for a 20 cm source in stable flow.
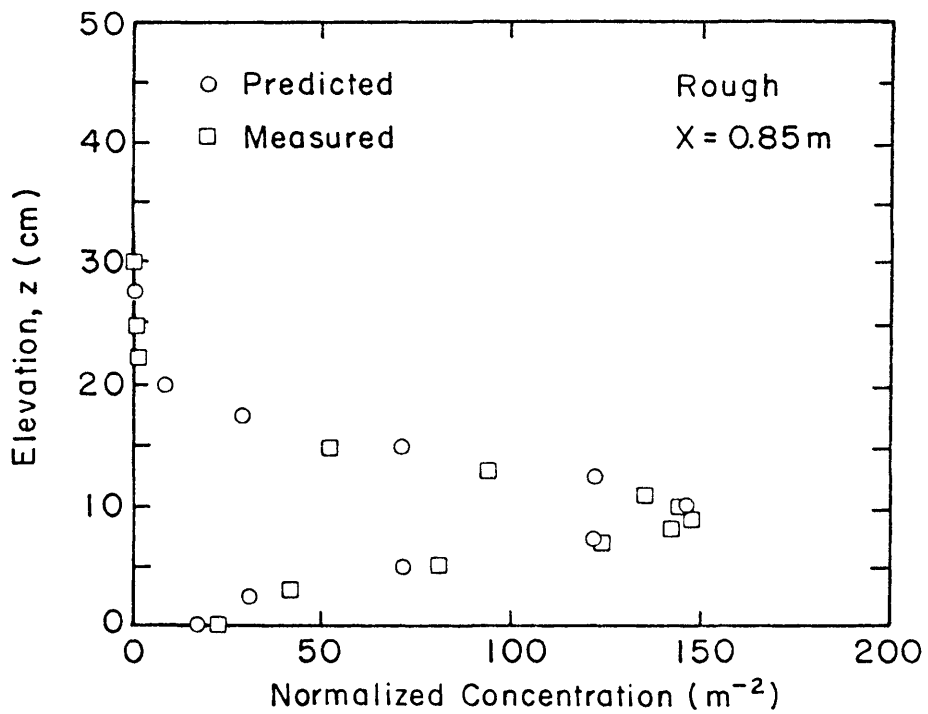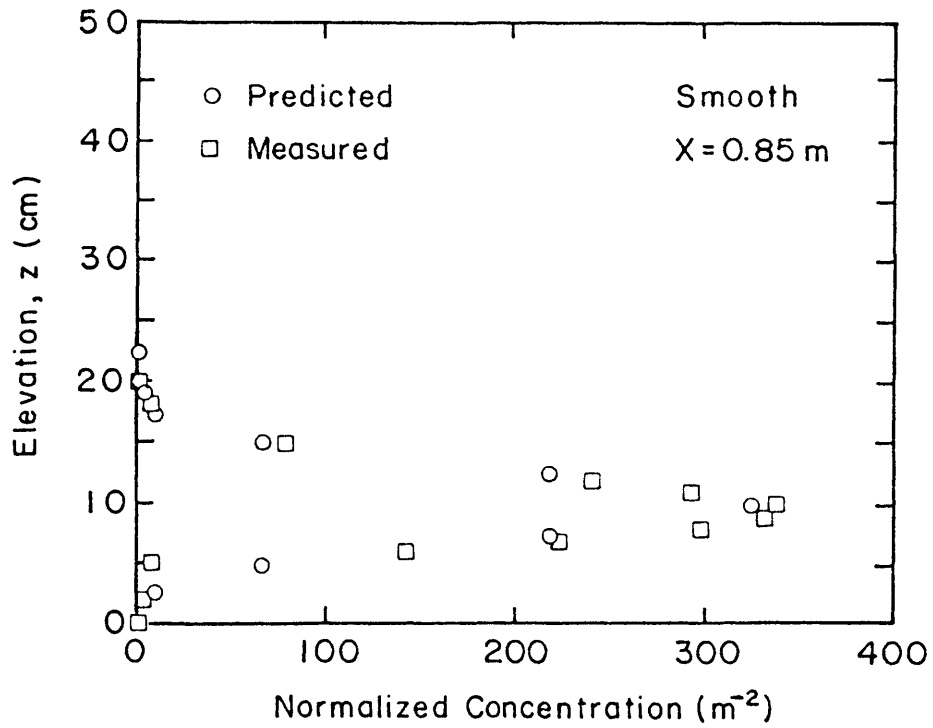
Figure 4-16. Vertical concentration profiles for a 10 cm source in stable flow.
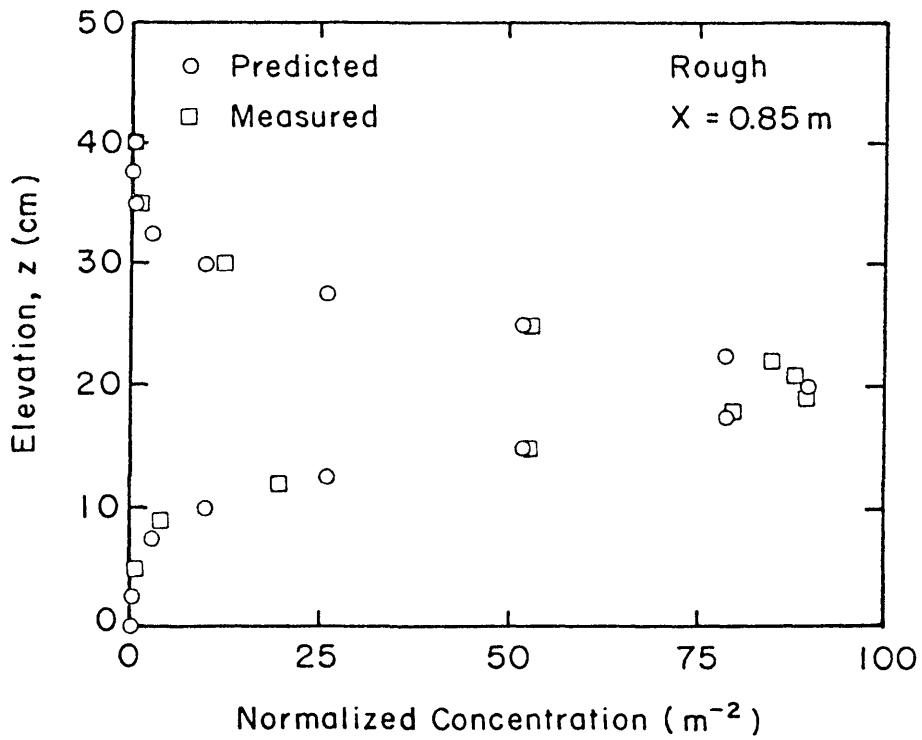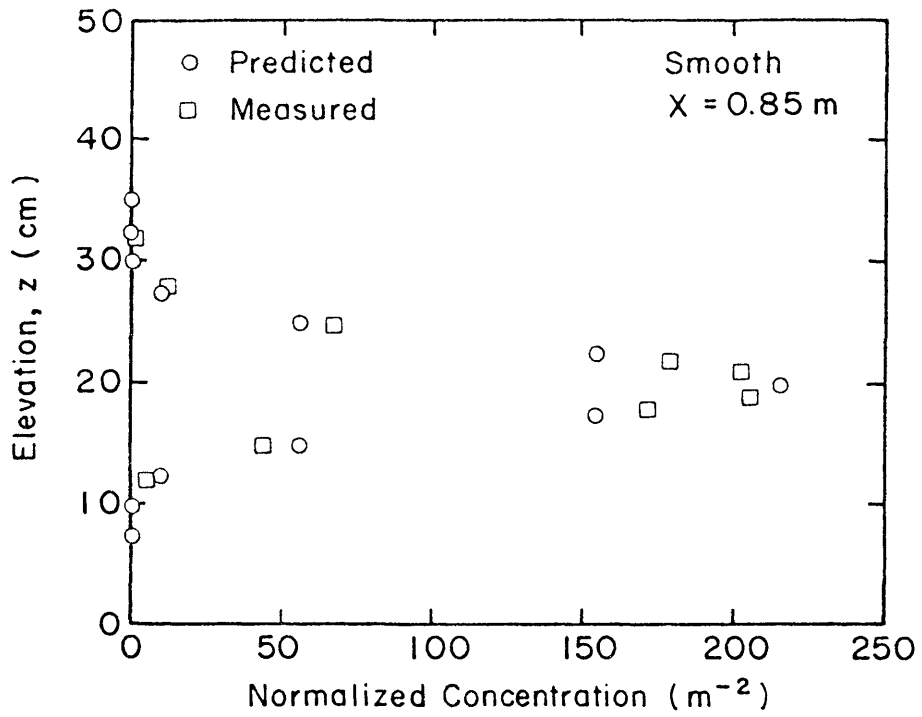
Figure 4-17. Vertical concentration profiles for a 20 cm source in stable flow.
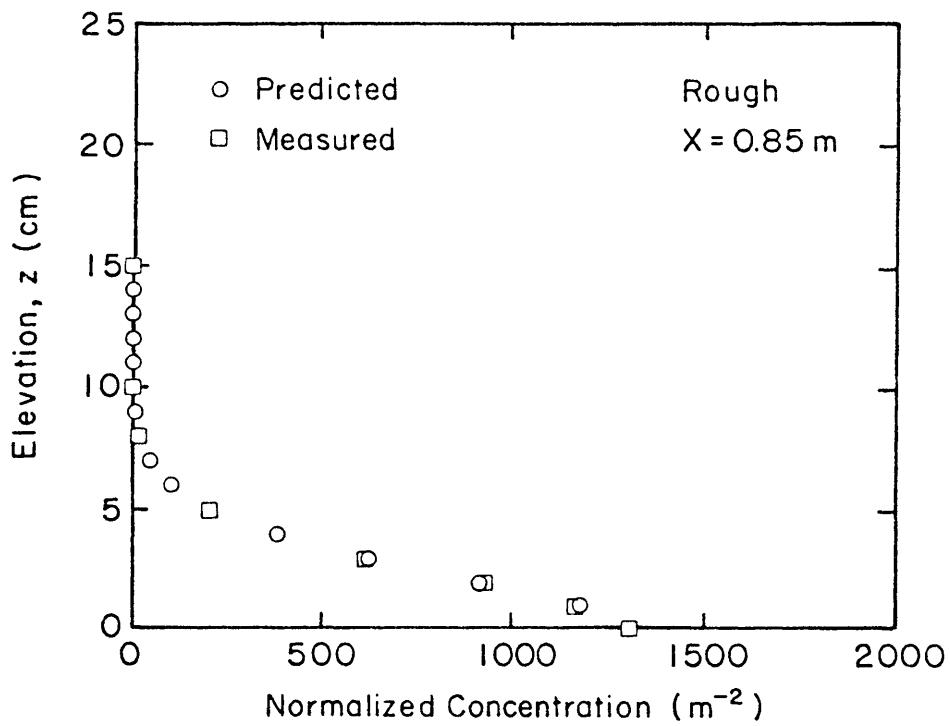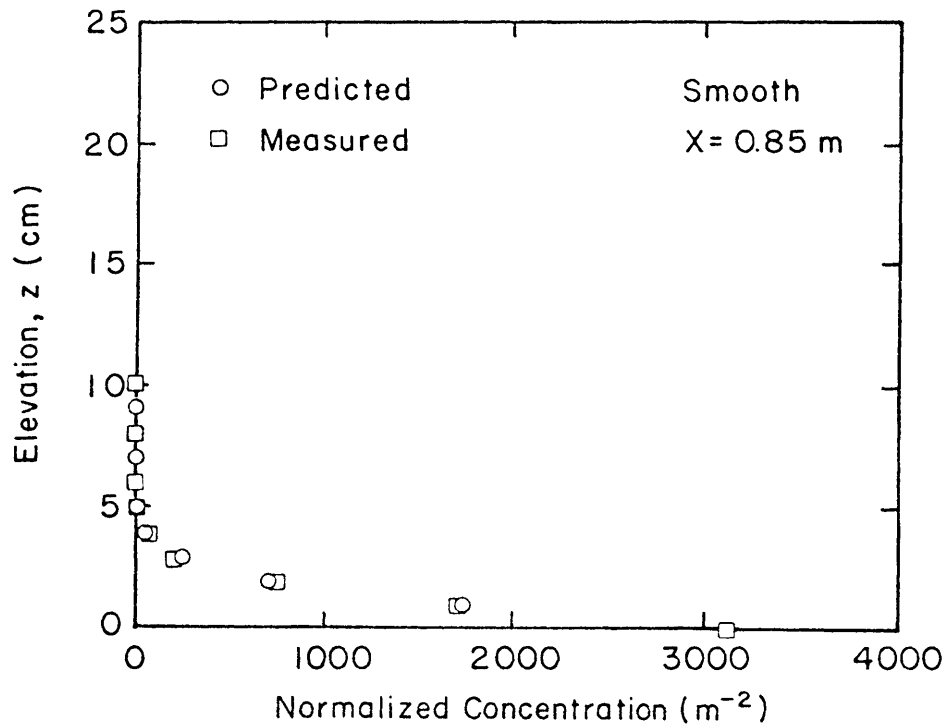
Figure 4-18. Velocity concentration profiles for a ground-level source in stable flow.

5.0 UNSTABLE FLOW

5.1 Velocity Field over the Smooth Floor

Measurements of the temperature profiles at the position of the source (x = 0) and at x = 2.80 m and x = 6.05 m, are shown in Figure 5-1.

The measurements reveal an inversion of the temperature gradient at a height h above the ground. The height h is slightly increasing in the direction of the flow, from h = 0.55 m at x = 0 to h = 0.85 m at x = 6.05 m. The value h = 0.75 m, at x = 2.80 m appears to be a representative height of the unstable layer for the smooth-floor configuration. Using this value, a specific heat flux $w'\theta' = 0.63°K\text{-}m/sec$ and an average temperature $\theta = 283°K$, the representative value of the convective velocity is estimated to be approximately $w^* = 0.25$ m/sec.

The measured mean velocity distributions u(z) at x = 0, x = 2.80 m and x = 6.05 m are presented in Figure 5-2. A mild horizontal non-homogeneity is observed indicating, as shown by Antonia and Luxton (1972), that the boundary layer as a whole recovers very slowly after a rough-to-smooth change in the surface roughness. Nevertheless, both the horizontal and the vertical nonhomogeneities in the convective layer are mild and the dimensionless distance $X = xw^*/(\bar{U}h)$ in this layer may be calculated with sufficient accuracy using the average value $\bar{U}$ = 1.90 m/sec. According to Antonia and Luxton, the shear stress after a rough-to-smooth change in the surface roughness, increases throughout the central region of a boundary layer instead of monotonically decreasing. On the other hand, the surface shear stress is drastically reduced, then increases at a lower rate, with x. The shear stress measurements at x = 0, 2.80 m and 6.05 m which are presented in Figure 5-3 show similar behavior.

74

The average value of the shear velocity in this region is estimated from Figure 5-3 to be $u^* = 0.085$ m/sec, which implies that the Monin-Obukhov length for this flow was on the order of 0.07m and $-h/L \sim 10.7$. The Monin-Obukhov length, L, which is a measure of the thickness of the surface layer where the shear stress plays a dominant role, is defined as

$$L = -(u^*)^3 \; \theta/k \; g \; \overline{w'\theta'} \quad . \tag{5-1}$$

Since in this experiment the shear stresses in the central region of the boundary layer were slightly larger than the shear stress at the wall, it is plausible that the surface layer extends beyond the above esti-mated height, or in other words, the effective value of $-h/L$ is smaller.

The measured normalized vertical velocity fluctuations, $w'^2/(w^*)^2$, are plotted in Figure 5-4. The values for the flow over the smooth floor vary between 0.1 to 0.3 and are of the same order of magnitude as the field measurements in the Ashchurch and Minnesota experiments (see Lamb, 1981, Figure 4.18).

It may be concluded that although the unstable boundary layer developed in the wind tunnel over the smooth floor is not a perfect model of an ideal CBL, its major characteristics are typical of many real convective atmospheric boundary layers.

5.2 Velocity Field over the Rough Floor

The temperature distributions for this case are shown in Figure 5-5. The values of h at the different stations are slightly higher for this case and the representative value of h is estimated to be $h = 0.90$ m.

The mean velocity profiles, shown in Figure 5-6, indicate that the horizontal nonhomogeneity of the velocity field in this case is smaller, apparently because the relative change in the surface roughness was smaller. Distribution of shear stresses at the different stations, shown in Figure 5-7, are also more similar. Using these data, the average horizontal velocity for this flow is estimated to be $\bar{U} = 1.70$ m/sec and the average shear velocity is estimated to be $v* = 0.115$ m/sec. Thus, the convective velocity scale and the Monin-Obukhov scale for the flow over the rough floor are of the order of $w* = 0.28$ m/sec and $L = 0.16$ m. One may conclude that the added roughness increased the thickness of the surface layer and reduced the convective nature of the flow. The ratio $-h/L$ for this case is smaller than six and the vertical velocity fluctuations have also decreased, as seen from Figure 5-4.

5.3 Measured Concentration Field

More than 40 concentration profiles were measured in the study. Representative dimensionless vertical concentration profiles, $C(x,0,z)\bar{U}h^2/Q$ plotted versus z/h, are shown in Figures 5-8a through 5-8ℓ. The concentration profiles, Figures 5-8a,b,c, measured immediately downwind from the ground-level source have an approximate Gaussian shape. The profiles are, however, better described by the function

$$C = C(0) \exp \left[-\beta(z/\lambda_z)^s \right] , \qquad (5-2)$$

where $\beta = \ell n(2)$ and s is a power smaller than 2. The calculated values of s are 1.21, 1.31 and 1.41 and 1.39 at $x = 0.45$, 0.85, 0.135 and 1.95 m from the source for a smooth boundary. Figures 5-8d,e,f indicate that the maximum concentrations at $x = 2.8$ m, $X = 0.49$m, $x = 3.9$ m, $X = 0.68$, and at $x = 6.05$ m, $X = 1.06$, are no longer at ground-level.

The heights of the maximum concentration of the vertical profiles downwind from the elevated sources, Figure 5-8g, are initially at the height of the source, but rapidly approach the ground. Figure 5-8h shows for example, that it is impossible to tell whether the concentration profile at X = 0.49 and z^s/h = 0.133 is due to an elevated or a ground-level source. This pattern is also observed in neutral flow, however, the vertical profile at X = 1.06, Figure 5-8i, shows that the position of the maximum concentration is beginning to rise above the ground.

The same pattern is observed for the unstable flow above the rough boundary.

The variation of the measured maximum ground-level concentration $C(x,0,0)\bar{U}h^2/Q$ is plotted in Figure 5-9 for the smooth boundary and in Figure 5-10 for the rough boundary. As seen from these figures, the ground-level concentrations from an elevated source exceed after a certain distance the ground-level concentrations from lower-level sources. Comparison with Figure 5-11 shows a very close similarity between the calculated and the measured diffusion pattern, and the dimensionless concentration values in the two figures are of the same order of magnitude, although not identical. Comparison of the rough and smooth floors data shows that the increased shear has slightly decreased the maximum ground-level concentration for the source at z^s/h = 0.133 and has slightly modified the values of the dimensionless concentrations at different points, however, the basic pattern of diffusion has not changed.

Figures 5-12 and 5-13 show the cross-wind spread of the plume and its dependence on the height of the source. It can be seen that σ_y is larger for ground-level sources, as predicted by Lamb (1979). The

measured values of σ_y/h are, however, larger than the calculated values (see Lamb, 1981, Figure 5.3).

Figure 5-14 compares the measured values of the cross-wind spread over the smooth floor with the Prairie Grass data and the results of Deardorff and Willis (1975) and Lamb (1979). It appears that the wind-tunnel measurements at small values of $xw^*/(h\bar{U})$, give larger values of σ_y/h. However, they are consistent with some Prairie Grass measure-ments. At larger distances the wind-tunnel data is in better agreement with the few available field measurements.

The difference between the values of σ_y/h for short distances could be due to the effect of the surface layer present in the wind-tunnel experiment.
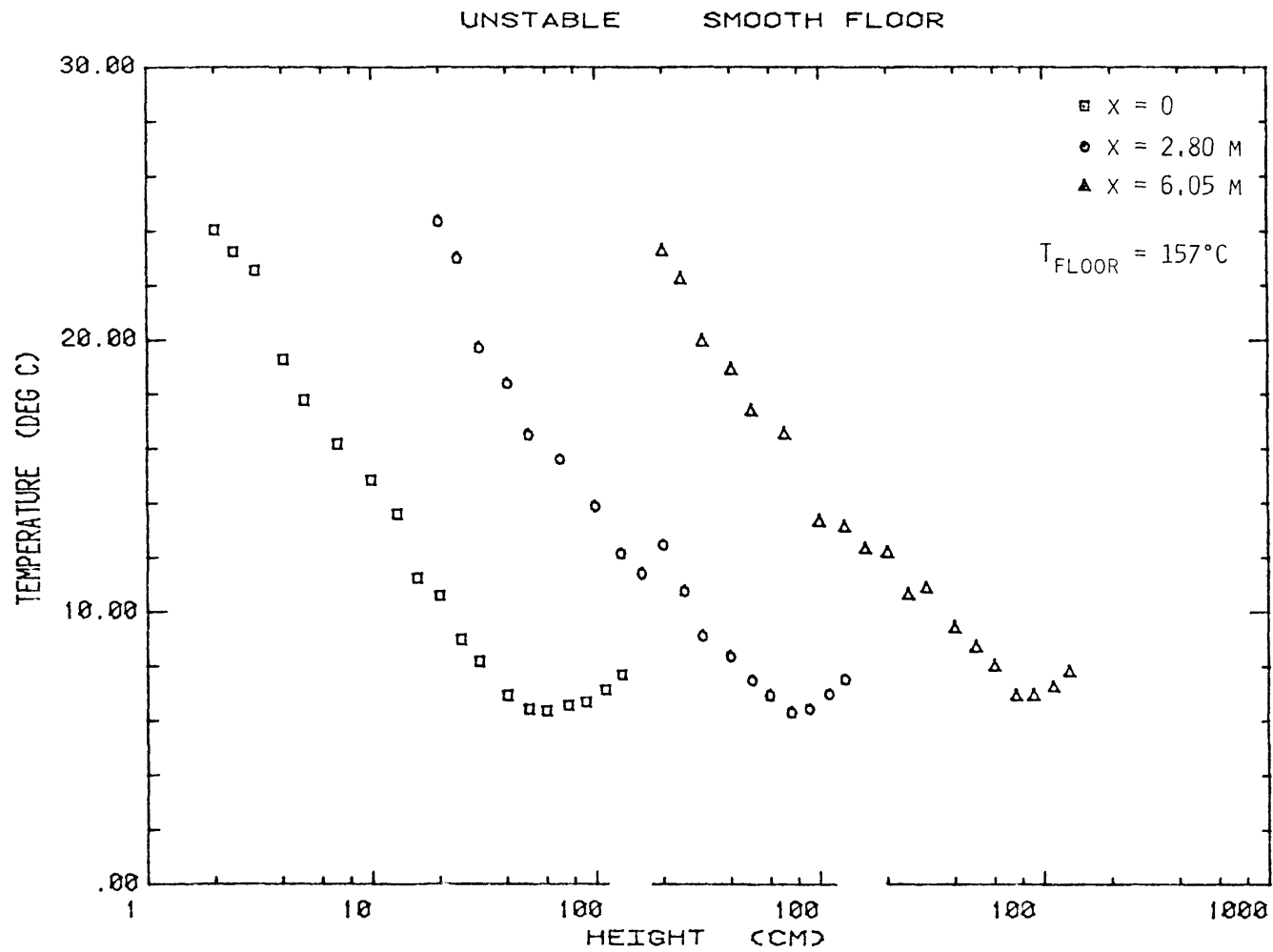
Figure 5-1. Temperature profiles, smooth floor.

79
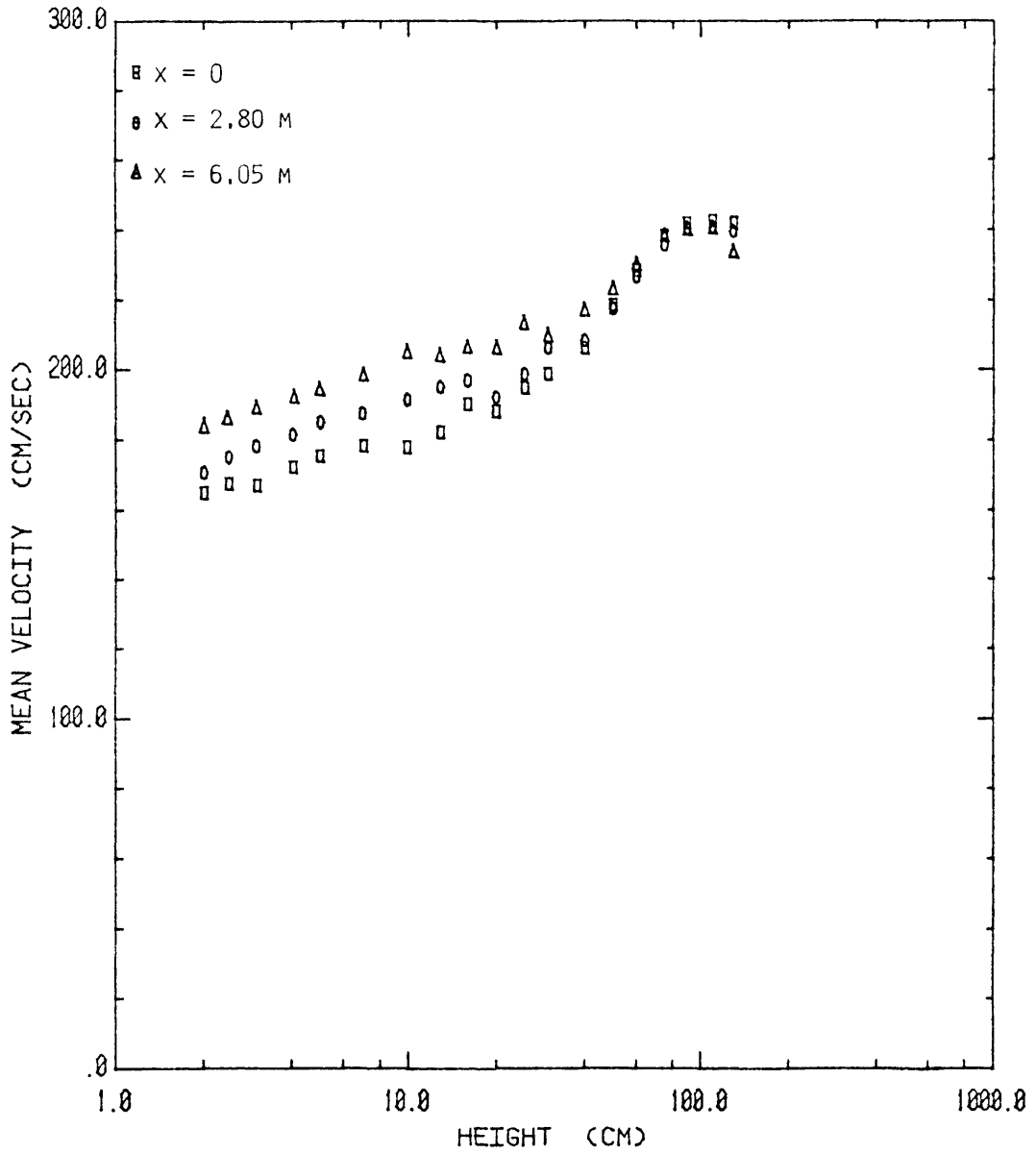
Figure 5-2. Mean velocity profiles, smooth floor.
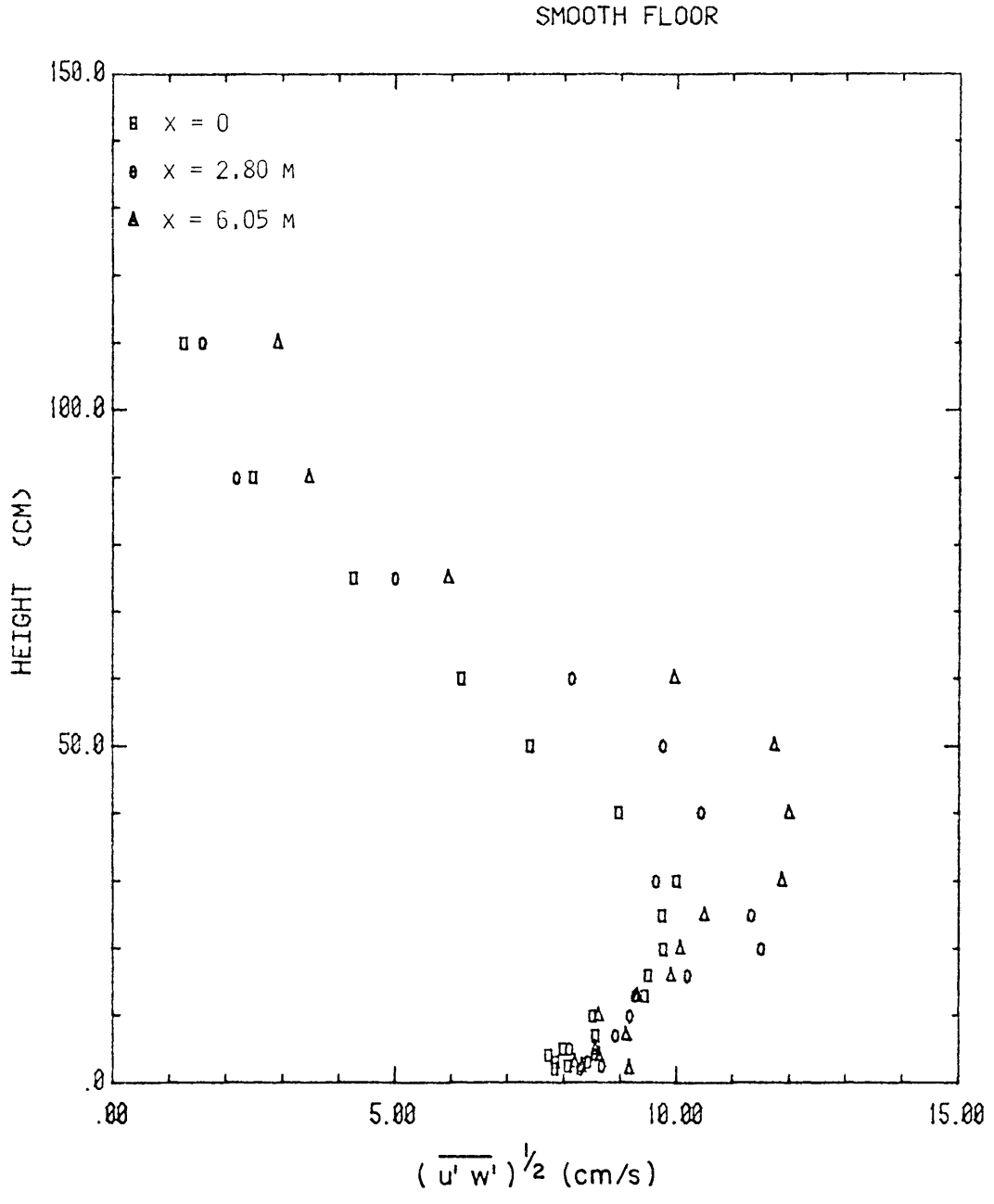
Figure 5-3. Vertical distribution of shear stress $(\overline{u'w'})^{\frac{1}{2}}$, smooth floor.
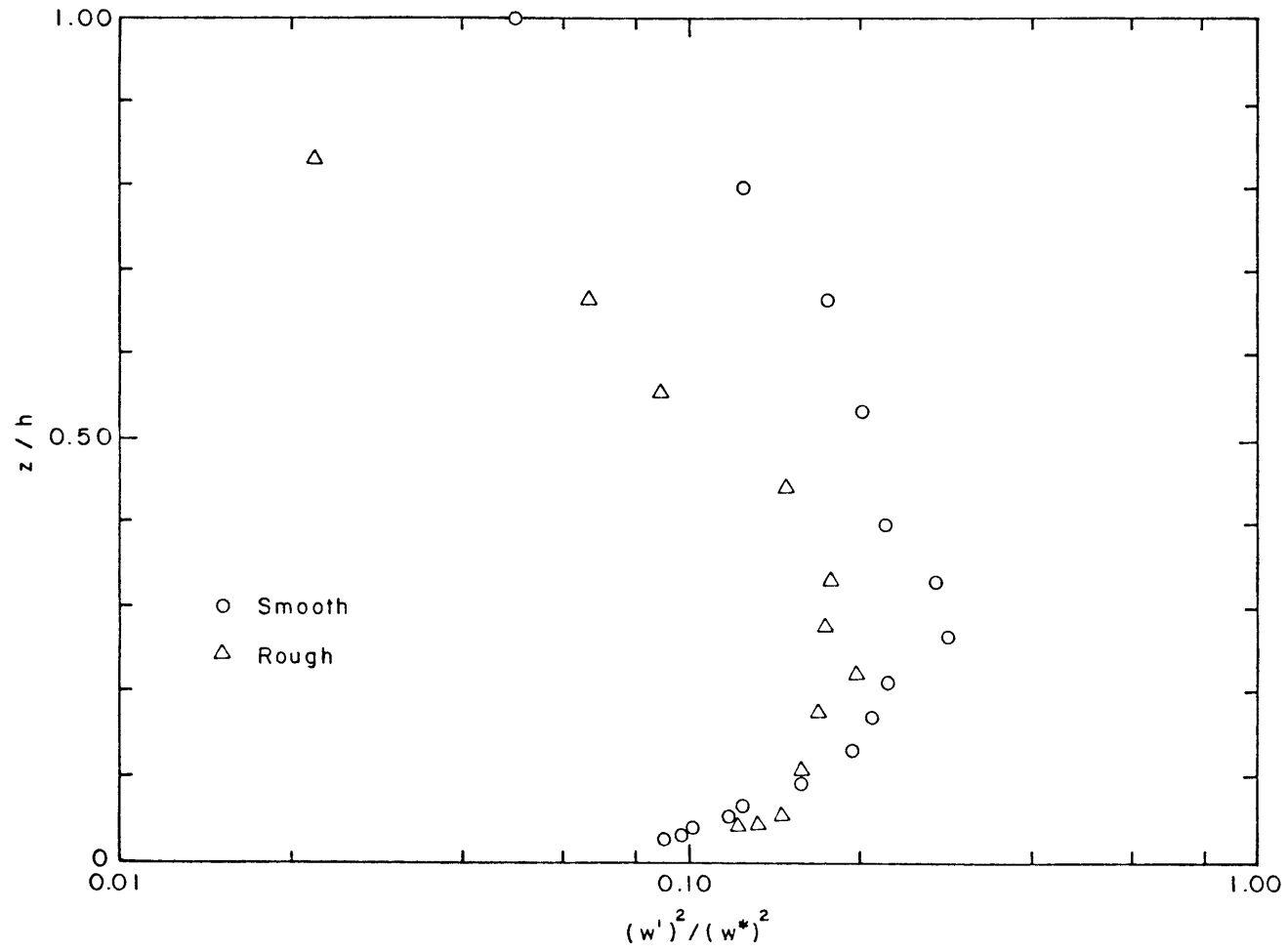
Figure 5-4. Vertical distribution of the vertical velocity fluctuations $(w')^2/(w^*)^2$.
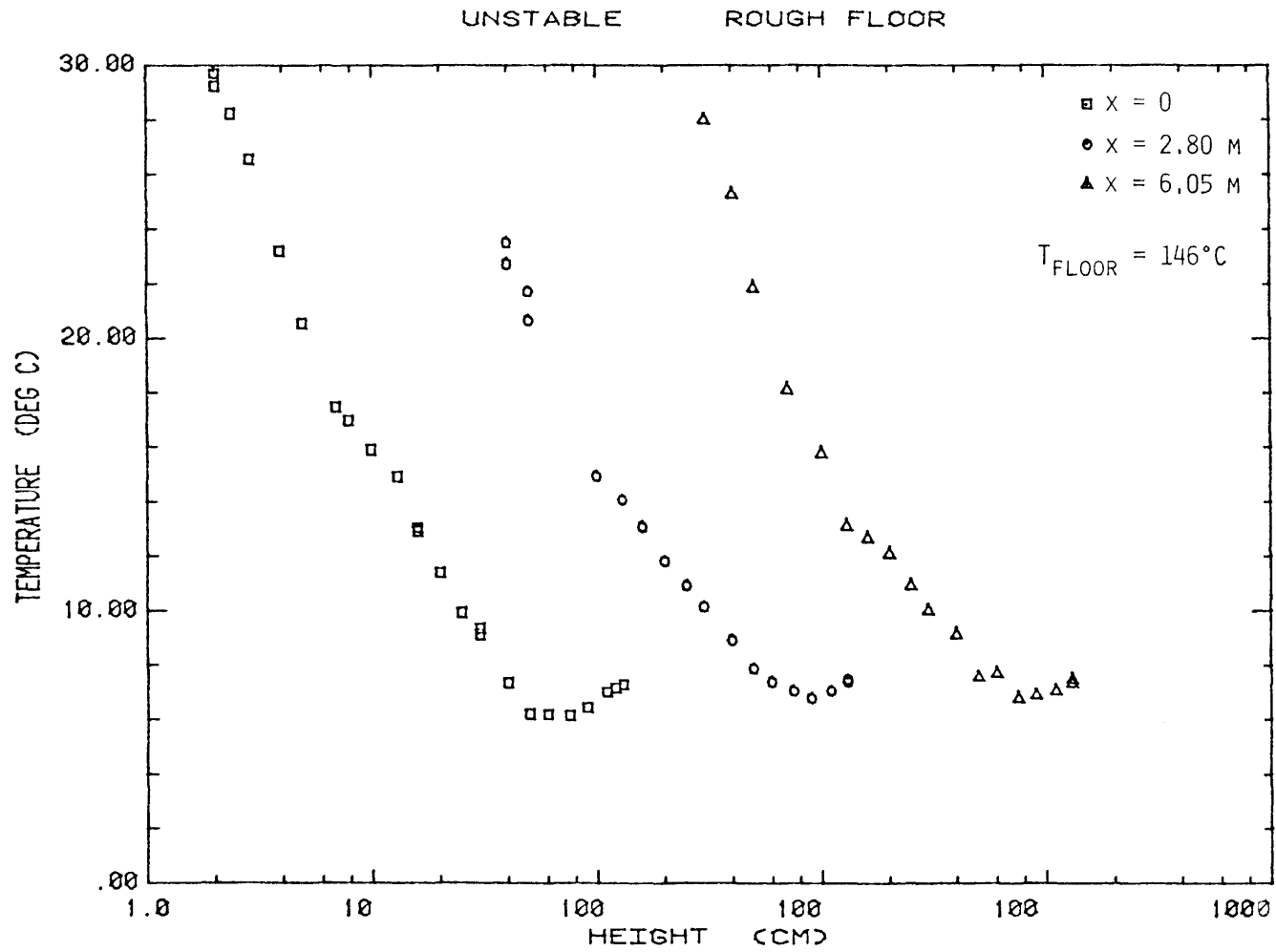
Figure 5-5. Temperature profiles, rough floor.
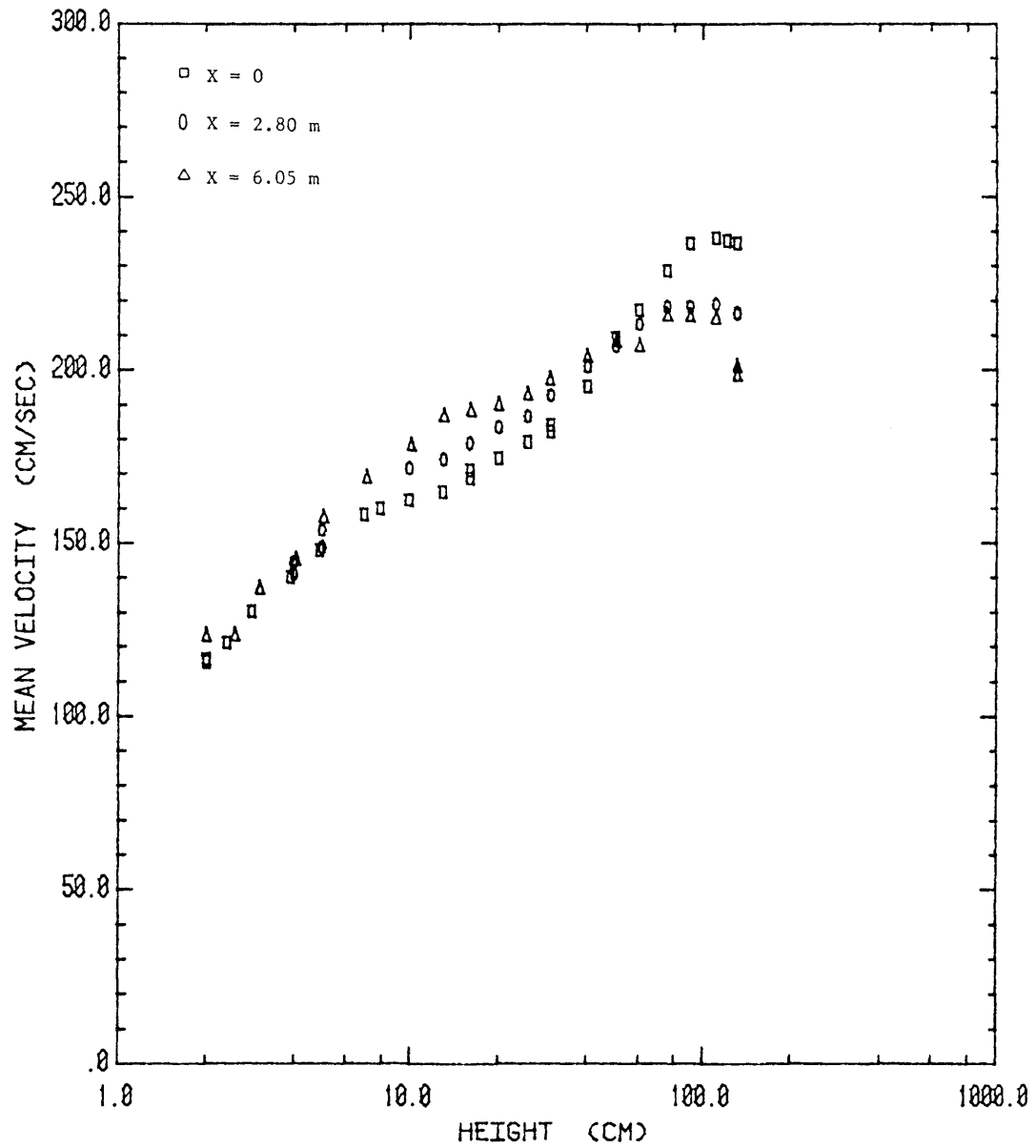
Figure 5-6. Mean velocity profiles, rough floor.
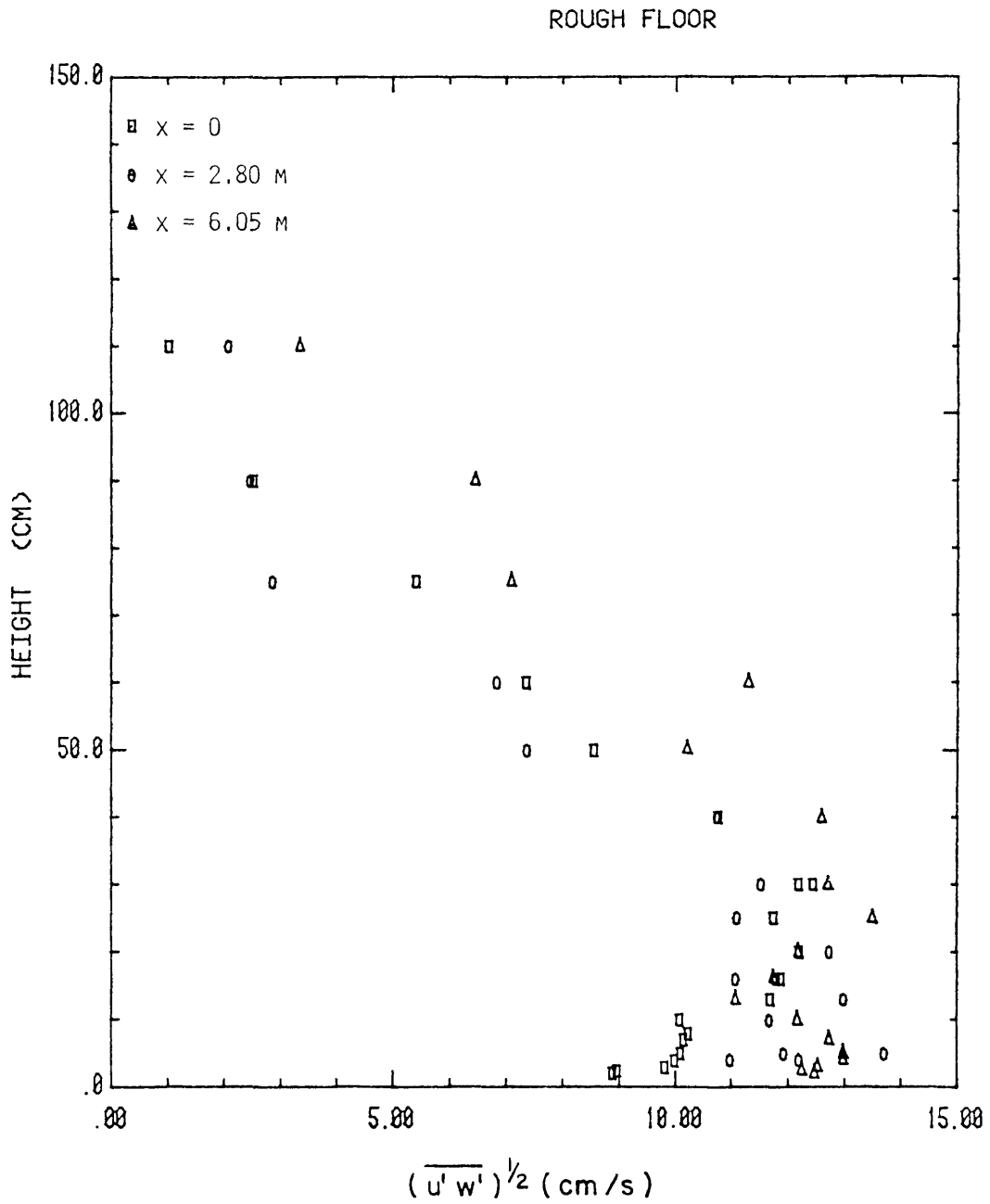
Figure 5-7. Vertical distribution of shear stress $(\overline{u'w'})^{\frac{1}{2}}$, rough floor.
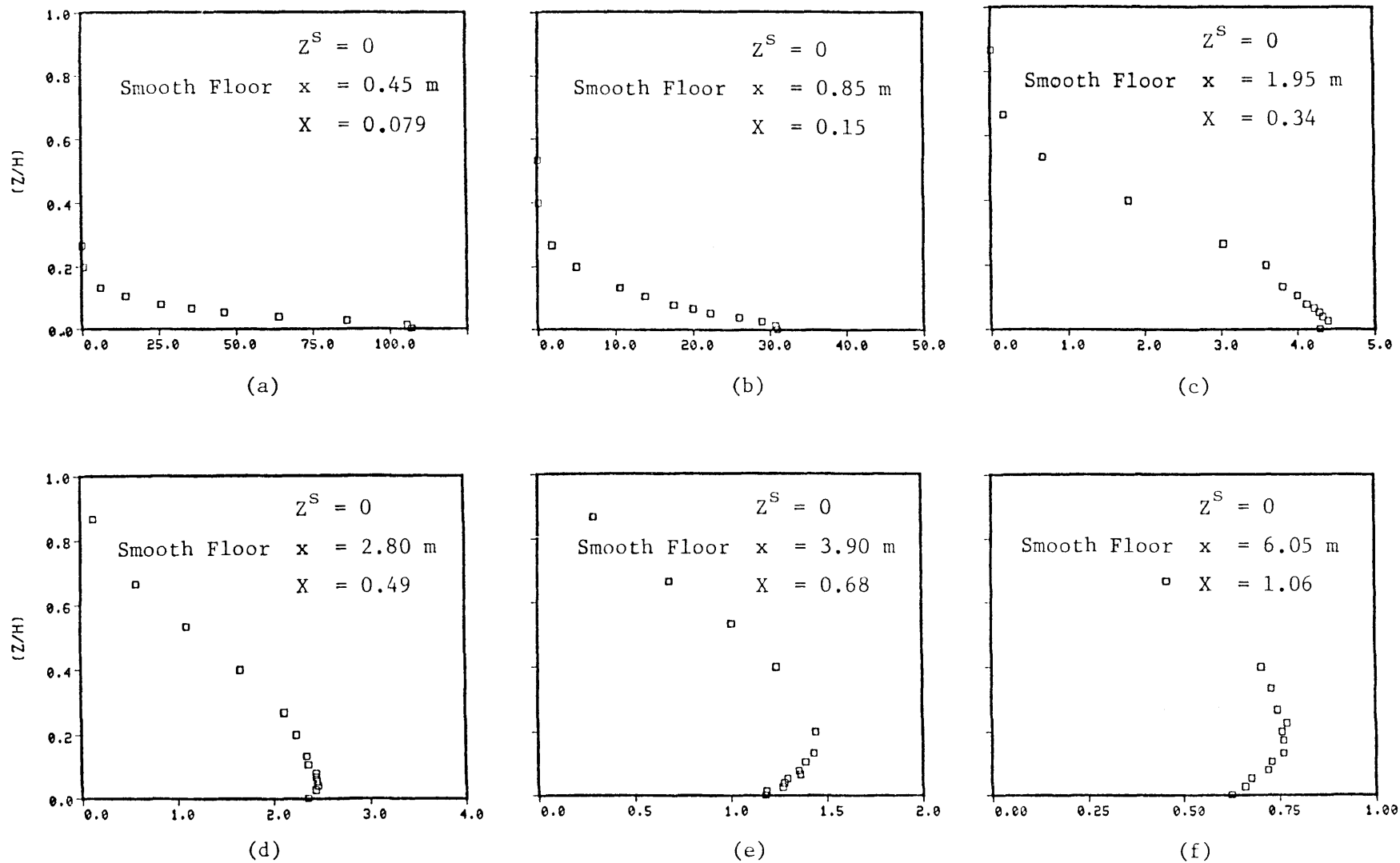
Figure 5-8. Selected dimensionless concentration profiles $C(x,0,z)$ $\bar{U}h^2/Q$, for smooth floor $z^S = 0$
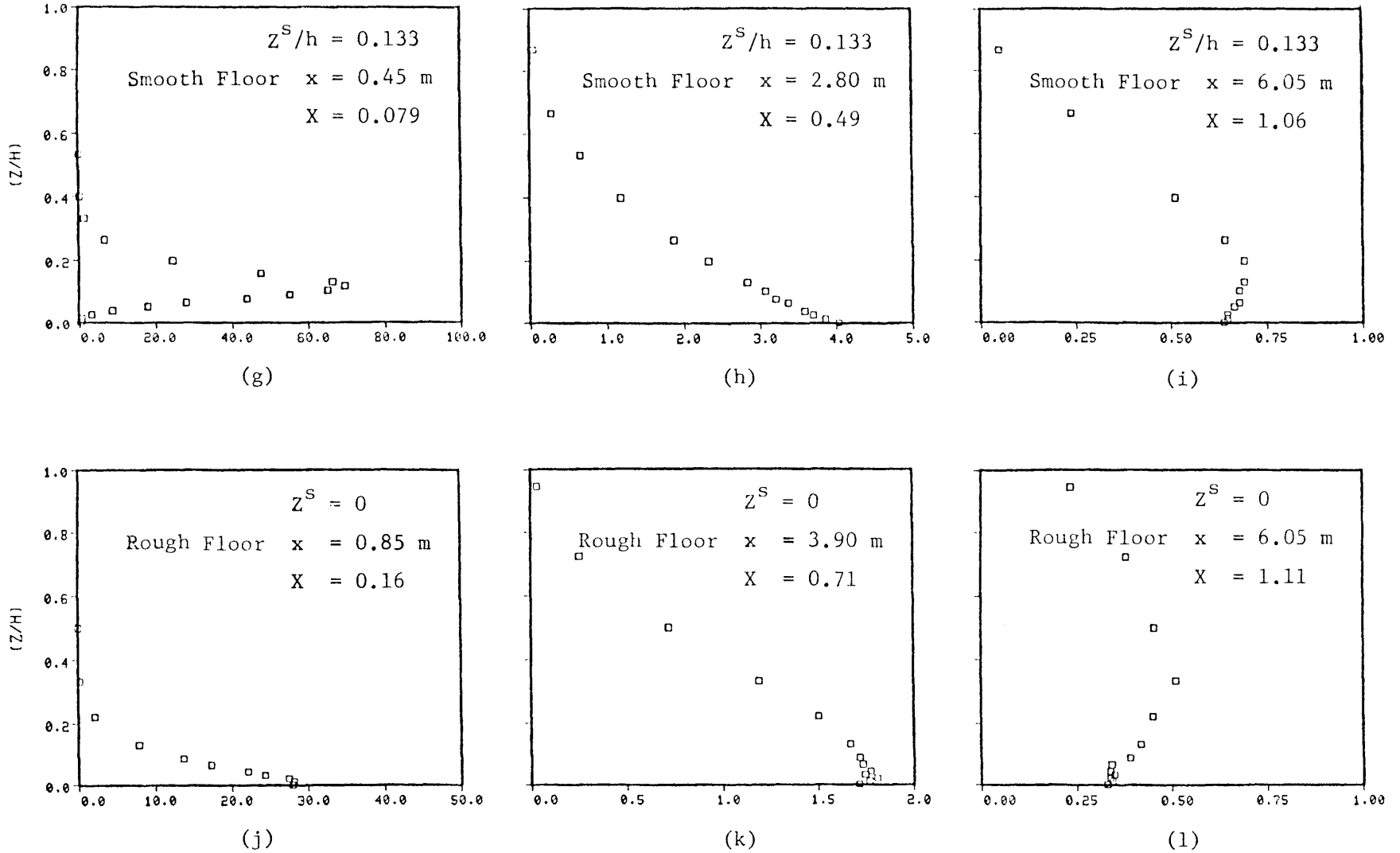
Figure 5-8. Selected dimensionless concentration profiles $C(x,0,z)$ $\bar{U}h^2/Q$, for smooth floor (SF) $z^s/h = 0.133$ and rough floor (RF) $z^s = 0$ (continued).
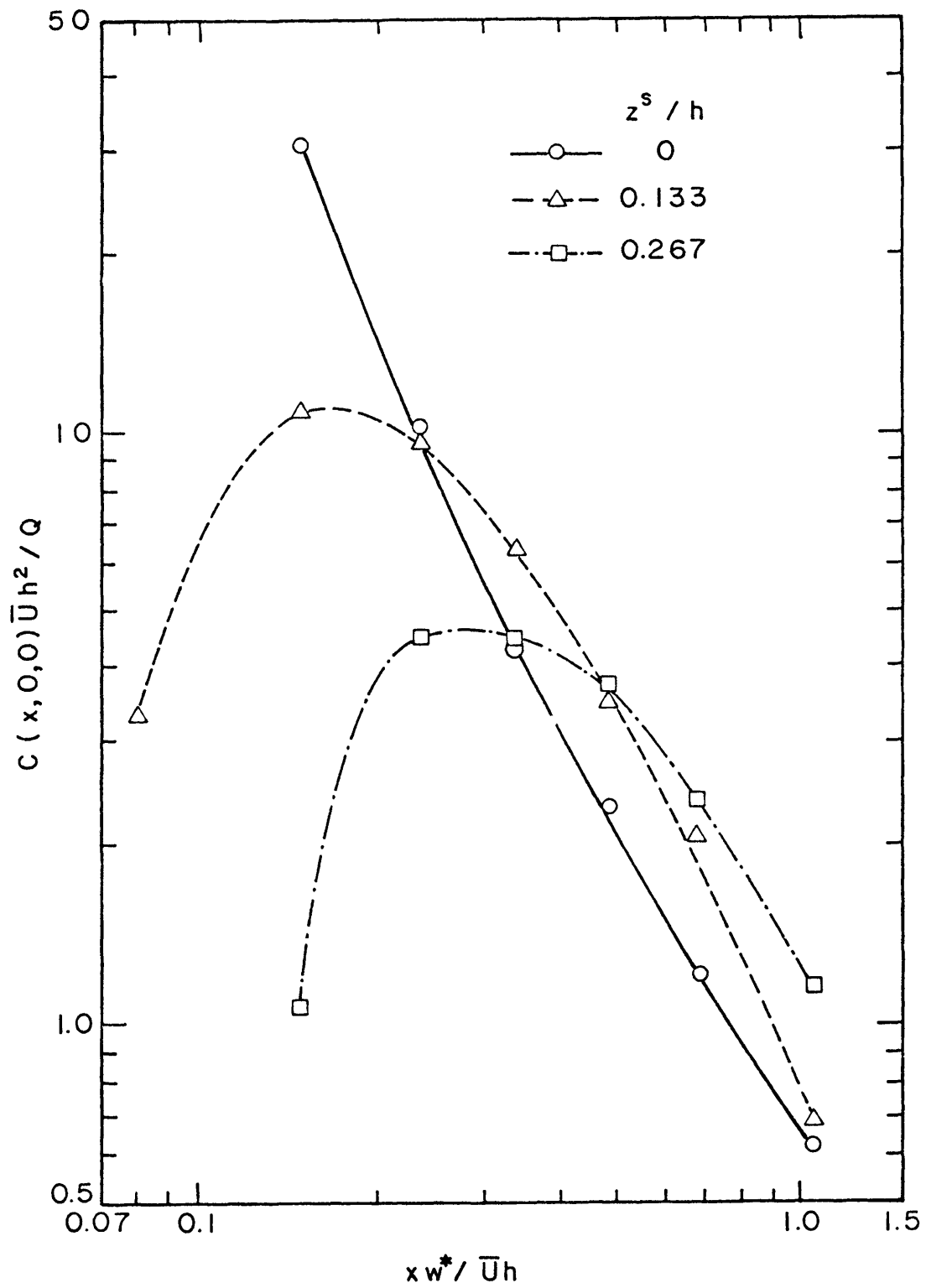
Figure 5-9. Dimensionless maximum ground-level concentrations, smooth floor.
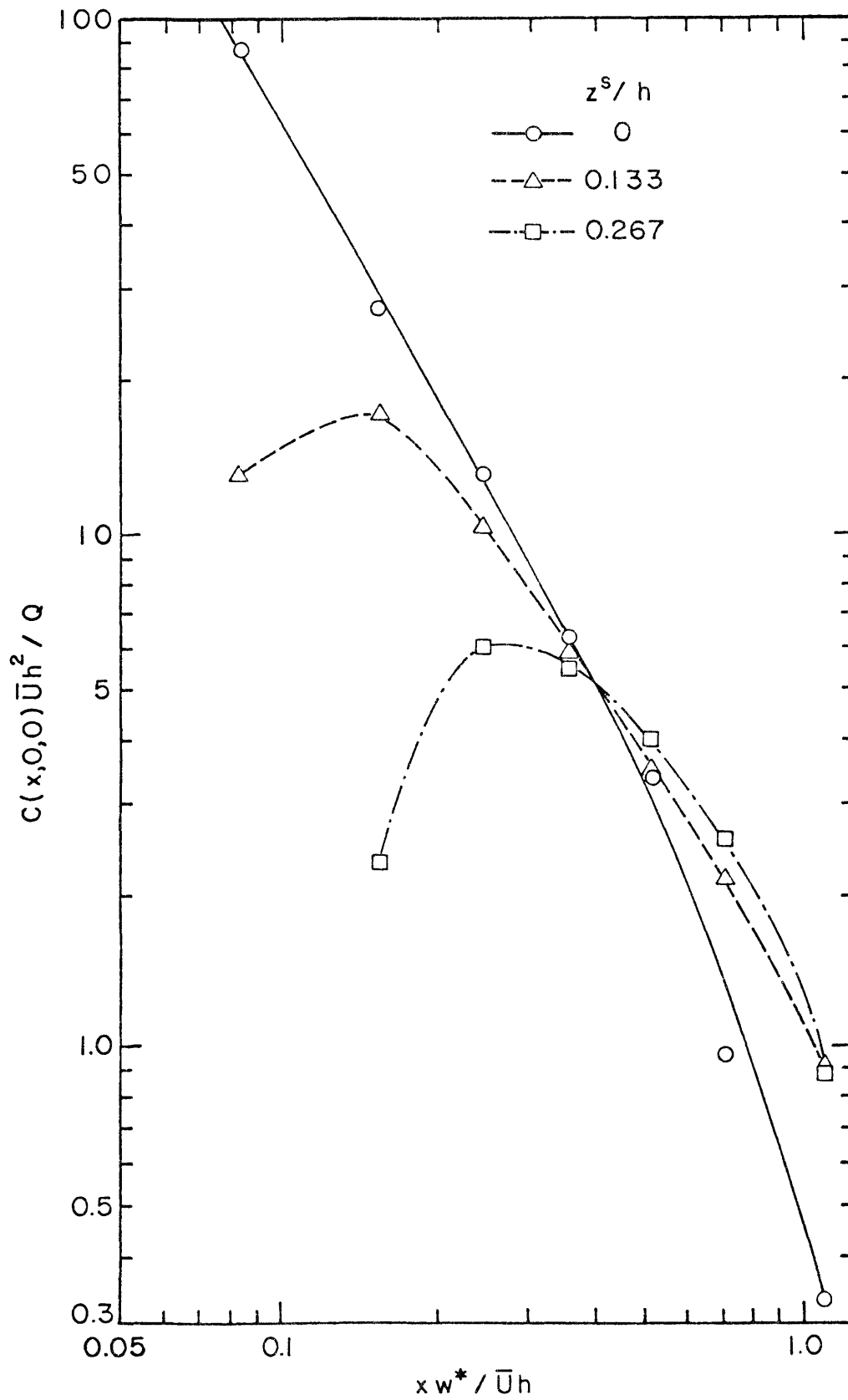
Figure 5-10. Dimensionless ground-level concentrations, rough floor.
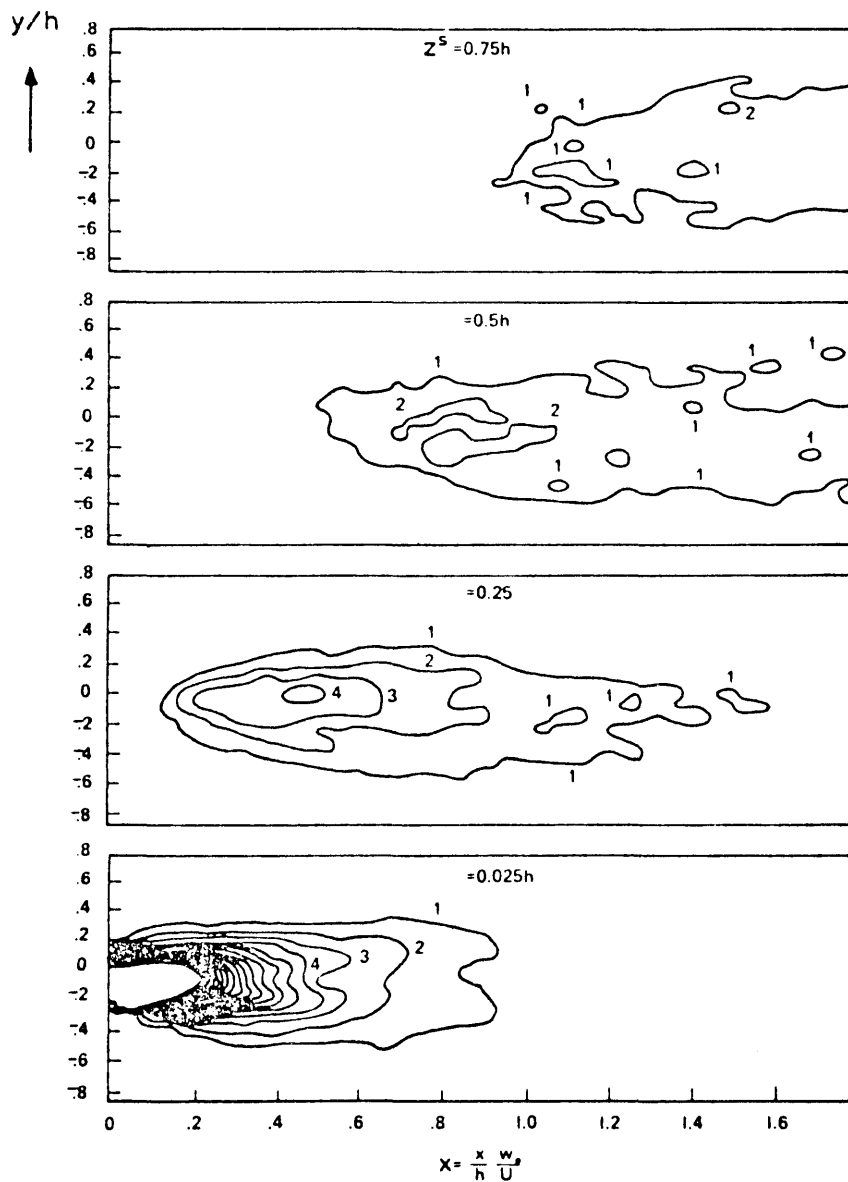
Figure 5-11. Calculated non-dimensional ground-level concentration $C(x,y,0)\bar{U}h^2/Q$ for point sources of heights $z^s = 0.75$ h, 0.5 h, 0.25 h and 0.025 h (Lamb, 1979).
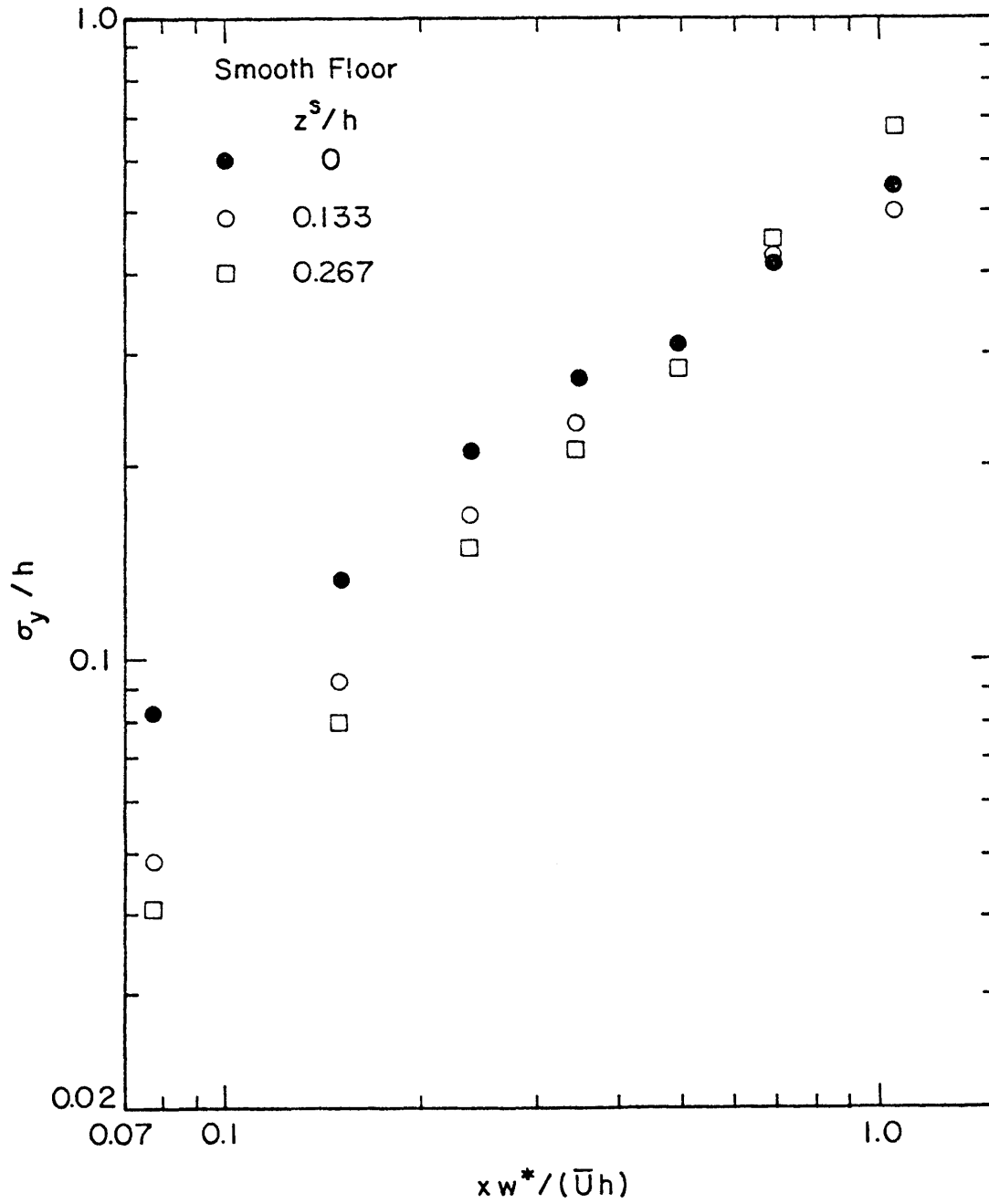
Figure 5-12.   Cross-wind spread, smooth floor.
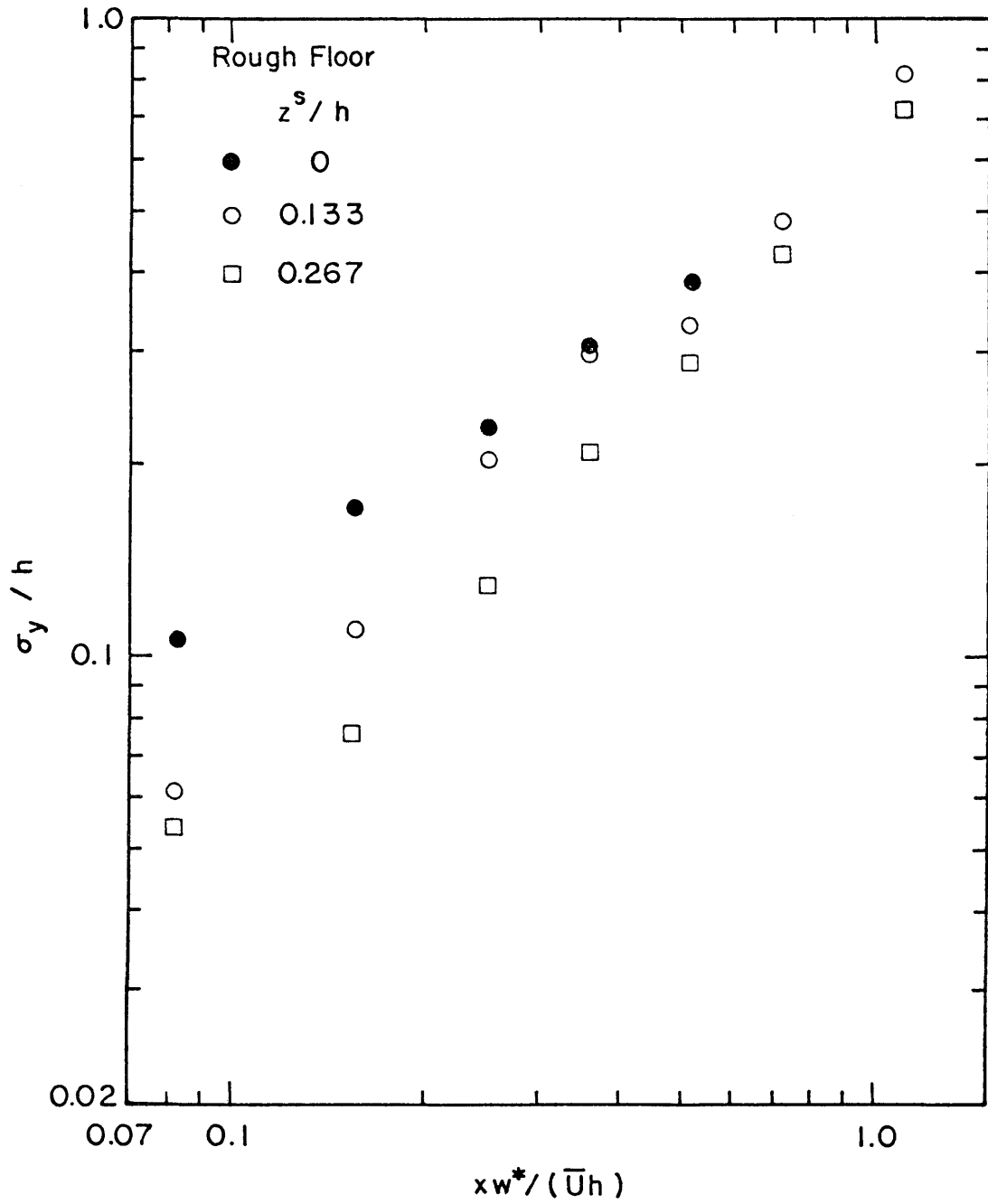
Figure 5-13. Cross-wind spread, rough floor.
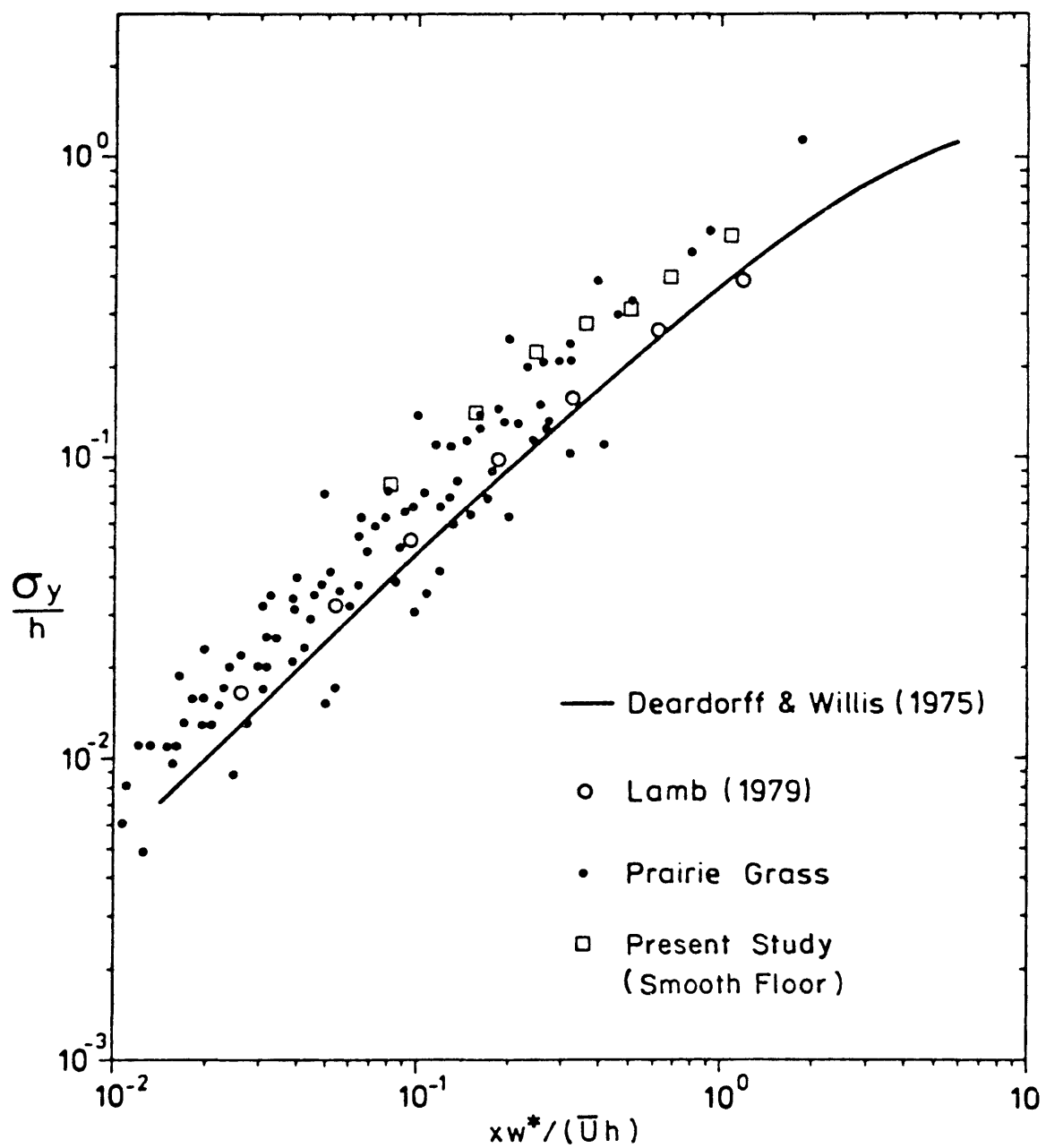
Figure 5-14. Cross-wind spread of plumes from ground-level sources.

6.0 CONCLUSIONS AND COMMENTARY

Measurements of mean and turbulent velocities and temperatures over smooth and rough floors for stable, neutral and unstable flows in the MWT at CSU were found to be similar to those measured in many typical boundary layers corresponding to the appropriate stability.

The wind-tunnel stable boundary layer flows had a Monin-Obukhov length-scale of approximately 16 cm for the smooth floor and 25 cm for the rough floor. In the unstable boundary layer, the corresponding length scales were 7 cm and 16 cm respectively.

Diffusion patterns in the neutral boundary layer from a ground-level source were similar to those found in the Marchwood Engineering Laboratory experiments by Robins (1978), and these measurements were also in good agreement with Pasquill's diffusion estimates. Diffusion data in the vertical plane from the elevated source, for both surface roughnesses considered, showed that near the source the maximum con-centration occurred at the height of the source, then it rapidly approached the ground with increasing distance from the source.

In stably stratified turbulent flows, wind-tunnel data showed that with increasing distance from the source, vertical diffusion of the gas was much less than under neutral stratification. This is easily ex-plained since increasing vertical displacement in stable flows requires a steady input of energy, assuming that the density of the diffusing gas remains unchanged. Hence in stable flows, with increasing distance from the source, the plume center remains at approximately a constant height, equal to the release height of the gas.

The patterns of diffusion from ground-level and elevated sources in unstable flows, for both the smooth floor and the rough floor, were

similar to that found in the water-tank experiment of Deardorff and Willis (1975) and in numerical models. The measurements confirmed the predicted rise of plumes from ground-level sources after a travel time on the order of $0.5 \ h/w^*$ and an initial rapid descent of plumes from elevated sources. They also showed that after a certain distance from the source, ground-level concentrations from an elevated source were higher than ground-level concentrations from sources at lower elevations.

The measured cross-wind spreads, σ_y, were found to be in agreement with the Prairie Grass measurements. The measurements confirmed the numerical predictions, that σ_y is larger for ground-level sources than for elevated sources.

Thus, it may be concluded that the wind-tunnel measurements confirm the predicted unique features of diffusion in a CBL, which cannot be described by a simple Gaussian model or by a conventional Eulerian type mass balance differential equation. They also indicate the CBL diffusion pattern can be found for values of $-h/L$ on the order of 6 which are often encountered in the atmosphere. The effect of surface roughness on the diffusion pattern is found to be small.

The work exhibits the value of physical simulations in wind tunnels, which can be used to model stratified flows with much more complicated boundary conditions as well as diffusion of buoyant and negatively buoyant flows in ASL. Such problems cannot easily be simulated numerically (Lamb, 1981).

7.0 ACKNOWLEDGEMENTS

The research documented in this report was performed within the Fluid Dynamics and Diffusion Laboratory (FDDL), Fluid Mechanics and Wind

Engineering Program, Colorado State University, under a contract (No. DAA 11-82-K-0004) with the United States Army Armament Research and Development Command (ARRADCOM). Initial formulation of the research program was accomplished with guidance by Dr. Edward W. Stuebing, Chemical Systems Laboratory, ARRADCOM, and Dr. J.R. Brock, Department of Chemical Engineering, University of Texas (Austin).

8.0 REFERENCES

1. Antonia, R. A. and R. E. Luxton (1972), "The Response of a Turbulent Boundary Layer to a Step Change in Surface Roughness." Part 2. Rough-to-smooth. J. Fluid Mech., part 4, pp. 737-757.

2. Barad, M. L. and D. A. Haugen (1959), "A Preliminary Evaluation of Sutton's Hypothesis for Diffusion from a Continuous Point Source," Journal of Meteorology, No. 16, pp. 12-20.

3. Barad, M. L. and J. J. Fuquay (1962), "The Green Glow Diffusion Program," Geophysical Research Paper No. 73, Vols. 1 and 2.

4. Cermak, J. E. (1971), "Laboratory Simulation of Atmospheric Boundary Layer," AIAA Journal, Vol. 9, No. 9, pp. 1746-1754.

5. Cermak, J. E. (1981), "Wind Tunnel Design for Physical Modelling of Atmospheric Boundary Layer," Journal of the Engineering Mechanics Division, ASCE, Vol. 107, No. EM3, Proc. Paper 16340, pp. 623-642.

6. Cermak, J. E. (1982), "Simulation of the Natural Wind," Preprint 82-518, ASCE Convention and Exhibit, New Orleans, Louisiana.

7. Deardorff, J. W. and G. E. Willis (1975), "A Parameterization of Diffusion into the Mixed Layer." J. Appl. Meteo., 14, pp. 1451-1458.

8. Lamb, R. G. (1979), "The Effects of Release Height on Material Dispersion in the Convective Planetary Boundary Layer." Preprint vol. AMS Fourth Symposium on Turbulence, Diffusion and Air Pollution, Reno, Nevada.

9. Lamb, R. G. (1979), "A Numerical Simulation of Dispersion from an Elevated Point Source in the Convective Planetary Boundary Layer." Atmos. Environ., 12, pp. 1297-1304.

10. Lamb, R. G. (1981), "Diffusion in the Convective Boundary Layer," (from Nieuwstadt, F. T. M. and H. Vandap, Atmospheric Turbulence and Air Pollution Modelling, D. Reidel Publishing Company, 1982).

11. Pasquill, F. (1974), Atmospheric Diffusion, 2nd ed., New York, John Wiley and Sons.

12. Robins, A. G. (1978), "Plume Dispersion from Ground-Level Sources in Simulated Atmospheric Boundary Layers." Atmospheric Environment, 12, pp. 1033-1044.

APPENDIX A

WIND-TUNNEL SIMULATION OF PARTICLE PLUMES

IN THE ATMOSPHERIC SURFACE LAYER

TABLE OF CONTENTS

LIST OF SELECTED SYMBOLS

Symbol	Definition	Dimension
A	cross-sectional area of source	L^2
d	diameter of particles	L
D	downward shift of plume	L
F	buoyancy flux	L^4T^{-3}
g	acceleration due to gravity	LT^{-2}
h	height of source	L
ΔH	plume rise	L
Iz	constant of Equation (3)	-
ℓ	scale of turbulent eddies	L
Q	volumetric discharge rate	L^3T^{-1}
r	relative fall velocity of particles = Vg/U	-
r_o	radius of plume at source	L
s	characteristic response length of particle	L
t	diffusion time	T
U	characteristic mean velocity of air	LT^{-1}
$\bar{U}$	mean velocity of air at effective stack height	LT^{-1}
V	volume	L^3
Vg	particle fall velocity	LT^{-1}
w	exit velocity of plume	LT^{-1}
x,y,z	a right-hand coordinate system with origin at the base of the simulated point source	L
x_m	position of maximum deposition rate of particles	L
z_o	aerodynamic surface roughness length	L
β	ratio of Lagrangian/Eulerian time scale	-
ρ	mass density of plume	ML^{-3}

λ_L model length scale   -

λ_U model velocity scale   -

σ_z standard deviation of the vertical plume spread   L

τ particle relaxation time   T

L - length
T - time
M - mass

WIND-TUNNEL SIMULATION OF PARTICLE PLUMES IN THE
ATMOSPHERIC SURFACE LAYER

One of the objectives of the first year's program was to explore possible methods of modelling the dispersion of stable aerocolloidal particle-plumes in the wind tunnel and to design (on the basis of this investigation) the second year's research program (Tasks 2-A and 2-B).

The results of this investigation are presented herein.

1.   Classification of Heavier-than-Air Particle Plumes

The following analysis focuses, initially, on steady-state, stable, particle-plumes (PP) from ground-level, or elevated sources. Two parameters which significantly affect the behavior of such plumes are: the relative fall velocity of the individual particles $r = V_g/U$, where V_g is the particle fall velocity and U the characteristic mean velocity of the air; and the relative negative buoyancy of the air-particle mixture.

Several types of particle-plumes which can be classified, according to these two parameters follow.

> Particle-plumes with both negligible relative particle fall velocity and negligible plume buoyancy. The dispersion of such PP is identical to that of passive tracer plumes and, as shown in previous investigations (Cermak, 1981 and Snyder, 1981), they can be satisfactorily simulated in meteorological wind tunnels.
>
> Local concentrations of the tracer gas in such simulations are proportional to the spatial probability density function of particles dispersing from the same source,

and local flux values $\vec{cu} \cdot \vec{ds}$ are proportional to the probability of particles passing through the area $\vec{ds}$.

This limiting case will be designated as the Passive Reference Plume (PRP). Its dispersion characteristics at different categories of atmospheric stability and surface roughness were simulated in Task 1-B of the project.

When the concentration of particles is increased, the plume may be exposed to buoyancy effects, even though the relative fall velocity of the individual particles remains negligible. (This study refers only to negatively buoyant plumes, although it is theoretically possible to obtain buoyant plumes using lighter-than-air particles.) Such plumes behave like negatively buoyant gas plumes and, as shown in previous investigations by Snyder (1981) and Poreh (1981), they can be fully simulated in meteorological wind tunnels by keeping the dimensionless buoyancy flux constant in the model and atmosphere.

This type of plume is designated as a Buoyant Plume (BP). Its dispersion characteristics are scheduled for investigation during the second year of the project (Task 2-A).

It is not easy to produce large buoyancy effects in the atmosphere with large concentrations of particles. However, they may be produced from a mixture of particles and a carrier gas whose density is less than that of air.

A different limiting case is obtained when the concentration of the particles in the plume remains small. However, the relative fall velocity of the individual particles is no longer negligible. Each particle will experience a gravity

103

force which causes a mean downward motion and an early deposit on the ground. No interaction between particles is expected in this case and motion of the particles is not expected to modify the atmospheric flow. Thus, the time averaged plume characteristics are also equal to the ensemble average of a single particle dispersion. This type of plume will be referred to as a Heavy Particle Plume (HPP). Only monodispersed HPP should be investigated and characterized, whereas the PRP and the BP could be composed of different size particles, so long as the relative fall velocity of the largest size particles remains negligible.

When only a small fraction of a polydispersed particle-plume has a non-negligible relative fall velocity, that fraction will disperse as a HPP, whereas the rest of the particles will disperse as a PRP. When the rest of the plume behaves as a BP, modifications to the velocity field may occur, particularly near the source, and the dispersion of that fraction, which is affected by the velocity field, will differ from that of the HPP. This is called an HPP/BP combination.

Figure A-1 provides a graphic relationship of the four defined particle-plume regimes in terms of relative fall velocity (V_g/U) and dimensionless buoyancy flux ($F/(xu^3)$ x 10^6).

2. Required Relative Particle Fall Velocities

The properties of an HPP depend on the relative particle fall velocity, r. When r is small, the buoyancy effect, which distinguishes the HPP from the PRP, will not be detectable. Thus it is of

primary interest to estimate the relative fall velocities at which the effect can be detected.

Figure A-2 shows the effect of a 0.4 σ_z downward shift of a Gaussian plume on the vertical concentration distribution. It appears from the figure that positive identification of the differences between HPP and PRP characteristics require that the downward shift, D, satify the inequality

$$D \geq 0.4 \ \sigma_z \ . \tag{A-1}$$

The downward shift of the plume is expected to be of the order of

$$D \sim V_g \cdot t = V_g \ x/U, \tag{A-2}$$

where t is the diffusion time and U is the average velocity of the plume, taken as the velocity at the height of the source.

In order to satisfy Eq. 2 it is required that

$$r = V_g/U \geq 0.4 \ \sigma_z/x = 0.4 \ I_z \ . \tag{A-3}$$

The ratio I_z is a mild function of x. However, for our estimates, an average constant value of I_z may be used for each stability category. These values were estimated using modified estimates of σ_z (Pasquill, 1974, p. 375) for $z_o = 10$ cm at $x_p = 1$ km (approximately 1.66 m in the wind tunnel) and are shown in Table A-1, together with the calculated values of r . This table also contains the corresponding fall velocities and diameters of unit density spheres descending in still air at those fall velocities, assuming U = 2.0 m/s.

The downward motion of the HPP affects the distribution of the ground-level concentrations. Stewart (1967) compared his experimental data to estimates obtained from the "Classical Theory" and "Statistical Theory" methods for predicting the diffusion of particles. The

105

"Classical Theory" appears to predict more accurately the position of the maximum deposition rate of particles, x_m, whereas the "Statistical Theory" provies better estimates of the deposition rate.

Figure A-3, from Stewart (1967), shows the theoretical estimates of x_m/h, where h is the height of the source, for different values of I_z and r . The figure indicates that the value of r = 0.03 would give a 10-15 percent decrease of x_m/h for unstable flows (B). A similar change would occur for r = 0.015 and 0.01 in neutral and stable flows. These results confirm the previous estimates of the minimum relative particle fall velocities required for obtaining detectable HPP characteristics in wind-tunnel experiments shown in Table A-1.

3.   Criteria for HPP Simulations

Dispersion in wind-tunnel models requires that the ASL flow is correctly simulated. It is evident from the preceding discussion that an additional requirement for the simulation of HPP is

$$\left(\frac{V_g}{U}\right)_m = \left(\frac{V_g}{U}\right)_p \quad .$$
(A-4)

It is usually not difficult to satisfy this requirement. The ratio I_z should also be equal in the model and the atmosphere. This condition is satisfied when the ASL is correctly simulated.

To simulate the dispersion of heavy particles, it is also required that the particles' response to the turbulent eddy motion be correctly modelled. When a free falling particle encounters a small change in the ambient air velocity it will adjust to the new conditions within a time of the order of

$$\tau = V_g/g \quad ,$$
(A-5)

which is designated as the _particle relaxation time_. During this time
the particle will descend a vertical distance of

$$s = V_g^2/g .$$

The length scale, s, may be termed the _characteristic response length_ of
the particle.

To achieve a similar response of the particles in the model it is
required that the dimensionless number

$$\left(\frac{V_g^2/g}{\ell} \right)_m = \left(\frac{V_g^2}{g\ell} \right)_p$$

(A-7)

where ℓ is a typical scale of the turbulent eddies. The scale of
eddies in the model is proportional to the linear scale of the model and
thus it follows that when the model scale is $\lambda_L = \ell_m/\ell_p = L_m/L_p$, all
the velocities in the model should scale as

$$\lambda_U = \frac{V_{g_m}}{V_{g_p}} = \frac{U_m}{U_p} = \lambda_L^{1/2} .$$

(A-8)

This requirement implies a considerable reduction of the model Reynolds
number, which is scaled down as $\lambda_L^{3/2}$. The model Reynolds number may
not be reduced below a critical value and thus the above requirements
can be met only in large models, or when simulating high wind speeds.
At high wind speeds, however, most particle plumes behave as PRP and
such cases are of no interest in the proposed study.

Fortunately, when $V_g^2/g\ell$ becomes very small (namely the response
length of the particles is small compared to the length of the eddies),
the dispersion of particles would be approximately equal to that of
"tagged" fluid particles and independent of particle inertia. Using the

analysis of Csanady (1961), as summarized by Pasquill (1974), p. 152, Eq. 3.133, it is estimated that when

$$\frac{V_g^2}{g\ell} < \frac{1}{2\pi} \sim 0.16 \qquad\qquad (A-9)$$

(where ℓ is the smallest significant eddy size in the flow), the particle's motion will be independent of its inertia and will fully respond to the turbulent motion.

Consider diffusion from an elevated source. The size of the energy containing eddies is of the order of h, where h is the height of the source above ground. The energy contained in eddies whose size is smaller than 0.1 h is small and their effect on the diffusion can be neglected. Thus, Eq. A-9 with $\ell = 0.1$ h, or

$$\frac{V_g^2}{gh} < 0.015 \quad , \qquad\qquad (A-10)$$

is a necessary condition to ensure that the particle inertia is not affecting diffusion.

According to Smith's (1961) analysis on the growth of a cluster of particles descending in a turbulent flow, the size of the cluster, σ, would decrease when the fall velocity V_g became large, due to the fact that the particles were crossing the turbulent eddies. Smith's analysis suggests that for large times (see Pasquill, 1974, p. 15, Eq. 3.130), the reduction in cluster size for small V_g/U would be of the order of $V_g^2\beta^2/(4\ U^2)$, where β is the ratio of the Lagrangian/Eulerian time scales (see Pasquill 1974, p. 135, Eq. 3.89). When $\beta = 5$

$$\frac{V_g}{U} < 0.125 \qquad\qquad (A-11)$$

and the effect of the fall velocity on σ is less than 10 percent.

108

The effect of the fall velocity on continuous PP is expected to be smaller than its effect on clusters of particles, but in view of the uncertainties in the analysis and the estimate of β, the requirement of Eq. A-11 will be adopted in this analysis. It follows that when both Eq. A-9 and A-11 are satisfied, the diffusion of particle plumes is independent of inertia and response time and, therefore, Eq. A-8 need not be satisfied. However, the limitations imposed per Eqs. A-9 and A-11 must be satisfied in both model and atmosphere.

As evidenced in Figure A-4, many cases of atmospheric HPP will satisfy Eq. A-11 and usually also satisfy Eq. A-10, as well. However, the simulated HPP will satisfy the latter equation only if the scale of the model is not too large. Figure A-4 reveals the dependence of the scale reduction factor, $1/\lambda_L$, on the relative fall velocity, r, of the particles and the wind-tunnel speed, U, at an elevation corresponding to a 60 m high prototype source. The figure reveals an inverse relationship between r and $1/\lambda_L$, for a given wind-tunnel velocity. Maximum size of the model is, however, limited by the physical dimsnions of the wind tunnel.

The average ABL is typically 600 m high (Robins, 1978). In the MWT it is possible to generate a shear layer 1.2 m thick so that with a scale of 1:500, the entire ABL can be modelled. However, it is usually sufficient to create a shear layer whose thickness is four times the height of the source. Therefore, a minimum scale of 1:200 will suffice to model a 60 m tall prototype source in the MWT. This constraint is also shown in Figure A-4. In spite of the multiple limitations it appears from the figure that a variety of HPP could satisfactorily be simulated in the Meteorological Wind Tunnel.

4. Negatively Buoyant Particle Plumes

When the combined density of the air-particle mixture leaving the source is larger than that of the ambient air, the plume will descend below the source height in exactly the same way as a hot buoyant plume would rise above the stack height.

It is important to examine the conditions at which such a descent would be detectable, both in wind-tunnel experiments and in the atmosphere. The effect can be estimated using Briggs (1969) plume rise equation (see Pasquill, 1974, pp. 242 and 248),

$$\Delta H = 1.8 \ F^{1/3} \ x^{2/3} \ \bar{U}^{-1} \tag{A-12}$$

where

$$F = \omega r_o^2 \ g \ \Delta\rho/\rho = Qg \ \Delta\rho/(\pi\rho) \tag{A-13}$$

is the buoyancy flux (divided by π), r_o - the radius of the initial jet, ω - the exit velocity and Q - the (volumetric) discharge at the origin.

It is necessary to determine for which conditions

$$\frac{\Delta H}{\sigma_z} \geq 0.4 \ , \tag{A-14}$$

at $x_m = 1.67$ m and $x_p = 1000$ m, in neutral flows, where σ_z/x is approximately 0.04. It follows from Eq. A-14 that the above conditions require that

$$\frac{F}{U^3 x} > 0.4 \times 10^{-6} \ . \tag{A-15}$$

Using the values $U = 1.5$ m/sec and $x_m = 1.67$ m, it is found that

$$F_m > 4.0 \times 10^{-6} \ m^4/sec^3 \ , \tag{A-16}$$

whereas for the prototype,

$$F_p > 2.4 \times 10^{-3} \text{ m}^4/\text{sec}^3 \quad . \tag{A-17}$$

By assuming a 6 mm orifice for a source diameter and establishing ω and $\bar{U} = 1.5$ m/sec the source strength, $Q = \omega A$ becomes

$$Q = 42 \times 10^{-6} \text{ m}^3/\text{sec} = 0.25 \text{ lit/min} \tag{A-18}$$

The required density difference in the wind tunnel thus becomes

$$\frac{\Delta\rho}{\rho} = \frac{F_m \cdot \pi}{Q_m \cdot g} = 0.03 \quad . \tag{A-19}$$

The density ratio of glass/air is approximately 2000. Therefore the relative volume fraction of the glass particles is

$$\Delta V/V = 15 \times 10^{-6} \ , \tag{A-20}$$

and only 0.015 cc, or 0.033 gram, of glass need be added to each liter of air.

The linear void ratio of the mixture in this case is

$$1 - (\Delta V/V)^{1/3} = 1 - 0.024 \cong 0.976 \tag{A-21}$$

so that the "separation" between particles will be approximately 40 diameters.

The above buoyancy flux was calculated for $\Delta H/\sigma_z = 0.4$, which is estimated to be the minimum descent which can accurately be measured in the wind tunnel. It would probably require that

$$\frac{\Delta H}{\sigma_z} < 0.16 \tag{A-22}$$

to completely eliminate negative buoyancy effects. Since ΔH is proportional to $F^{1/3}$, it would be necessary to reduce $\Delta\rho/\rho$, or F, by a factor of 15 to achieve this requirement. Similarly, to increase the effect by a factor of m, the buoyancy flux would have to be increased by m^3.

In most atmospheric PP, the particles will descend due to their own fall velocity and not by modifying the density of the plume. Buoyancy effects can also be created by a mixture of particles and a heavier, or a lighter, carrier gas.

5. Conclusions

The various types of PP are classified according to their relative fall velocities and dimensionless buoyancy flux:

PRP   -   Passive Reference Plume

BP   -   Buoyant Plumes

HPP   -   Heavy Particle Plumes

HPP/BP -   Heavy Particle Plume diffusing together with a Buoyant Plume.

All four types of plumes can be simulated in the wind tunnel. The simulation of HPP is restricted, however, to a finite range of relative fall velocities which depend on the scale of the model and the height of the source.

Figure A-1 schematically describes the regions where the four types of plumes occur for neutrally stable flows.

6. References

Briggs, G. W. (1969), Plume Rise, U.S. Atomic Energy Commission, Division of Technical Information.

Cermak, C. E. (1981), Wind Tunnel Design for Physical Modelling of Atmospheric Boundary Layers, Jour. of the Engineering Mech. Division, ASCE, 107, pp. 623-642.

Csanady, G. T. (1963), Diffusion of Heavy Particles with Atmosphere, Jour. of Atmospheric Sciences, 20, 201.

Pasquill, F. (1974), Atmospheric Diffusion, 2nd Edition. John Wiley and Sons, New York.

Poreh, M. and A. Kacherginsky (1981), Simulation of Plume Rise in Small Wind-Tunnel Models, Jour. of Wind Engineering and Industrial Aerodynamics, 7, pp. 1-14.

Smith, F. B. (1961), The Turbulent Spread of a Falling Cluster, in Atmospheric Diffusion and Air Pollution, Edited by F. N. Frenkill and P. H. Sheppard, Advances in Geophysics, 6, Academic Press.

Snyder, S. H. (1981), Guideline for Fluid Modeling of Atmospheric Diffusion. U.S. Environmental Protection Agency, Research Triangle Park, NC, APA-600/8-81-009.

Stewart, R. E. 1967), Atmospheric Diifusion of Particulate Matter Released from an Elevated Continuous Source. Presented at the 60th Annual Meeting APCA, Cleveland, OH, 1967. Florida Eng. and Ind. Exp. Station Tech. Rept. 388.

Table A-1. Minimum Settling Velocities for HPP

Stability Category	σ_z/x (at 1 km)	V_g/U (-)	V_g[1] cm/sec	d_1[2] μm	$d_{0.25}$[3] μm
B	0.080	0.032	6.4	47	94
D	0.038	0.015	3.0	32	64
E	0.023	0.010	2.0	26	52

(1) Assuming U = 2.0 m/sec.
(2) Assuming U = 7.0 m/sec and a unit density sphere.
(3) Assuming U = 2.0 m/sec and 0.25 gm/cc density.
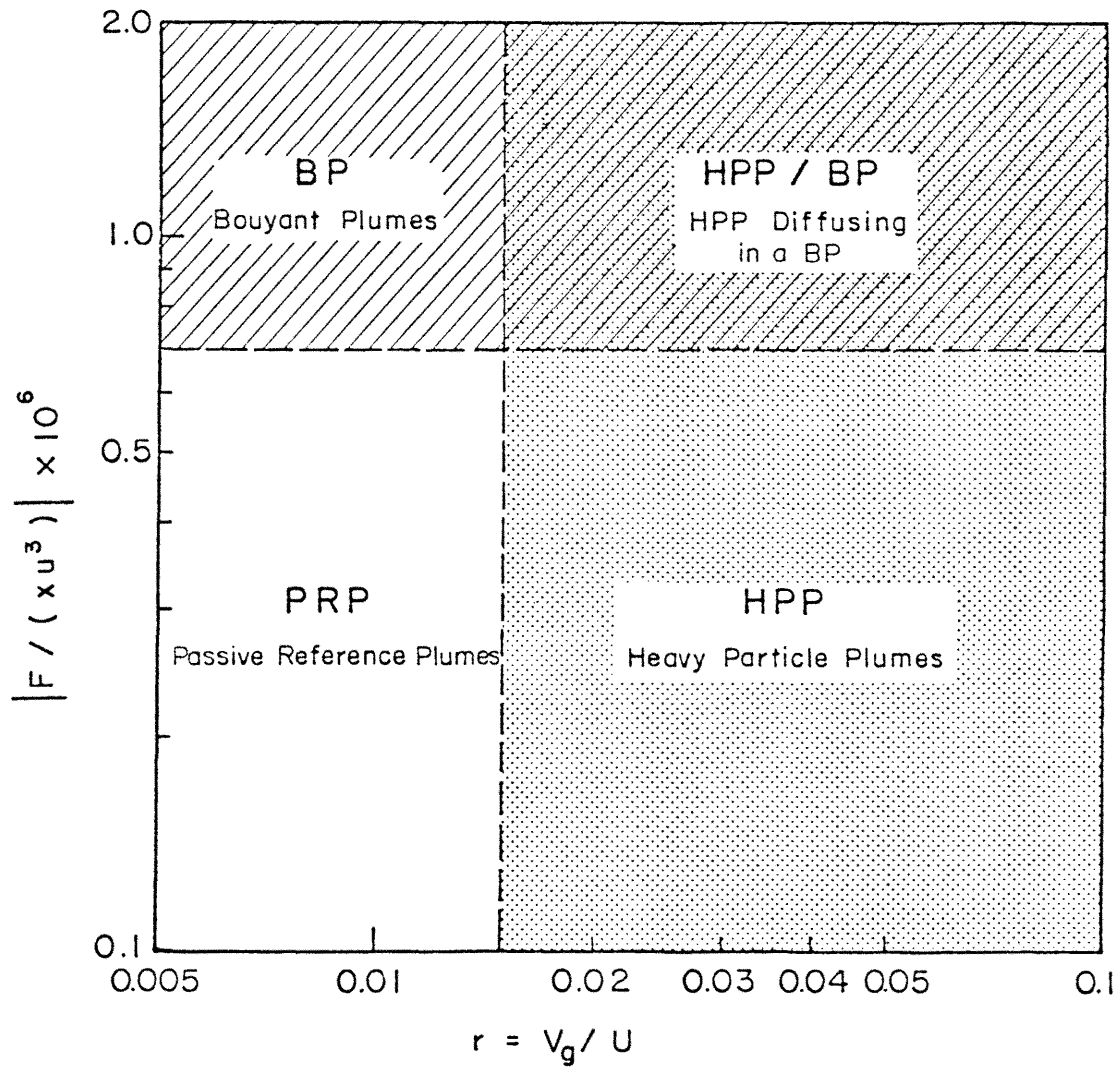
Figure A-1. Classification of Particle Plumes for Neutrally Stratified ASL
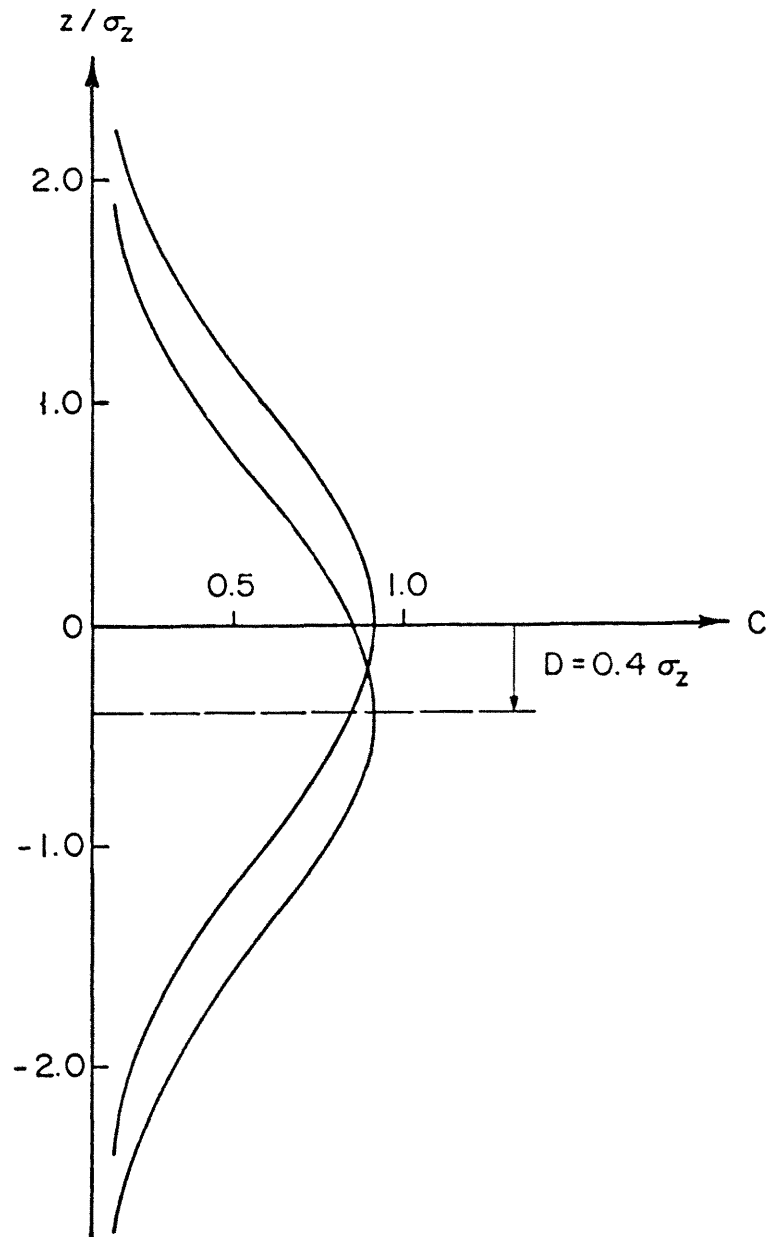
Figure A-2. The Effect of a Vertical Descent D = $0.4\sigma_z$ on the Concentration Distribution

116
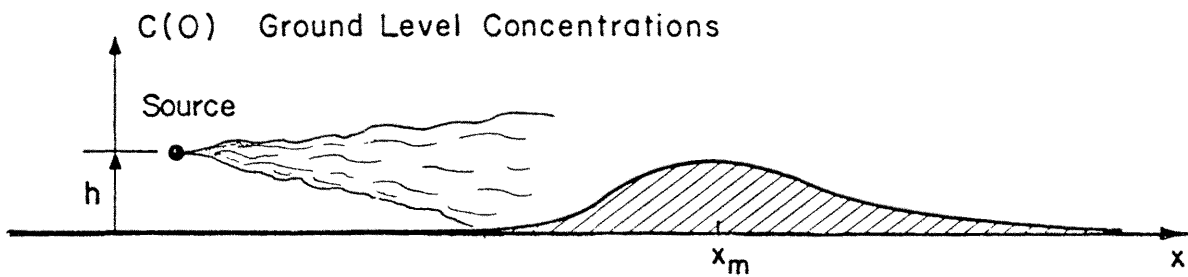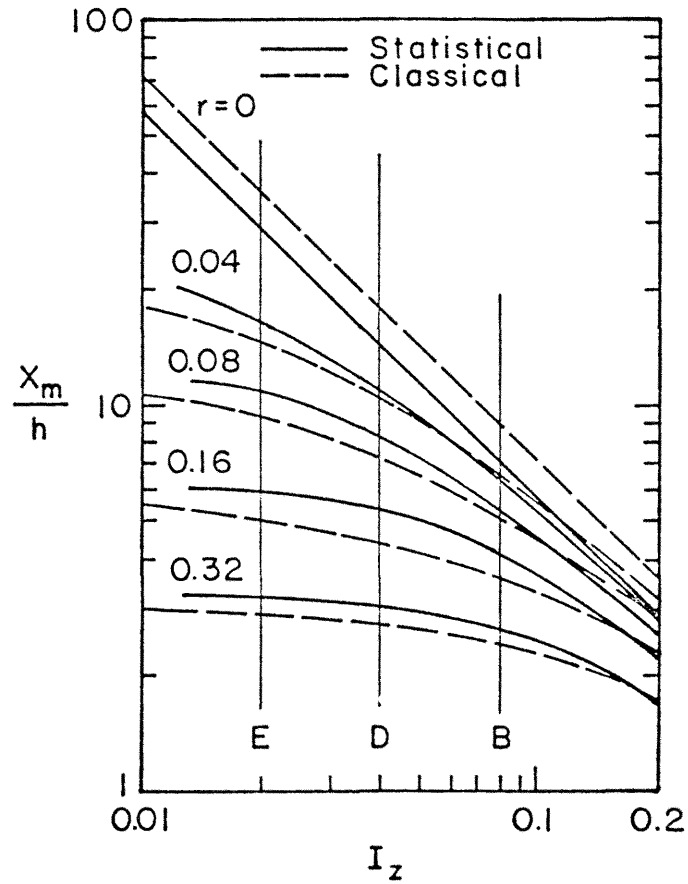
Figure A-3. Comparison of Theoretical Estimates of the Location of Maximum Deposition for Various Values of r and I_z, from Stewart (1967).

117
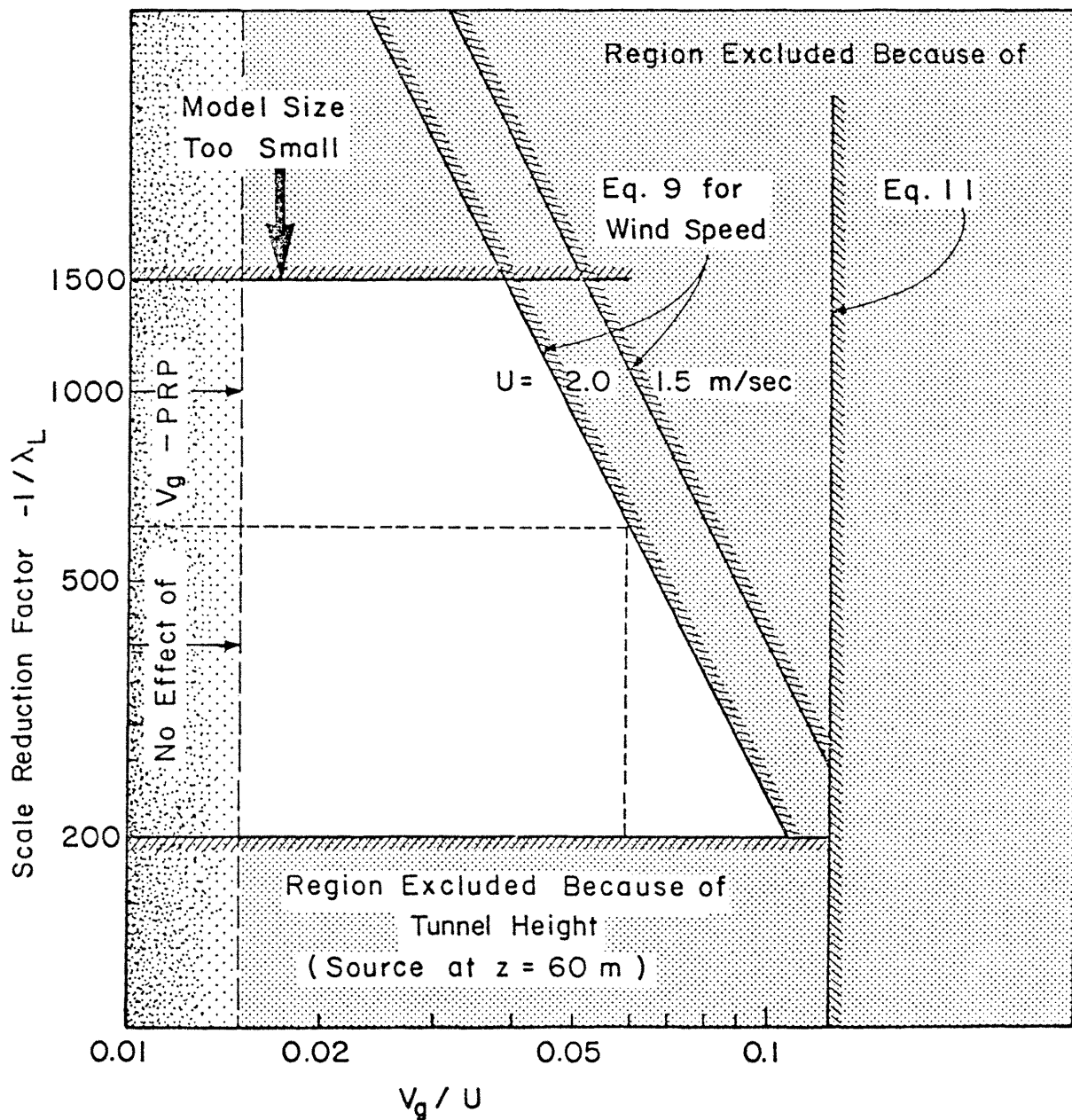
Figure A-4.   Constraints for Wind-Tunnel Simulation for a HPP Source
              Height 60 m, Neutral ASL.   (Example: U = 2.0 m/sec,
              $V_g/U = 0.06$, $200 < \lambda_L \leq 600$).

APPENDIX B

LENGTH-SCALES DESCRIBING THE VERTICAL DIFFUSION

FROM GROUND-LEVEL SOURCES

TABLE OF CONTENTS

LIST OF SELECTED SYMBOLS

Symbol	Definition	Dimension
$A(s,n)$	function of shape factor and velocity profile exponent, defined by equation 39	-
$B(s,n)$	function of shape factor and velocity profile exponent, defined by equation 41	-
C	Gaussian concentration function	ML^{-3}
C_{max}	maximum concentration	ML^{-3}
CWIC	cross-wind integrated concentration	ML^{-2}
$f(z)$	dimensionless concentration profile	-
h	source height	L
Im	mth moment of dimensionless concentration profile	L^{m+1}
Jm	flux related moment	$L^{m+2}T^{-1}$
Ky	lateral mass diffusivity	$L^{2}T^{-1}$
Kz	vertical mass diffusivity	$L^{2}T^{-1}$
n	exponent of velocity profile	-
Q	source height	MT^{-1}
s	shape parameter	-
u^*	shear velocity	LT^{-1}
$\bar{U}$	mean velocity	LT^{-1}
U_R	reference velocity	LT^{-1}
x,y,z	a right-hand coordinate system with origin at the base of the simulated point source	L
$\bar{z}$	centroid of concentration profile	L
$\bar{z}_f$	flux distribution centroid	
z_R	reference length	L
$\alpha(s,n)$	function of shape factor and velocity profile exponent, defined by equation 46	-

121

β	constant ($= \ell n2 = 0.693$)	-
λ_z	height at which $C/C_{max} = 0.5$	L
σ_f	flux standard deviation	L
σ_y	standard deviation of horizontal plume spread	L
σ_z	standard deviation of vertical plume spread	L
σ_{zc}	centroid-centered standard deviation	L
σ_{ze}	estimated standard deviation	L

L - length
T - time
M - mass

LENGTH-SCALES DESCRIBING THE VERTICAL
DIFFUSION FROM GROUND-LEVEL SOURCES

1. Introduction

The vertical growth of passive plumes diffusing from ground-level sources measured in wind-tunnel simulations appears to have a considerably lower rate of growth than that given in widely used predicting schemes, like the Pasquill-Gifford (PG) σ curves, as demonstrated in Figure B-1 taken from Robins (1978).

It will be shown that part of this difference may be due to the use of different length-scales for describing the vertical size, σ_z, of the plume. Length-scales used in the literature to describe diffusing plumes will be reviewed and correlated analytically, making it possible to compare different data sets and to improve predictions of ground-level concentrations.

2. Simple Gaussian Model and the Sigma Curves

A solution of the diffusion equation for a homogeneous field,

$$\bar{U} \frac{\partial C}{\partial x} = K_y \frac{\partial^2 C}{\partial y^2} + K_z \frac{\partial^2 C}{\partial z^2} \quad , \tag{B-1}$$

where the velocity $\bar{U}$, and the eddy diffusivities K_y and K_z are constants, is the Gaussian concentration function,

$$C(x,y,z) = \frac{Q}{2\pi\sigma_y\sigma_z\bar{U}} \exp\left(- \frac{y^2}{2\sigma_y^2}\right) \exp\left(- \frac{(z-h)^2}{2\sigma_z^2}\right), \tag{B-2}$$

where h is the height of the source, Q is the source strength, σ_y and σ_z are the standard deviations of the concentration profile in the y and z direction. The values of $\sigma_y(x)$ and $\sigma_z(x)$ in this solution are

$$\sigma_{y,z} = (2K_{y,z} \, x/\bar{U})^{\frac{1}{2}} \quad . \tag{B-3}$$

For ground-level sources, with no flux at the ground (z=0),

$$C(x,y,z) = \frac{Q}{\pi\sigma_y\sigma_z\bar{U}} \exp(-\frac{y^2}{2\sigma_y^2}) \exp(-\frac{z^2}{2\sigma_z^2}) \, , \qquad \text{(B-4)}$$

giving a maximum concentration at z=0 and y=0.

$$C_{max}(x) = \frac{Q}{\pi\sigma_y\sigma_z\bar{U}} \, . \qquad \text{(B-5)}$$

The concentration distribution downwind of an elevated source is given by,

$$C(x,y,z) = \frac{Q}{2\pi\sigma_y\sigma_z\bar{U}} \exp(-\frac{y^2}{2\sigma_y^2})[\exp(-\frac{(z-h)^2}{2\sigma_z^2}) + \exp(-\frac{(z+h)^2}{2\sigma_z^2})], \quad \text{(B-6)}$$

where h is the height of the source.

The pioneering field experiments in the British Meteorological Office in 1958 (Pasquill, 1974) indicated that neither σ_y nor σ_z follow the $x^{\frac{1}{2}}$ law (Eq. B-3), and therefore, empirical curves for predicting the lateral and vertical spreads of plumes were proposed. Perhaps most common are the PG σ_y and σ_z curves which were adopted in Turner's "Workbook of Atmospheric Dispersion Estimates" (1969). Several improved curves for different stability categories and surface conditions have appeared since (Briggs, 1973), but the so-called Simple Gaussian Model (SGM) (Eqs. B-4, B-5 and B-6) remains the basis for calculation of the concentration field from the σ_y and σ_z curves.

One of the known limitations of the SGM is its use of a constant characteristic velocity $\bar{U}$ to describe the flow field. In cases of elevated sources it is customary to assume that $\bar{U}$ equals the mean velocity at the effective height of the source,

124

$$\bar{U} = u(h) \; , \tag{B-7}$$

or the mean velocity through the vertical extent of the plume, $(h-2\sigma_z)$ < z < $(h+2\sigma_z)$ (Turner, 1969), which is usually close to u(h).

No accepted convention has been adopted for ground-level sources. Turner (1969) remarks that "the surface wind is most applicable to surface or low-level emissions, especially under stable conditions". Indeed, the most widely used value is probably that of u at z=10 m, which usually appears in meteorological data. However, the value of u at z = 2 m, and other heights, is also used. Several authors choose a characteristic velocity at the "effective height" of the plume in the particular experiment or application. In practice only one value of $\bar{U}$ is used in the calculations, even when this recommendation is followed (see for example problems 1 and 2 in Turner's workbook).

Inherent problems make it difficult to measure the vertical distribution of the concentration in field experiments and thus the vertical plume standard deviation has usually been estimated from Eq. B-5, namely:

$$\bar{\sigma}_{ze} = \frac{Q}{\pi \sigma_y C_{max} \bar{U}} \; . \tag{B-8}$$

The length-scale obtained in this procedure is denoted by $\bar{\sigma}_{ze}$, rather than σ_z, and will be referred to as the Estimated Standard Deviation to distinguish it from the σ_z value obtained by direct calculation of the second moment of the actual vertical concentration profile.

Different values of $\bar{U}$ will obviously alter the value of $\bar{\sigma}_{ze}$. Moreover, since Eqs. B-1 through B-5 are mass-balance equations for a uniform flow field, the use of a constant value of $\bar{U}$, which does not

vary with x, violates the mass-balance equations and large errors could occur if a $\bar{\sigma}_{ze}(x)$ curve calculated from field data at short distances were extrapolated to longer distances.

3. Vertical Distribution of Concentrations

Wind-tunnel simulation of turbulent diffusion from ground-level line sources by Shlien and Corrsin (1976) revealed a deviation in the vertical concentration profile from the Gaussian model, as did similar studies by Poreh and Cermak (1964). Malhotra and Cermak (1964) also found similar deviations in wind-tunnel simulations of diffusion from point sources in both neutral and unstable conditions. Their data fit the form,

$$C(z) = C_{max} \exp[- \beta(z/\lambda_z)^S], \qquad\qquad (B-9)$$

where $\beta = \ln(2) = 0.693$ and λ_z is the height where $C/C_{max} = 0.5$, with a value of s = 1.4. Similar experiments in neutral flows by Robins (1978) fit the same form with s = 1.7. Field observations (Pasquill, 1974, pp. 204-205) also indicated that Eq. B-9, with s < 2, described the measured vertical profile better than the Gaussian curve (s = 2). The Porton experiment gave s = 1.15 at x = 100 m, whereas the Cardington experiments gave s = 1.5 at x = 229 m. Both experiments were conducted in a neutral atmosphere. The Prairie Grass experiments suggest that s = 1.48 ± .28 at x = 100 m. The higher values of s correlate with fairly stable atmospheric conditions.

Several solutions of the diffusion equation with variable u(z) and $K_2(z)$, reviewed by Pasquill (1974) and Robins (1978), also show departures from the Gaussian form.

Thus, it appears that the concentration field downstream from a point source can be described in the form,

$$C = C_{max} \exp(- y \qquad \text{(B-10)}$$

or the equivalent form

$$C = C_{max} \exp[- \beta(y/\lambda_y)^2] \, f(z), \qquad \text{(B-11)}$$

where

$$f(z) = \exp[- \beta(z/\lambda_z)^s], \qquad \text{(B-12)}$$

with s varying in the range $1 < s \le 2$.

4. Vertical Plume Length-Scales

Various length-scales are used to characterize the vertical size of plumes. These are defined using the dimensionless concentration profile $f(z) = C(z)/C_{max}$ and its moments I_m, where

$$I_m = \int_0^\infty z^m \, f(z) \, dz \quad . \qquad \text{(B-13)}$$

The one-half peak concentration height, λ_z, is defined by

$$f(\lambda_z) = 0.5 \quad . \qquad \text{(B-14)}$$

Similarly, heights corresponding to other fractions of the peak have been used, such as the one-tenth peak height. The one-half peak height is easier to determine because of the large gradient at that height.

The standard deviation, σ_z, is the most commonly used vertical measure of the plume. It is defined by

$$\sigma_z = (I_2/I_0)^{\frac{1}{2}} \quad . \qquad \text{(B-15)}$$

The centroid of the concentration profile, $\bar{z}$, is defined as

$$\bar{z} = I_1/I_0 \quad . \qquad \text{(B-16)}$$

The centroid-centered standard deviation, σ_{zc}, is defined as

$$\sigma_{zc} = \int_0^\infty (z-\bar{z})^2 \, f(z) \, dz \, / I_0 \, , \qquad (B-17)$$

and it is related to σ_z by

$$\sigma_{zc}^2 = \sigma_z^2 - \bar{z}^2 \, . \qquad (B-18)$$

The length-scales $\bar{z}$ and σ_{zc}, according to Shlien and Corrsin, are important because $\bar{z}$ is approximately equal to the mean particle displacement perpendicular to the wall, and the second centroid-centered moment is approximately equal to the dispersion of the particles around the centroid.

The previously defined Estimated Standard Deviation, $\bar{\sigma}_{ze}$, was calculated from the ground-level concentration (Eq. B-8). A similar length-scale is defined by

$$h = \frac{Q}{CWIC \cdot u^*} \, , \qquad (B-19)$$

where u^* is the shear velocity and CWIC is the Cross-Wind Integrated Concentration, defined as

$$CWIC = \int_{-\infty}^\infty C(y,0) \, dy \, . \qquad (B-20)$$

Since $C(y)$ is well described by a Gaussian form, it follows that

$$CWIC = \sqrt{2\pi} \, C_{max} \, \sigma_y \qquad (B-21)$$

and

$$h = \sqrt{2/\pi} \, (\bar{U}/u^*) \, \bar{\sigma}_{ze} \, . \qquad (B-22)$$

The advantage of using h, rather than $\bar{\sigma}_z$, is that the shear velocity is clearly defined. However, it is more difficult to determine shear

velocity than it is to determine the mean velocity, at an agreed upon height, say 10 m.

Using the vertical concentration profile given by Eq. B-11, the four length-scales σ_z, $\bar{z}$, σ_{zc} and λ_z can be correlated.

$$I_m = \int_0^\infty z^m \exp[-\beta(z/\lambda_z)^s] \, dz$$

$$= \beta^{-(m+1)/s} \lambda_z^{m+1} s^{-1} \Gamma[(m+1)/s] \qquad \text{(B-23)}$$

and thus,

$$\frac{\sigma_z}{\lambda_z} = \beta^{-1/s} [\Gamma(3/s)/\Gamma(1/s)]^{\frac{1}{2}} \qquad \text{(B-24)}$$

and

$$\frac{\bar{z}}{\lambda_z} = \beta^{-1/s} \Gamma(2/s)/\Gamma(1/s) \; . \qquad \text{(B-25)}$$

The value of σ_{zc}/λ_z can be calculated from

$$\left(\frac{\sigma_{zc}}{\lambda_z} \right)^2 = \left(\frac{\sigma_z}{\lambda_z} \right)^2 - \left(\frac{\bar{z}}{\lambda_z} \right)^2 \; . \qquad \text{(B-26)}$$

Table B-1 and Figure B-2 show the dependence of the above ratios on the shape parameter, s.

5. Flux Related Length-Scales

The length-scales $\bar{z}(x)$ and $\sigma_z(x)$ are related to the concentration distribution at the distance x and thus give information on the "residing" matter at that position. The moments

$$J_m = \int_0^\infty z^m u(z) \, f(z) \, dz \qquad \text{(B-27)}$$

on the other hand, are related to the distribution of the flux at each distance, normal to the mean wind-direction, and may be useful in describing the motion of clouds and particles.

The moment J_0 is proportional to the total flux, Q

$$J_0 = \int_0^\infty u(z) \; f(z) \; dz = Q/(\sqrt{2\pi} \; \sigma_y) . \qquad \text{(B-28)}$$

The <u>flux</u> <u>distribution</u> <u>centroid</u> is given by

$$\bar{z}_f = J_1/J_0 \qquad \text{(B-29)}$$

and the <u>flux</u> <u>standard</u> <u>deviation</u> is given by

$$\sigma_f = (J_2/J_0)^{\frac{1}{2}} . \qquad \text{(B-30)}$$

To calculate the above moments and length-scales, the vertical velocity distribution, $u(z)$, must be known. Two forms of describing this distribution are widely used: the Law of the Wall representation, which has a sound theoretical basis; and the power-law representation, which is often used in practical applications since it is more convenient for calculations. Estimates of the power n for various surface and stability classes were made by Irwin (1979) and are shown in Table B-2, taken from Hanna (1982).

Using the power law

$$\frac{u}{U_R} = (\frac{z}{z_R})^n , \qquad \text{(B-31)}$$

where z_R is a convenient reference height within the region described by the power law, the various flux related moments become

$$J_m = \frac{U_R}{z_R^n} \int_0^\infty z^{m+n} \; f(z) \; dz = \frac{U_R}{z_R^n} \; I_{m+n} . \qquad \text{(B-32)}$$

It follows that

$$J_0 = \frac{Q}{C_{max}\sqrt{2\pi} \; \sigma_y} = \frac{U_R}{z_R^n} \; \beta^{-(1+n)/s} \; \lambda_z^{1+n} \; s^{-1} \; \Gamma \left[(1+n)/s \right] \qquad \text{(B-33)}$$

$$\frac{\bar{z}_f}{\lambda_z} = \beta^{-\frac{1}{s}} \left[\Gamma \left(\frac{2+n}{s} \right) / \Gamma \left(\frac{1+n}{s} \right) \right] \tag{B-34}$$

$$\frac{\sigma_f}{\lambda_z} = \beta^{-\frac{1}{s}} \left[\Gamma \left(\frac{3+n}{s} \right) / \Gamma \left(\frac{1+n}{s} \right) \right]^{\frac{1}{2}} \tag{B-35}$$

$$\frac{\sigma_f}{\sigma_z} = \frac{\Gamma[(3+n)/s] \, \Gamma (1/s)}{\Gamma(3/s) \, \Gamma [(1+n)/s]} {}^{\frac{1}{2}} \tag{B-36}$$

and

$$\frac{\bar{z}_f}{\bar{z}_c} = \frac{\Gamma [(2+n)/s] \, \Gamma (1/s)}{\Gamma (2/s) \, \Gamma [(1+n)/s]} \; . \tag{B-37}$$

The dependence of these ratios on s and n is also shown in Table B-1 and Figure B-2. Using Eqs. B-24 and B-33, the flux, Q, can be written as

$$Q = \pi \, \lambda_y \, \lambda_z \, \bar{U}_r \, C_{max} \cdot (\lambda_z/z_R)^n \, A(s,n) \; , \tag{B-38}$$

where

$$A(s,n) = 0.9493 \, \sqrt{2/\pi} \, \beta^{-(1+n)/s} \, s^{-1} \, \Gamma[(1+n)/s] \; , \tag{B-39}$$

or

$$Q = \pi \, \sigma_y \, \sigma_z \, \bar{U}_R \, C_{max} \, (\sigma_z/z_R)^n \, B(s,n) \; , \tag{B-40}$$

where

$$B(s,n) = \frac{\sqrt{2/\pi} \, s^{-1} \, \Gamma [(1+n)/s]}{[\Gamma(3/s) / \Gamma(1/s)]^{(1+n)/2}} \tag{B-41}$$

The dependence of $A(s,n)$ and $B(s,n)$ on s and n is shown in Table B-1 and Figures B-3 and B-4, respectively.

The relationship between σ_z and σ_{ze} can be calculated directly from Eqs. B-8 and B-40,

$$\frac{\sigma_{ze}}{\sigma_z} = \frac{U_R}{\bar{U}} \left(\frac{\sigma_z}{z_R} \right)^n B(s,n) \; . \tag{B-42}$$

Since $\bar{U}z^{-n}$ is a constant in a boundary layer satisfying Eq. B-31,

$$\frac{\sigma_{ze}}{\sigma_z} = (\frac{\sigma_z}{z_U})^n \ B(s,n) \ , \tag{B-43}$$

where $z_{\bar{U}}$ is the height where $\bar{U}$ is being measured, or

$$\frac{\sigma_z}{\sigma_{ze}} = (\frac{z_u}{\sigma_{ze}})^{\frac{n}{1+n}} \ B^{-1/(1+n)} = \frac{z_u}{\sigma_{ze}}^{n/(1n)} \ B^{-1/(1+n)} . \tag{B-44}$$

The above relationship clearly reveals that for a given s, n and $z_{\bar{U}}$, σ_z is proportional to $\sigma_{ze}^{1/(1+n)}$ and thus the rate of growth of σ_z with x is expected to be smaller than that of σ_{ze}, which is compatible with the measurements shown in Figure B-1.

Equation B-43 may also be written in the form

$$\frac{\sigma_{ze}}{\sigma_z} = (\frac{\sigma_z}{\alpha \, z_U})^n \tag{B-45}$$

where

$$\alpha(s,n) = B(s,n)^{-\frac{1}{n}} \tag{B-46}$$

Equation B-45 may be used to determine the height, relative to σ_z, at which the effective velocity, $\bar{U}$, should be measured to ensure that $\sigma_{ze} = \sigma_z$. Unfortunately, $\alpha(s,n)$ varies considerably with both s and n. For example, $\alpha(1.5, 0.15) = 4.42$, $\alpha(1.5, 0.20) = 6.12$ and $\alpha(2.0, 0.2) = 1.69$. Thus, it appears that measuring $\bar{U}$ at σ_z, or at a constant fraction of it, will not ensure the above desired equality.

6.   Improving Concentration Predictions

Given semi-empirical values for $\sigma_z(z)$ for different stability categories and surface roughnesses, it is essential to determine whether

132

these values represent the true standard deviation of the plume concentration or estimated values obtained from ground-level concentrations and an effective velocity measured at a certain height.

Ground-level concentrations can be calculated directly from the estimated values of $\bar{\sigma}_{ze}$ using Eq. B-5. Elevated concentration levels, particularly for $z \geq \sigma_{ze}$ should be estimated, however, using Eq. B-9. To carry out such a procedure it is necessary to estimate both n and s.

Given estimates of σ_z, Eq. B-40 should be used to determine C_{max} at ground-level, using the velocity at any reference height, except very close to the ground where the power law is not expected to hold. It is necessary, of course, to estimate both s and n. The value of n can be estimated using Table B-2. No procedure for estimating s is available, but even a rough estimate of the shape parameter will usually give a more accurate prediction than one obtained by the simple Gaussian model.

7. References

Briggs, G.A. (1973), Diffusion estimation for small emissions. 1974 Annual Report of the USAEC, Report ATDL-106, National Oceanic and Atmospheric Administration.

Hanna, S. R. (1982), Applications in modelling, in Atmospheric Turbulence and Air Pollution Modelling, Ed. by F.T.M. Nieuwstadt and H. van Dop, D. Reidel Publishing Co., Boston, USA.

Irwin, T. S. A theoretical variation of the wind profile power law exponent as a function of surface roughness and stability. Atmospheric Environment 13, 191-194 (1979).

Malhotra, R. C. and Cermak, J. E. (1964), Mass diffusion in neutral and unstable stratified boundary-layer flows. Int. J. Heat Mass Transfer, 7, pp. 169-186.

Pasquill, F. (1974), Atmospheric Diffusion, 2nd ed. New York, John Wiley & Sons.

Poreh, M. and J. E. Cermak (1964), Study of diffusion from a line source in a turbulent boundary layer. Int. J. Heat Mass Transfer, 7, 1083-1095.

Robins, A.G. (1978), Plume dispersion from ground level sources in simulated atmospheric boundary layers. Atmospheric Environment, 12, pp. 1033-1044.

Shlien, D. H. and Corrsin, S. (1976), Dispersion measurements in a turbulent boundary layer. Int. J. Heat Mass Transfer 19, pp. 285-295.

Turner, B. D. (1969), Workbook of atmospheric dispersion estimates. U.S. Department of Health, Education and Welfare.

n	s	σ_z/λ	$\bar{z}/\lambda$	σ_{zc}/λ	σ/λ	$\bar{z}_f/\lambda$	σ_{fc}/λ	$\sigma_z/\bar{z}$	σ_{zc}/σ	$\sigma_f/\bar{z}$	σ_{fc}/σ_f	σ_f/σ_z	z_f/z	σ_{fc}/σ_{zc}	A	B
.05	1.20	1.473	1.085	.996	1.522	1.134	1.015	1.357	.676	1.342	.667	1.033	1.044	1.019	.848	.665
.05	1.40	1.189	0.902	.775	1.225	0.939	0.786	1.318	.651	1.304	.642	1.030	1.041	1.015	.781	.766
.05	1.60	1.025	0.794	.648	1.054	0.825	0.656	1.290	.632	1.278	.622	1.028	1.038	1.012	.740	.848
.05	1.80	0.921	0.725	.567	0.944	0.751	0.573	1.269	.616	1.257	.606	1.026	1.036	1.010	.713	.915
.05	2.00	0.849	0.678	.512	0.870	0.701	0.516	1.253	.603	1.242	.593	1.025	1.034	1.008	.694	.970
.05	2.20	0.798	0.644	.472	0.817	0.665	0.475	1.241	.592	1.229	.582	1.024	1.033	1.006	.681	1.016
.10	1.20	1.473	1.085	.996	1.570	1.182	1.033	1.357	.676	1.328	.658	1.066	1.089	1.038	.834	.641
.10	1.40	1.189	0.902	.775	1.260	0.975	0.798	1.318	.651	1.292	.633	1.059	1.081	1.030	.762	.742
.10	1.60	1.025	0.794	.648	1.082	0.854	0.663	1.290	.632	1.266	.613	1.055	1.075	1.024	.718	.823
.10	1.80	0.921	0.725	.567	0.968	0.777	0.578	1.269	.616	1.246	.597	1.052	1.071	1.019	.690	.889
.10	2.00	0.849	0.678	.512	0.891	0.724	0.520	1.253	.603	1.231	.583	1.049	1.068	1.015	.670	.944
.10	2.20	0.798	0.644	.472	0.836	0.685	0.478	1.241	.592	1.219	.572	1.047	1.065	1.012	.656	.989
.15	1.20	1.473	1.085	.996	1.617	1.229	1.051	1.357	.676	1.316	.650	1.098	1.133	1.056	.823	.621
.15	1.40	1.189	0.902	.775	1.295	1.011	0.809	1.318	.651	1.280	.625	1.089	1.121	1.044	.746	.720
.15	1.60	1.025	·0.794	.648	1.109	0.883	0.670	1.290	.632	1.255	.604	1.082	1.112	1.035	.700	.801
.15	1.80	0.921	0.725	.567	0.991	0.802	0.583	1.269	.616	1.236	.588	1.076	1.105	1.027	.669	.867
.15	2.00	0.849	0.678	.512	0.911	0.746	0.523	1.253	.603	1.221	.574	1.072	1.100	1.021	.648	.921
.15	2.20	0.798	0.644	.472	0.853	0.705	0.480	1.241	.592	1.210	.563	1.069	1.096	1.017	.633	.966
.20	1.20	1.473	1.085	.996	1.665	1.277	1.068	1.357	.676	1.304	.642	1.130	1.176	1.073	.815	.603
.20	1.40	1.189	0.902	.775	1.329	1.046	0.819	1.318	.651	1.270	.616	1.117	1.160	1.057	.733	.701
.20	1.60	1.025	0.794	.648	1.136	0.912	0.677	1.290	.632	1.245	.596	1.108	1.148	1.045	.683	.781
.20	1.80	0.921	0.725	.567	1.014	0.826	0.587	1.269	.616	1.227	.579	1.101	1.139	1.036	.651	.846
.20	2.00	0.849	0.678	.512	0.930	0.767	0.526	1.253	.603	1.212	.566	1.095	1.132	1.028	.629	.900
.20	2.20	0.798	0.644	.472	0.871	0.725	0.483	1.241	.592	1.201	.554	1.091	1.127	1.021	.613	.946
.25	1.20	1.473	1.085	.996	1.712	1.324	1.085	1.357	.676	1.293	.634	1.162	1.219	1.090	.809	.587
.25	1.40	1.189	0.902	.775	1.363	1.081	0.829	1.318	.651	1.260	.608	1.146	1.198	1.070	.721	.684
.25	1.60	1.025	0.794	.648	1.163	0.940	0.683	1.290	.632	1.236	.588	1.134	1.184	1.055	.669	.763
.25	1.80	0.921	0.725	.567	1.036	0.850	0.591	1.269	.616	1.218	.571	1.125	1.172	1.043	.635	.829
.25	2.00	0.849	0.678	.512	0.950	0.789	0.529	1.253	.603	1.204	.557	1.118	1.164	1.033	.611	.883
.25	2.20	0.798	0.644	.472	0.888	0.744	0.484	1.241	.592	1.193	.545	1.113	1.157	1.025	.594	.928
.30	1.20	1.473	1.085	.996	1.758	1.370	1.102	1.357	.676	1.283	.627	1.194	1.263	1.106	.805	.573
.30	1.40	1.189	0.902	.775	1.396	1.116	0.839	1.318	.651	1.251	.601	1.174	1.237	1.083	.712	.669
.30	1.60	1.025	0.794	.648	1.189	0.968	0.690	1.290	.632	1.228	.580	1.160	1.219	1.064	.656	.748
.30	1.80	0.921	0.725	.567	1.057	0.874	0.596	1.269	.616	1.210	.563	1.149	1.205	1.050	.620	.813
.30	2.00	0.849	0.678	.512	0.968	0.809	0.532	1.253	.603	1.197	.549	1.140	1.194	1.039	.595	.867
.30	2.20	0.798	0.644	.472	0.905	0.763	0.486	1.241	.592	1.186	.537	1.133	1.186	1.029	.578	.912
.40	1.20	1.473	1.085	.996	1.850	1.463	1.133	1.357	.676	1.265	.612	1.256	1.348	1.138	.803	.550
.40	1.40	1.189	0.902	.775	1.462	1.184	0.857	1.318	.651	1.235	.586	1.229	1.312	1.106	.698	.645
.40	1.60	1.025	0.794	.648	1.240	1.023	0.701	1.290	.632	1.212	.565	1.209	1.287	1.082	.636	.723
.40	1.80	0.921	0.725	.567	1.100	0.920	0.603	1.269	.616	1.196	.548	1.195	1.268	1.063	.596	.788
.40	2.00	0.849	0.678	.512	1.005	0.850	0.537	1.253	.603	1.183	.534	1.183	1.254	1.048	.568	.841
.40	2.20	0.798	0.644	.472	0.937	0.799	0.489	1.241	.592	1.172	.522	1.174	1.242	1.036	.549	.886
.50	1.20	1.473	1.085	.996	1.941	1.555	1.163	1.357	.676	1.249	.599	1.318	1.432	1.168	.809	.533
.50	1.40	1.189	0.902	.775	1.526	1.251	0.874	1.318	.651	1.220	.573	1.283	1.386	1.129	.691	.627
.50	1.60	1.025	0.794	.648	1.290	1.076	0.712	1.290	.632	1.199	.552	1.258	1.354	1.098	.621	.705
.50	1.80	0.921	0.725	.567	1.141	0.964	0.610	1.269	.616	1.183	.534	1.239	1.330	1.075	.577	.769
.50	2.00	0.849	0.678	.512	1.040	0.888	0.541	1.253	.603	1.171	.520	1.225	1.311	1.057	.547	.822
.50	2.20	0.798	0.644	.472	0.969	0.834	0.492	1.241	.592	1.161	.508	1.213	1.296	1.041	.525	.867
.60	1.20	1.473	1.085	.996	2.031	1.645	1.191	1.357	.676	1.235	.587	1.379	1.516	1.197	.822	.521
.60	1.40	1.189	0.902	.775	1.589	1.316	0.890	1.318	.651	1.207	.560	1.336	1.459	1.149	.688	.614
.60	1.60	1.025	0.794	.648	1.338	1.127	0.721	1.290	.632	1.187	.539	1.306	1.419	1.113	.611	.691
.60	1.80	0.921	0.725	.567	1.181	1.007	0.616	1.269	.616	1.172	.522	1.283	1.389	1.086	.562	.755
.60	2.00	0.849	0.678	.512	1.074	0.926	0.545	1.253	.603	1.160	.507	1.265	1.366	1.064	.529	.809
.60	2.20	0.798	0.644	.472	0.999	0.868	0.494	1.241	.592	1.151	.495	1.251	1.348	1.046	.505	.853

Table B-2. Estimates of the Power n in Eq. 31* by Irwin
from Hanna (1982)

$Z_o(m)$	Class:	A	B	C	D	E	F
0.01		0.05	0.06	0.06	0.12	0.34	0.53
0.10		0.08	0.09	0.11	0.16	0.32	0.54
1.00		0.17	0.17	0.20	0.27	0.38	0.61
3.00		0.27	0.28	0.31	0.37	0.47	0.69

* $z < 100$ m.
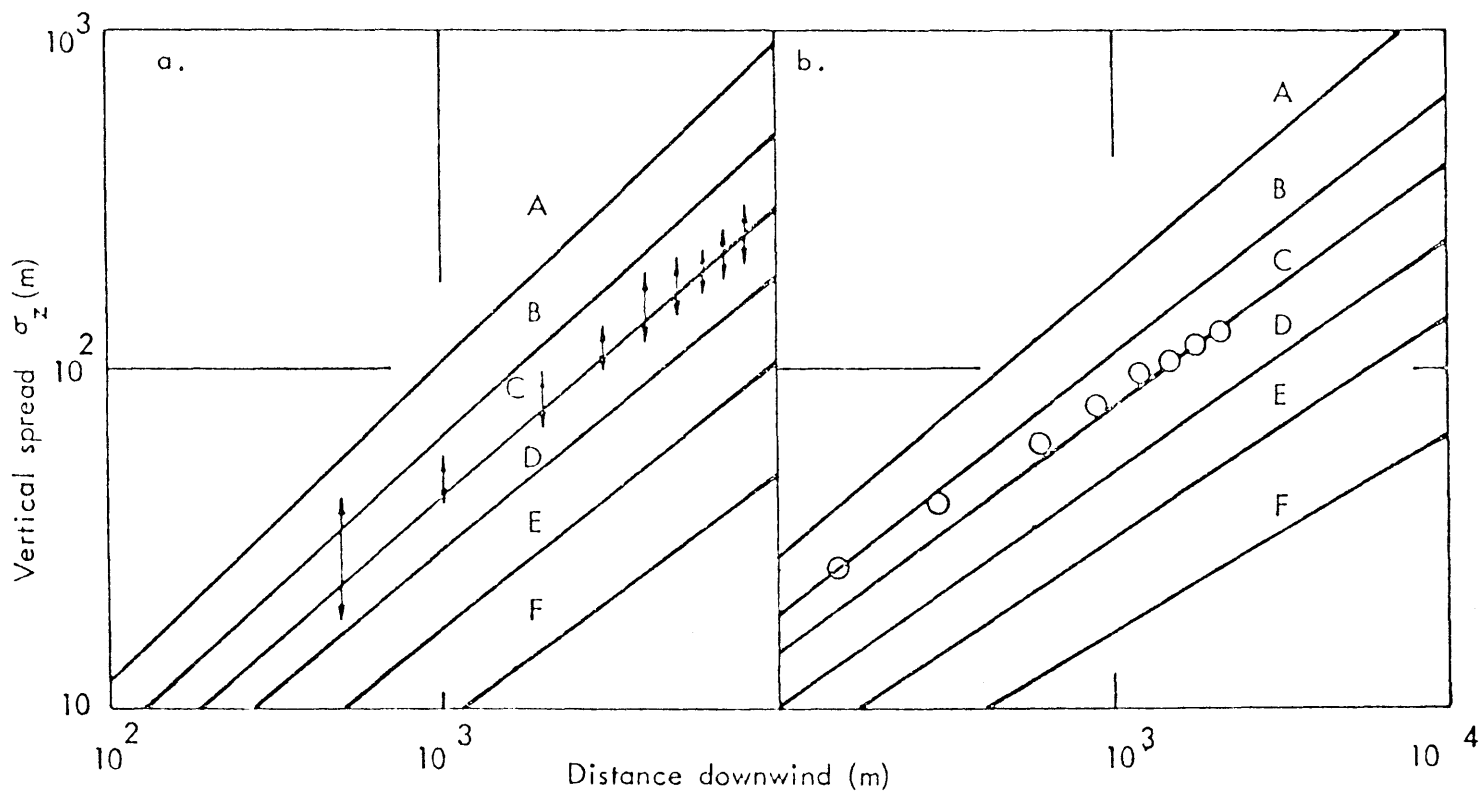
Figure B-1. Comparison of Measured Vertical Plume Spread with Pasquill Estimates (a. Rural; b. Urban), from Robins (1978)
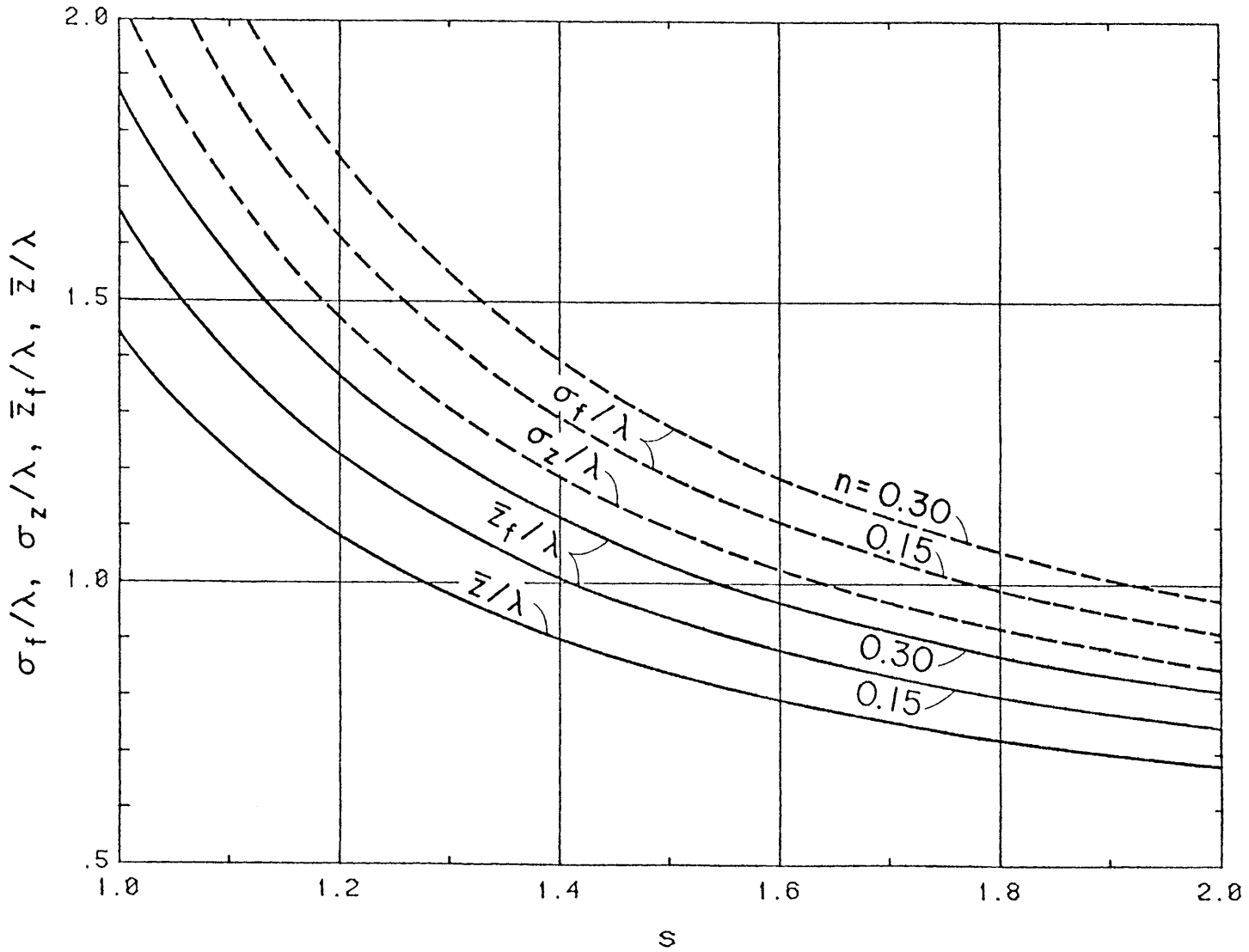
Figure B-2. The Dependence of Different Length-Scale Ratios on the Shape Parameter, s
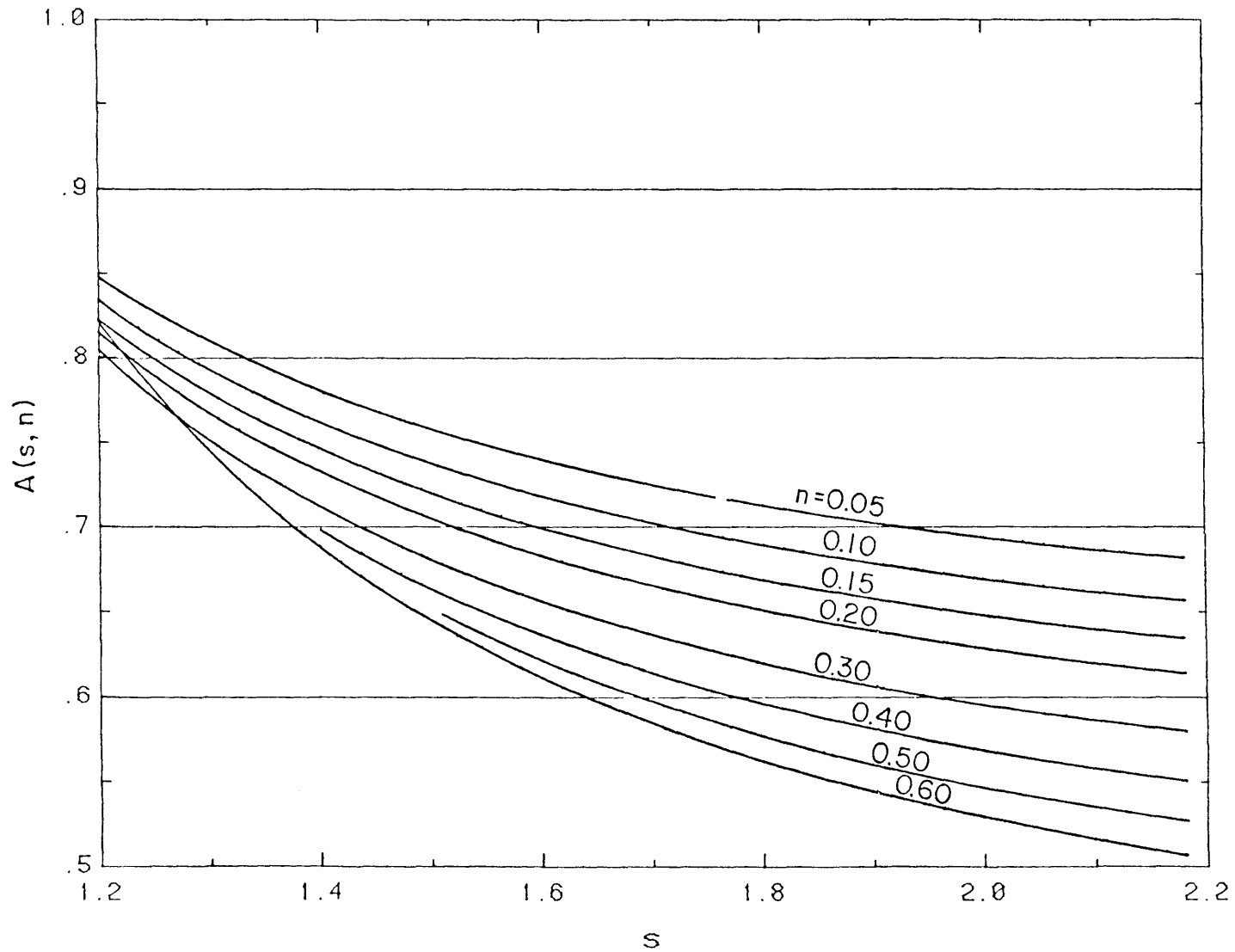
Figure B-3.   The Variation of the Function   A(s,n)
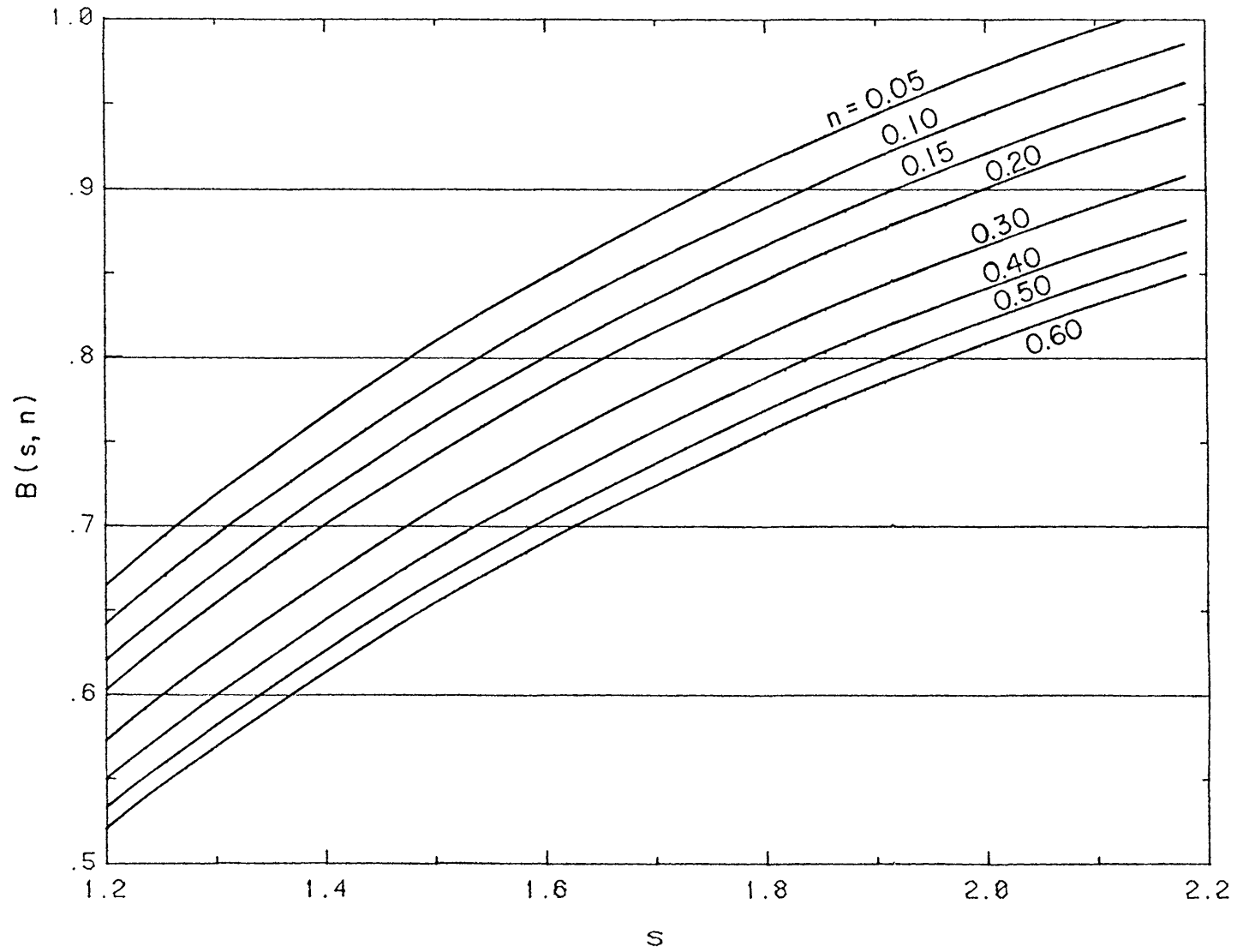
Figure B-4.   The Variation of the Function   B(s,n)